Distribution of velocities and acceleration for a particle in Brownian correlated disorder: Inertial case

Pierre Le Doussal, Aleksandra Petković, and Kay Jörg Wiese

Laboratoire de Physique Théorique-CNRS, Ecole Normale Supérieure, 24 rue Lhomond, 75005 Paris, France

We study the motion of an elastic object driven in a disordered environment in presence of both dissipation and inertia. We consider random forces with the statistics of random walks and reduce the problem to a single degree of freedom. It is the extension of the mean-field Alessandro-Beatrice- Bertotti-Montorsi (ABBM) model in presence of an inertial mass m. While the ABBM model can be solved exactly, its extension to inertia exhibits complicated history dependence due to oscillations and backward motion. The characteristic scales for avalanche motion are studied from numerics and qualitative arguments. To make analytical progress, we consider two variants which coincide with the original model whenever the particle moves only forward. Using a combination of analytical and numerical methods together with simulations, we characterize the distributions of instantaneous acceleration and velocity, and compare them in these three models. We show that for large driving velocity, all three models share the same large-deviation function for positive velocities, which is obtained analytically for small and large m, as well as for $m = 6/25$. The effect of small additional thermal and quantum fluctuations can be treated within an approximate method.

I. INTRODUCTION

The dynamics of a large class of classical and quantum systems can be modeled within the description of an elastic manifold driven by an applied external force through a disordered medium [1–3]. Some examples are domain walls in magnetic systems in the presence of time-dependent magnetic fields [4], flux-line lattices in type-II superconductors driven by an applied transport current [5], charge-density waves in solids in an electric field [6,7], pinned or driven Wigner crystals [8–11], dislocations in metals [12], interface between two fluids in a porous medium [13], earthquakes [1], and crack fronts in brittle materials [14]. In all these systems, the competition between elastic forces, quenched disorder, and external driving shapes the dynamics. As a result, the response is usually complicated.

If the driving force is sufficiently small, the system is trapped due to disorder in a metastable state. When increasing the external driving, some weakly pinned parts will start moving. They will be stopped by elastic forces that describe interactions between weakly and strongly pinned regions of the manifold. Further increase of the driving usually results in jumps of a segment of the system, and avalanche motion.

One example occurs in soft magnets. When smoothly increasing the magnetic field (H), the magnetization (M) changes in an irregular way. This process can be explained by considering the motion of domain walls separating regions of opposite magnetization. The derivative of the magnetization with respect to the magnetic field, $\partial M / \partial H$, is known as Barkhausen noise and can be related to avalanche motion [15,16]. An important step towards modeling the dynamics in these systems was made by Alessandro, Beatrice, Bertotti and Montorsi (ABBM). On a phenomenological basis, they introduced [17,18] a Langevin equation for the velocity of a single degree of freedom, i.e., a particle, which represents the center of mass of the domain wall. It is simple enough to allow for an exact solution. Their approach is known as the

ABBM model. It was successful in explaining the distribution of sizes and the duration of pulses in the Barkhausen signal, both for an extremely small and for a finite increase rate of the external field [4,19–21]. In the ABBM model, the probability of the instantaneous domain-wall velocity is found to be $P(\dot{u}) \sim \dot{u}^{-\alpha} \exp(-\dot{u}/\dot{u}_0)$, where $\alpha = 1 - v$. Here v is proportional to the rate of increase of the field and $\dot{u}_0$ is some characteristic cutoff. The avalanche sizes S are distributed according to $P(S) \sim S^{-\tau}$ up to some large-scale cutoff, with $\tau = (3 - v)/2$. For vanishing rate $v \to 0^+$, different samples of different materials were found to be characterized by universal exponents α and τ, regardless of the specific microscopic details about the sample structure.

In their phenomenological theory, ABBM assumed that the random-force landscape seen by the particle has the long-range correlations of a Brownian motion, while the original disorder seen by the domain wall is of short-ranged nature. This approximation, made in order to explain experiments, turns out to be justified in some cases. First, in the limit of an interface with infinite-ranged interactions (i.e., a fully connected lattice model), it was shown that the ABBM model becomes exact, i.e., it describes exactly the center-of-mass motion [20]. It is believed to provide a mean-field model, which should be valid in particular to describe domain walls in situations where the long-ranged dipolar forces generate long-ranged elasticity and puts the system at its upper critical dimension [22].

Recently, two of us have developed a field theoretic approach to describe and compute avalanche-size distributions and velocity distributions for elastic interfaces of internal dimension d in short-ranged disorder [23–25]. It was shown that in the quasistatic limit $v \to 0^+$ the velocity of the center of mass is indeed described by the ABBM model at and above the critical dimension d_c, with corrections subdominant in the spring constant (parameter μ below). Deviations become important for $d < d_c$, and were computed in a $d = d_c - \epsilon$ expansion, where $d_c = 4$ for short-range elasticity, and $d_c = 2$ in case of dipolar forces. The theory also allows

us to predict the spatial dependence of avalanches [24,25] which can not be obtained from the ABBM model. It also provides an independent exact solution of the ABBM model at any driving velocity [26] based on the Martin-Siggia-Rose (MSR) formalism via the solution to a nonlinear saddle-point equation, called the instanton equation.

The ABBM model, and the subsequent field theoretical approach, provides a good description of avalanche motion in classical systems evolving with the simplest over-damped dynamics. One would like to extend these theories to describe elastic systems with a more general dynamics, including inertial and retardation effects, and to describe avalanche dynamics in quantum systems. Studies of classical models with stress overshoots [27,28] have shown that although the depinning transition may be not too much affected in the thermodynamic limit, the avalanche-size distributions can be quite different.

Retardation effects are important for instance in magnets. Apart from universal power laws discussed above (characterized by the exponents α and τ), pulses of different durations in Barkhausen noise are expected to collapse on the same curve after proper rescaling [29]. However, in some experiments on ferromagnetic alloys the pulse shape is found to be asymmetric [29–31]. This asymmetry was explained to be a transient effect of eddy currents [32,33]. Namely, the domain-wall motion generates eddy currents. The response is not immediate, but instead finite-time delays exist after the corresponding wall displacement is made. These effects of retardation can be taken into account by introduction of a negative mass of the domain wall [32,33].

Although the above-mentioned effects are important in some samples, inertial effects are always present in the domain-wall dynamics. A domain wall is characterized by the so-called Döring mass, which is due to gyromagnetic effects [34]. However, inertial effects are often neglected with respect to a larger damping present in the system, and simplified models excluding the mass are studied. In many other systems, the dynamics is only weakly dissipative and inertial effects can be important. Some examples are geological faults, motion of contact lines of a droplet on a dirty rough surface, and crack fronts in brittle materials. Domain walls with an internal degree of freedom also exhibit a nontrivial dynamics reminiscent of inertial effects [35].

The description of avalanches in quantum systems with quenched disorder is also a challenge. There is great current interest in nonequilibrium quantum systems and their full counting statistics [36–40]. Higher moments of the noise have been measured in avalanche processes and exhibit some resemblance to their classical counterparts [41]. Out of equilibrium elastic quantum systems in presence of disorder and a bath have been studied in the thermal and quantum-creep regimes [42,43] where the driving force is small and the dynamics is slow and governed by the time scales set by thermal or quantum tunneling over barriers. For a fixed driving force above the depinning threshold, however, there are no barriers. To study avalanches, it is convenient to drive the system with an external spring at fixed but small velocity v [24]. Then, the effective driving force changes in time, and the spring provides a restoring force that keeps the system near the depinning transition. In the stationary state, the system

is temporarily pinned, then unpins and jumps to the next metastable state, and so on. In that situation, while thermal or quantum fluctuations may help trigger an avalanche (see, e.g., p. 319 in Refs. [4] or [44]), they should be less important during the avalanche process itself, which usually involves much faster time scales than that of barrier crossing. During the avalanche the system is rolling down the potential hill, with possible overshoots and oscillations due to inertia. Thus, a semiclassical equation of motion keeping only inertia and damping into account should be a reasonable starting point.

Given these motivations, in this paper we study the ABBM model in presence of inertia. We consider the motion of a particle representing the center-of-mass position of an interface that is driven by a spring at velocity $v > 0$ in a Brownian correlated random-force landscape. The feature which makes the ABBM model solvable is that the motion is always forward. In presence of inertia, this property is lost. The disorder thus generates nontrivial correlations in time when the particle visits the same positions several times. To make progress, we thus consider two variants of the model.

One variant is a model "on a tree," i.e., such that when the particle changes the direction of motion, it experiences a different Brownian disorder. Although it may seem artificial, it could in fact be of relevance for interfaces since different parts of an interface are exposed to different disorder potentials, and in presence of inertia the backward motion of the center-of-mass does not have to involve the same segments of the system as the forward one. The advantage of this model is that it can again be studied using a Fokker-Planck equation, which however does not appear to be exactly solvable. We determine the joint distribution of velocity $\dot{u}$ and acceleration a: (i) in perturbation theory at small and large mass, (ii) for large driving velocity v, and (iii) numerically. We then compare with a numerical solution of the original model, i.e., the ABBM model with inertia.

The second variant we call the $\sqrt{\dot{u}}$ model. It is the model for which the method developed in Ref. [24] naturally extends. The nonlinear instanton equation is now a differential equation of second order in the time variable. It is the saddle-point equation of the MSR action for the ABBM model with inertia under the assumption that the particle moves in the direction of the drive only. We are unable to solve it exactly for generic values of the mass. We solve it (i) in perturbation at small and large mass, and (ii) for a magic value of the mass where exact solutions exist, related to the Abel equation. It is also easy to solve numerically and from it we obtain, for that model, the Fourier-Laplace transform of the velocity distribution. Also, we calculate exactly the moments characterizing the distribution function $\overline{(a^k \dot{u}^n)}$ for arbitrary v and mass. The only unpleasant feature of this model is that due to backward motion, complex velocities appear. As long as they have a small probability, e.g., for large v or small mass, it gives the correct physics. In fact, by comparing with numerics, we find that this model provides quite interesting approximations to the ABBM model even for not so small values of mass and velocities.

Although the three models, namely, the original one, the tree model, and the $\sqrt{\dot{u}}$ model, do correspond to different ways to treat the negative velocities, it appears that they share the same *large-deviation function* at positive instantaneous velocity.

The latter describes the large-v limit (i.e., driving velocity) of the probability distribution of the (instantaneous) velocity and acceleration. Hence, we conjecture that we have obtained in this paper the exact large-deviation function for the ABBM model with inertia in the positive-velocity domain. This conjecture is explained and argued for in details, and supported by numerics. We find that the large-deviation function is determined by the nonlinear instanton equation and we obtain its analytical form (i) in perturbation for small m and for large m; (ii) for the magic value of the mass. In addition, we discuss for all three models the probability that the particle, starting with given acceleration and velocity, reaches zero velocity before or at time t. We refer to the latter as the exit probability.

Although our calculation is performed at zero temperature and $\hbar$, the distribution of velocities and accelerations in an avalanche is expected to be robust, and should survive at low temperatures, as well as in the presence of quantum fluctuations. More precisely, from the above discussion, it should be valid as long as avalanche durations remain small compared to barrier-crossing time scales, which is the regime studied in this paper. A more complete theory, however, yet to be worked out, would need to incorporate several additional effects: (i) the renormalization of disorder by fluctuations; (ii) in the under-damped limit the total avalanche duration may be notably increased as the system oscillates before settling into the next metastable state; (iii) the scale dependence of these effects. Although the present approach is only a first step, it is expected to capture some of the effects of inertia in classical and quantum avalanches. In particular, at the end of the paper we show how to incorporate some of the thermal and quantum effects in the moving system by studying the $\sqrt{\dot{u}}$ model in presence of an additional thermal or quantum noise.

The paper is organized as follows. First, in Sec. II, we rederive the distribution of velocities for the ABBM model and make the connection with the MSR formalism employed in Ref. [24]. Then we start analyzing inertial effects. In Sec. III, we introduce the ABBM model with inertia and analyze the results of a numerical simulation. Then, in Sec. IV, we consider a particle on "the tree." The model is introduced in Sec. IV A. In Sec. IV B, we solve the corresponding Fokker-Planck equation perturbatively in the inertia, and determine the corresponding probability distribution. The large-v limit is discussed in Sec. IV C. In Sec. IV D, we solve the Fokker-Planck equation perturbatively in $1/m$ and give a solution for the $\sqrt{\dot{u}}$ model in the same limit. In Sec. IV E, we solve the Fokker-Planck equation numerically, and finally compare analytical and numerical results in Sec. IV F. Then, in Sec. V A, we consider the $\sqrt{\dot{u}}$ model. We start with the definition and its basic properties in Sec. V B. Then, we connect the instanton and Fokker-Planck approaches in Sec. V C. In Sec. V D, we calculate exactly the moments characterizing the distribution function. We solve the instanton equation perturbatively in the mass and from that we find a perturbative expansion of the distribution function in Sec. V E, while in Sec. V G we solve it exactly for the "magic" value of the mass. In Sec. V F, we analyze in more detail one fixed value of the mass. In Sec. VI, we introduce and discuss the large-deviation function. Its perturbative expansion in small and large m is given in Secs. VI C and VI D, respectively, while in Sec. VI E we give

its exact result for the magic value of the mass. Supplementary material is relegated to Appendices A to I.

II. ABBM MODEL

Before we start considering inertial and dissipative effects together, we first review the ABBM model [17,18] that neglects inertia, rederive its velocity distribution, and recall the connection to the saddle-point (instanton equation) approach of Ref. [24–26].

We study an elastic interface at zero temperature, the center-of-mass position of which is given by the equation of motion

$$\eta \dot{u}(t) = F(u(t)) + \mu^2 [vt - u(t)], \qquad (1)$$

where $\dot{u} = du/dt$ and F is the disorder force. It is Gaussian distributed with correlations

$$\overline{[F(u) - F(u')]^2} = 2\sigma |u - u'|. \qquad (2)$$

In Eq. (1), η measures dissipation and v is the driving velocity. For the specific realization in magnetic samples, the interface describes a domain wall and the term $\sim \mu^2 u$ models the demagnetizing field generated by free magnetic charges on the boundary of the sample [4]. In general, this term is a restoring force and μ^2 the spring constant by which the particle (representing the center of mass) is driven.

For $v > 0$, the Middleton theorem [45] states that the particle always moves forward in the steady state (and for all $t > 0$ if its initial velocity at $t = 0$ is positive). The above equations can be solved via the Fokker-Planck equation

$$\frac{\partial P(\dot{u},t)}{\partial t} = -\frac{\partial}{\partial \dot{u}} j(\dot{u},t). \qquad (3)$$

Here, $j(\dot{u},t)$ is the probability current

$$j(\dot{u},t) = \left(\frac{\mu^2 v}{\eta} - \frac{\mu^2 \dot{u}}{\eta}\right) P(\dot{u},t) - \frac{\partial}{\partial \dot{u}}\left(\frac{\sigma \dot{u}}{\eta^2} P(\dot{u},t)\right). \qquad (4)$$

The first term is the contribution from the drift and the second one from the diffusion.

Before proceeding further, let us recall the main scales for the ABBM model, and introduce the appropriate dimensionless units to be used in this paper. Times will be measured in units of the relaxation time of the quadratic well

$$\tau_\mu = \frac{\eta}{\mu^2}. \qquad (5)$$

Displacements (i.e., the u direction) will be measured in units of

$$S_\mu = \sigma/\mu^4, \qquad (6)$$

where S_μ gives an estimate of the large-size cutoff for the distribution of avalanche sizes, as defined in Ref. [23]. Velocities will be thus measured in terms of a velocity scale set by the disorder

$$v_\mu = \frac{\sigma}{\eta\mu^2} = \frac{S_\mu}{\tau_\mu}. \qquad (7)$$

With these units of time and space, the ABBM model contains only one parameter, the driving velocity $v := v/v_\mu$ in dimensionless units. Below, we will mostly use these units, keeping the freedom to restore dimension-full units when needed.

Let us now discuss the steady state of the ABBM model. In that case, $\partial_t P = 0$ and $j(\dot{u}) = $ const. However, from the condition that the particle always moves forward follows that $j(\dot{u}) = 0$. Solving Eq. (4) with this constraint, one obtains (in dimensionless units)

$$P(\dot{u}) = \frac{e^{-\dot{u}} \dot{u}^{v-1}}{\Gamma(v)} \theta(\dot{u}). \tag{8}$$

It is important to note the dramatically different behavior of $\lim_{\dot{u} \to 0} P(\dot{u})$ for $v < 1$ and $v > 1$. In the former it is divergent, while in the latter it tends to zero. The value $v = 1$ separates the regime of intermittent motion, where the particle is most of the time at rest, from the regime where it moves continuously.

Now we briefly discuss an alternative way of solving the Fokker-Planck equation and make connection with the approach introduced in Ref. [24] based on the instanton equation, and further studied in Ref. [26]. After performing the Laplace transform, we find

$$-\frac{\partial \hat{P}}{\partial t} + \lambda \frac{\mu^2 v}{\eta} \hat{P}(\lambda) - \frac{\mu^2}{\eta} \lambda \partial_\lambda \hat{P} + \frac{\sigma}{\eta^2} \lambda^2 \partial_\lambda \hat{P} + \text{BT} = 0. \tag{9}$$

Here, $\hat{P}(\lambda) = \int_0^\infty P(\dot{u}) e^{\lambda \dot{u}} d\dot{u}$ and the boundary terms (BT) are

$$\text{BT} = -[j(\dot{u},t) e^{\lambda \dot{u}}]\big|_0^\infty - \frac{\sigma \lambda}{\eta^2} [\dot{u} P(\dot{u}) e^{\lambda \dot{u}}]\big|_0^\infty. \tag{10}$$

We ignore for the moment the boundary terms and look for a solution of the form

$$\hat{P}(\lambda,t) = e^{v Z(\lambda,t)} \tag{11}$$

with $Z(0,t) = 0$ since $\hat{P}(\lambda = 0,t) = 1$. After introducing dimensionless quantities $\lambda' = \lambda \sigma / \eta \mu^2$ and $Z' = Z \sigma / \eta \mu^2$ and omitting primes, we find [24]

$$\frac{\partial Z(\lambda,t)}{\partial t} + \frac{\partial Z(\lambda,t)}{\partial \lambda}(\lambda - \lambda^2) = \lambda. \tag{12}$$

This equation admits a time-independent solution $Z(\lambda,t) = Z(\lambda)$ with $Z(0) = 0$:

$$Z(\lambda) = -\ln(1 - \lambda). \tag{13}$$

Hence, we recover the result of Ref. [24] for the steady state. Doing the inverse-Laplace transform of $\hat{P}(\lambda) = (1 - \lambda)^{-v}$ we obtain Eq. (8). Now, we can check that the boundary terms indeed vanish for $\lambda < 1$, i.e., in the domain in which $Z(\lambda)$ is defined.

In addition, one can make the connection to the instanton equation as follows. Equation (12) can be solved by the method of characteristics: Define a function $\lambda(t)$ which obeys the differential equation

$$\frac{d\lambda(t)}{dt} = \lambda(t) - \lambda^2(t). \tag{14}$$

Further define $Z(t) := Z[\lambda(t),t]$. Then, the total derivative using (12) is

$$\frac{dZ(t)}{dt} = \lambda(t). \tag{15}$$

Equation (14) is nothing but the instanton equation of Ref. [24], with here $\lambda(t) = \tilde{u}(t)$ there. It admits the solution

$$\lambda(t) = \frac{\lambda}{\lambda + (1 - \lambda)e^{-t}} \tag{16}$$

with boundary condition $\lambda(-\infty) = 0$. In addition,

$$Z(t) = \int_{-\infty}^t \lambda(t') \, dt', \tag{17}$$

where we have defined $\lambda(0) = \lambda$. Hence, if we express $Z(\lambda) := Z(t = 0)$ as a function of $\lambda = \lambda(0)$ we obtain precisely (13). In Refs. [24,25], Eqs. (14) and (17) were obtained not as the Laplace transform of the Fokker-Planck equation, but by a completely different route using the Martin-Siggia-Rose (MSR) dynamical action. This will be explained in more details below in the case where inertial terms are allowed.

Equation (12) is solved for any initial condition $Z(\lambda, t = 0) = Z_0(\lambda)$ as [25]

$$Z(\lambda,t) = -\ln(1 - \lambda + \lambda e^{-t}) + Z_0\left(\frac{\lambda}{\lambda + (1 - \lambda)e^t}\right). \tag{18}$$

Hence,

$$\hat{P}(\lambda,t) = (1 - \lambda + \lambda e^{-t})^{-v} \hat{P}_0\left(\frac{\lambda}{\lambda + (1 - \lambda)e^t}\right). \tag{19}$$

Using $\overline{u^n(t)} = \partial_\lambda^n \hat{P}(\lambda,t)|_{\lambda=0}$, we obtain the decay to the steady state after a change in the driving velocity $v = v_0 + \theta(t)(v - v_0)$:

$$\overline{\dot{u}(t)} = v(1 - e^{-t}) + e^{-t}\overline{\dot{u}(0)}, \tag{20}$$
$$\overline{\dot{u}(t)^2}^c = v(1 - e^{-t})^2 + 2\overline{\dot{u}(0)}e^{-t}(1 - e^{-t}) + e^{-2t}\overline{\dot{u}(0)^2}^c,$$

where the symbol c denotes connected correlation functions. This is in agreement with the results of Ref. [26], where it was obtained within the MSR approach. Note that for any $t > 0$, Eq. (19) behaves as $\hat{P}(\lambda,t) \sim A(t)(-\lambda)^v$ with $A(t) = (1 - e^{-t})^{-v} \hat{P}_0(-\frac{1}{e^t - 1})$, hence $P(\dot{u},t) \sim A(t)\dot{u}^{v-1}/\Gamma(v)$ and the current at the origin vanishes, which justifies ignoring the boundary terms above.[1]

III. ABBM MODEL WITH INERTIA

A. Definition of the model

In this section, we consider the generalization of the ABBM model to include the effect of inertia. The equations of motion in the laboratory frame are

$$\frac{d\dot{u}(t)}{dt} = a(t), \tag{21}$$

$$m\frac{da(t)}{dt} = \mu^2[v - \dot{u}(t)] - \eta a(t) + \partial_t F(u(t)), \tag{22}$$

where $F(u)$ is a function of u, and as for the ABBM model (2),

$$\overline{[F(u) - F(u')]^2} = 2\sigma|u - u'|. \tag{23}$$

In the limit $m \to 0$, the model simplifies to the ABBM model considered in the previous section.

---

[1]The next order at small u should be examined with the same conclusion.

For later use we note that *if* $u(t)$ is monotonously increasing, then the correlator of the random force $\partial_t F(u(t))$ in Eq. (22) is

$$\overline{\partial_t F(u(t))\partial_{t'} F(u(t'))} = 2\sigma \dot{u}(t)\delta(t-t')$$
$$= 2\sigma |\dot{u}(t)|\delta(t-t'). \qquad (24)$$

Note that *if* $\dot{u}(t) \geqslant 0$, both versions with and without the absolute value are equivalent. Under this assumption, an alternative way to model (23) is to replace

$$\partial_t F(u(t)) \rightarrow \sqrt{\dot{u}(t)}\,\xi(t)$$
$$= \sqrt{|\dot{u}(t)|}\,\xi(t) \qquad (25)$$

with

$$\langle \xi(t)\xi(t')\rangle = 2\sigma\delta(t-t'). \qquad (26)$$

We will get back to these formulations shortly. First, let us discuss the units. Keeping the same units for time and velocity (and space) as given by Eqs. (5) and (7), *the inertial model depends on two dimensionless parameters*, the driving velocity $v := v/v_\mu$ as before, and the dimensionless mass

$$m := \frac{m\mu^2}{\eta^2} = \frac{\tau_m}{\tau_\mu} = \frac{\tau_0^2}{\tau_\mu^2}. \qquad (27)$$

Indeed, two new time scales can be defined:

$$\tau_m = m/\eta, \quad \tau_0 = \sqrt{\tau_m\tau_\mu} = \sqrt{m}/\mu, \qquad (28)$$

where τ_m is the damping time beyond which damping overcomes inertia and τ_0 is the characteristic oscillation time of the harmonic oscillator in the absence of damping. These time scales are not independent, so there is really only one new time scale. The units of acceleration are $S_\mu/\tau_\mu^2 = \sigma/\eta^2$.

Below we study the model as a function of these two parameters m and v. Note that there are various limits of interest. We will in particular study the limit of small and large m, as well as the limit of large v. The large-m limit can be rephrased as the limit where disorder σ and damping η are both small. Note that the weak-disorder limit is more general since it is such that only σ is small.

Note a remarkable property of the ABBM model without inertia: while the space unit (6) depends on disorder, the characteristic relaxation time (5) remains *independent of the disorder*. Although at small v there is a broad distribution of time scales, the characteristic time remains τ_μ. In the language of renormalization group it means that the friction η is not corrected by disorder [24,26]: it is a consequence of the Brownian force landscape which can be proved using the Middleton theorem. In presence of inertia, the oscillation and damping time scales τ_0 and τ_m given in Eq. (28) are the bare ones (i.e., in the absence of disorder) and it remains to be understood whether characteristic oscillation and damping times are affected by disorder.

B. Phenomenology of the inertia model

The model defined by Eqs. (21)–(23) is difficult to analyze analytically since the particle may change its direction of motion. Let us therefore start with a numerical simulation and some qualitative considerations. We first describe how the typical trajectories change as m is increased, and then we show

some numerical results for the distribution of instantaneous velocities.

1. Qualitative features of trajectories

Let us start with a numerical simulation of Eqs. (21)–(23). We show in Fig. 1 some examples of typical trajectories $u(t)$, for different values of the mass and the driving velocity in the same realization of disorder, such that we can see how the trajectories are correlated with the disorder. In the first set we choose a small driving velocity $v = 0.01$ and in the second a larger one $v = 0.1$, so we can see the evolution from the avalanche regime (at small v) to the faster driven regime (at larger v).

For small v, we see that upon increasing the mass (up to moderate values) (i) time windows where the particle is pinned in a metastable state at position u_i (at zero or almost zero velocity) still exist but are shorter since the particle oscillates before coming to rest.[2] (ii) Hence, avalanches (from one metastable state to another one) can still be defined. (iii) Due to inertia, the avalanche starts more slowly, however, the particle overshoots and may not settle in the next metastable state (as for $m = 0$) but in one further away. These metastable states u_i are a subset of the metastable states for $m = 0$. As the mass increases, more and more of the metastable states at $m = 0$ get eliminated. Thus, as the mass increases, the smaller $m = 0$ avalanches (i.e., with smaller barriers to the next metastable state) are "eaten up" or merge. The larger $m = 0$ avalanches, with larger barriers, remain, although the dynamics is quite different. One notes that the frequency of oscillation increases as the particle settles to the new metastable state under the action of damping.

For larger v, as m increases the avalanche structure disappears and one enters into a regime better described by oscillations in the comoving frame (see Fig). 1. However, there remains some correlation with the $m = 0$ avalanche structure, the larger $m = 0$ avalanches seem to induce the largest oscillations (Fig. 1).

While for small mass the motion remains under-damped and the time scale remains $O(\tau_\mu)$, in the larger-mass regime $\tau_m \gg \tau_\mu$ ($m \gg 1$ in dimensionless units) the motion occurs on larger time scales. Let us describe qualitatively the avalanches in that regime. For that it is useful to rewrite the equation of motion as

$$\frac{d}{dt}E = \mu^2 v t\dot{u} - \eta\dot{u}^2, \qquad (29)$$

$$E = \frac{1}{2}m\dot{u}^2 + V(u) + \frac{\mu^2}{2}u^2, \qquad (30)$$

where $F(u) = -V'(u)$ and the disorder-potential fluctuations typically grow as $V(u) - V(0) \approx \sqrt{\sigma}u^{3/2}$. Balancing disorder with the quadratic well gives the avalanche cutoff size $u \sim S_\mu$. Hence, for $u \ll S_\mu$ the disorder term dominates. Consider an avalanche starting at $t = 0$. For small v and η, as the previous metastable state $u(t=0) = u_i$ becomes unstable, the particle will first oscillate with amplitude Δu between u_i and the smallest root of $V(u) - V(u_i) + \frac{\mu^2}{2}(u^2 - u_i^2)$, and the total

---

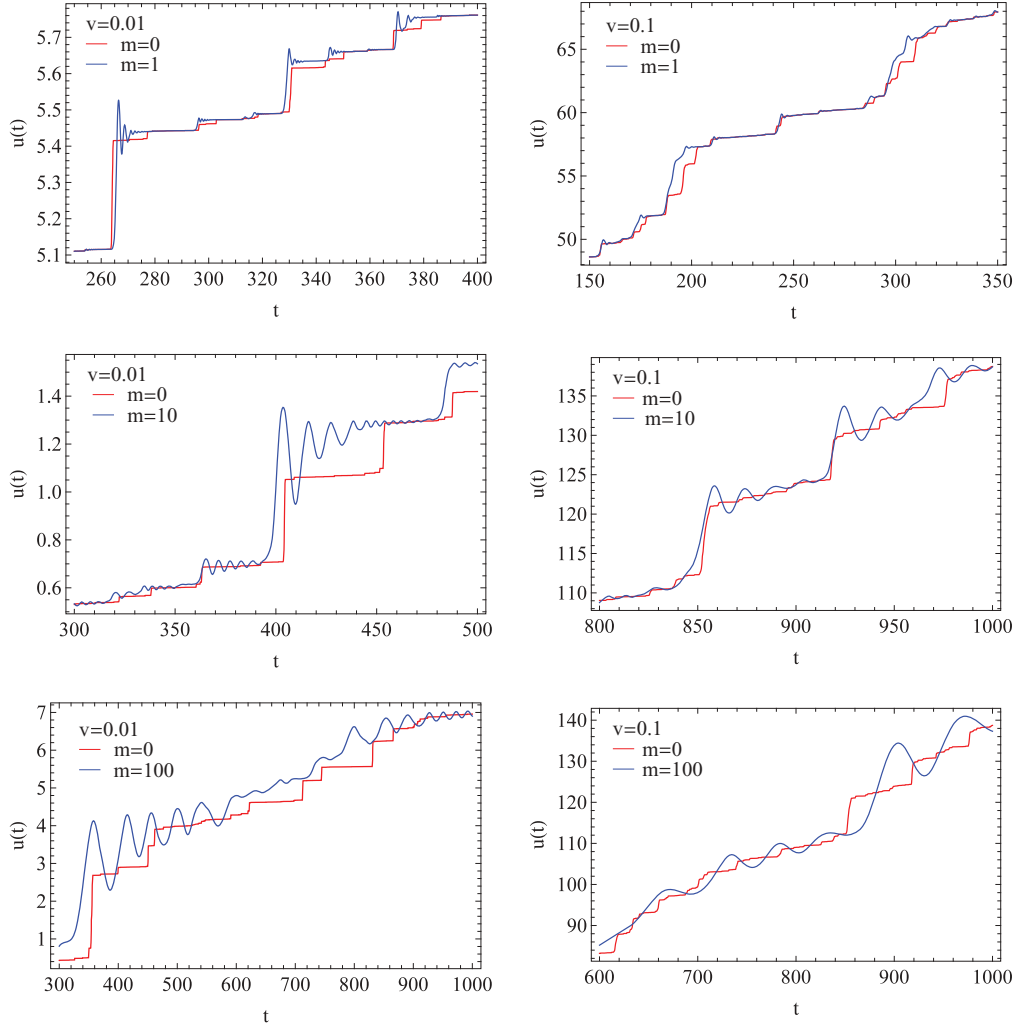[2]In the limit $v = 0^+$, metastable states can still be defined.

FIG. 1. (Color online) Each figure shows two trajectories in the same disorder realization and for the same driving velocity, but different values of the mass, as denoted.

energy E can be considered constant during a period.[3] There is clearly a distribution of amplitude Δu from the disorder, but we can estimate the typical oscillation time τ_{osc} as a function of the amplitude Δu as

$$\tau_{\text{osc}} \sim m^{1/2} (\Delta u)^{1/4} / \sigma^{1/4} \tag{31}$$

by balancing the kinetic energy with the disorder. The quadratic well controls the scale of the largest amplitudes $\Delta u \sim S_\mu$, which correspond to a time scale τ_0. The total energy E will decay on much larger time scale $\tau_m \gg \tau_0$, and the particle will settle in one of the available metastable states within the range of the first oscillation. From the above estimate (31) one sees that the frequency of oscillation will indeed increase as Δu decreases to zero. This picture requires that the quadratic well has moved by less than S_μ during the avalanche time, hence $v < v_m := S_\mu / \tau_m$ (in

dimensionless units this is $v < 1/m$). If $v > v_m$, the particle has no time to converge to a metastable state and the definition of an avalanche becomes less clear. In the regime $v_m < v < v_0 = S_\mu / \tau_0$, the motion still remains quite correlated to the disorder and plateaus would still be visible by averaging over oscillations. Finally, for $v > v_0$ (in dimensionless units this is $v > 1/\sqrt{m}$), multiple oscillations are not visible and the trajectory becomes smoother.

Note that $V(u)$ is a random acceleration process since $V''(u)$ is a white noise. Hence, in the large inertial mass limit, Δu can be seen as the first return to the origin of a random acceleration process. This leads to $P(\Delta u) \sim \Delta u^{-5/4}$ for small $\Delta u \ll S_\mu$, the distribution being cut off around S_μ. Similar arguments, although for a slightly different model, were made in Refs. [28, 46] using earlier results [47,48].

It is also interesting to note that in any time window $[t_i, t_f]$ where $\dot{u}(t) > 0$, one can parametrize trajectories as a function of the position $u(t) = \int_{t_i}^{t} dt' \dot{u}(t')$ and rewrite either model as a stochastic equation for $\dot{u}(u)$ as

$$\frac{d^2}{du^2} \left(\frac{1}{2} m \dot{u}^2 \right) + \frac{d}{du} (\eta \dot{u}) = \mu^2 \left(\frac{v}{\dot{u}} - 1 \right) + F'(u). \tag{32}$$

---

[3]In the limit $\eta, v = 0^+$, one can define the quasistatic motion of the edges of the oscillation interval $[u_{\min}(t), u_{\max}(t)]$. It should also proceed by jumps.
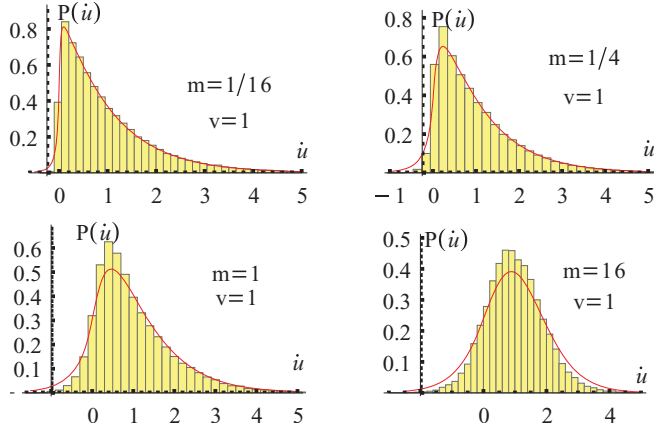
FIG. 2. (Color online) Probability density distribution of the instantaneous velocity $\dot{u}$ for the ABBM model with inertia in the form of a histogram for $v = 1$ and different masses. The red full line denotes the probability density obtained in Sec. IV E for the tree model. Note that the vertical axis is shifted from $\dot{u} = 0$ to the left.

In the limit of $m \to 0$ one recovers the standard ABBM stochastic equation [17,18] and $\dot{u}(u)$ can be mapped to the radial coordinate of a Brownian motion in dimension $d = 1 + v/v_\mu$ (see, e.g., Sec. VI B in Ref. [49]) leading to the distribution of avalanche sizes $P(S) \sim S^{-\tau}$ with $\tau = \frac{3}{2} - \frac{v}{2v_\mu}$ for $v < v_\mu$, for avalanches much smaller than the cutoff $S \ll S_\mu$ for which the quadratic well does not play a role. In presence of inertia, the above equation can be used between two zeros of the velocity, and for small η, μ leads again to an exit time for the random acceleration problem. Some considerations about exit times are given in Appendix H.

2. Velocity distributions

Consider on Fig. 2 the histograms of the distribution of the instantaneous velocity $\dot{u}$. We see that for driving velocity $v = 1$, by increasing the mass m from 1/16 to 16, the distribution becomes more and more symmetric, and peaked around $v = 1$. The same happens for larger driving velocities $v = 5/2$ (see Fig. 3). Note that all histograms have a nonvanishing tail for
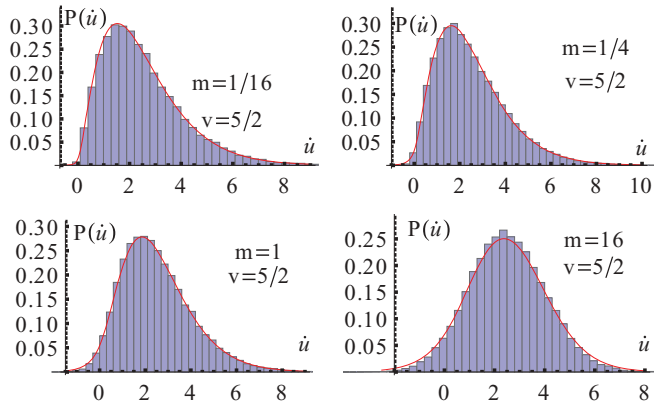

FIG. 3. (Color online) Histogram of the probability density distribution for the ABBM model with inertia for $v = 5/2$ and different masses. The red full line denotes the probability density obtained in Sec. IV E for the tree model. Note that the vertical axis is shifted from $\dot{u} = 0$ to the left.

negative $\dot{u}$, but that this tail gets smaller when decreasing the mass. (Attention: the axis on the figures is shifted from $\dot{u} = 0$ to the left.) By comparing Figs. 2 and 3, we see that when increasing the driving velocity v for a fixed mass, the probability for negative velocities decreases. This is clearly seen on the plots of Fig. 18 for mass $m = 1/4$, and $v = 1/10$, 1/2, and 5. The red lines (solid on Figs. 2 and 3, and dashed on Fig. 18) represent different approximations to be discussed later.

This negative tail renders the analytical analysis difficult, not per se due to the negative velocities, but since the particle moves backward through the same disorder, thus the disorder it sees becomes *correlated in time*, and the system has *memory*. Since we possess currently no powerful tool to tackle this situation, we will treat two different *local, memory-free* variants as explained in the Introduction: (i) the particle on the tree model that can be formulated by using for the random-force correlator the second line of Eqs. (24) or (25); and (ii) the $\sqrt{u}$ model given by the first line of Eqs. (24) or (25).

There is a strong motivation to consider these two variants. Let us look at Figs. 2 and 3. The red full lines represent the numerical solution for a particle on the tree. We see that when increasing v or decreasing m, the "particle on the tree" becomes a good *approximation* of the ABBM model with inertia. The same holds (not shown here) for the $\sqrt{u}$ model. The physical reason is simple: At higher and higher driving velocities or smaller and smaller mass, the particle will less and less often move backward, thus these events will lose their importance for $P(\dot{u})$.

We will indeed prove a much stronger statement. Consider the large-deviation function, defined (supposing the limit exists) by

$$F(x) := -\lim_{v \to \infty} \frac{\ln[P(xv)]}{v}. \tag{33}$$

We will show that $F(x)$ indeed exists for all three models, and that for $x > 0$ all three large-deviation functions coincide. We expect, but can not prove, that for $x < 0$ these functions will differ.

In Sec. IV, we start with the particle on the tree, which may be expected to be the most physical one. We then continue with the $\sqrt{u}$ model in Sec. V A, for which we have the most analytical results.

IV. TREE MODEL

A. Definition of the model

In this section we examine the motion of a particle, with finite mass m, in a Brownian correlated disorder force. Since the Middleton theorem does not hold, we assume that when the particle changes direction, it experiences a different disorder potential, uncorrelated with that experienced previously. The model describes the motion on a tree with constraint that the particle always chooses a different branch when changing its direction of motion. On each branch, the disorder satisfies Eq. (2). As mentioned in the Introduction, the model may be relevant to describe systems which do not visit the same microscopic configuration twice, while the center of mass is oscillating back and forth, i.e., systems with large deviations

from the Middleton theorem. Note that the tree is not defined from the start, but is generated dynamically, thus there is one tree associated to each trajectory or history. This may, however, be captured by the limit of a fixed tree with high branching rate.

The equation of motion in the laboratory frame is

$$\frac{d\dot{u}}{dt} = a, \tag{34}$$

$$m\frac{da}{dt} = \mu^2\left[v - \dot{u}(t)\right] - \eta a + \partial_t F_t[u], \tag{35}$$

where F is a functional of $u(t)$. Then, the effective disorder correlator becomes

$$\partial_t \partial_{t'} \overline{(F_t[u] - F_{t'}[u])^2} = -4\sigma|\dot{u}(t)|\delta(t - t'), \tag{36}$$

$$\overline{\partial_t F_t[u] \partial_{t'} F_{t'}[u]} = 2\sigma|\dot{u}(t)|\delta(t - t'). \tag{37}$$

In the limit of $m \to 0$, the model simplifies to the ABBM model considered in the previous section. Note that this tree model has the peculiarity that the system reaches a stationary state without being pinned, even in the *absence* of driving. The reason is that every time it changes the direction, the disorder is renewed. Only if the system starts at $a = \dot{u} = 0$ or arrives there "by accident," it remains there forever.

Now the probability distribution depends on two variables: velocity $\dot{u}$ and acceleration a. The corresponding Fokker-Planck equation is a parabolic differential equation and has the form

$$\frac{\partial P(\dot{u},a,t)}{\partial t} = -a\frac{\partial P}{\partial \dot{u}} + \frac{\partial^2}{\partial a^2}\left(\frac{\sigma|\dot{u}|P(\dot{u},a,t)}{m^2}\right)$$
$$-\frac{\partial}{\partial a}\left\{\left(-\frac{\mu^2}{m}\dot{u} - \frac{\eta}{m}a + \frac{\mu^2}{m}v\right)P(\dot{u},a,t)\right\}. \tag{38}$$

In the following two sections, we analyze this equation both analytically and numerically. There are several limits which can be studied analytically, namely, small or large m at fixed v, and large v at fixed m.

B. Perturbation expansion in small m

Equation (38) is complicated and an exact analytic solution is not known. There are many systems [4] where the mass term is small and could be treated as perturbation with respect to the other terms. Therefore, we start with perturbation theory in m, i.e., $m\mu^2/\eta^2 \ll 1$ in dimension-full units.

In dimensionless units, the Fokker-Planck equation simplifies, and effectively depends only on the two parameters, m and v:

$$\frac{\partial P(\dot{u},a,t)}{\partial t} = -a\frac{\partial P}{\partial \dot{u}} + \frac{\partial^2}{\partial a^2}\left(\frac{|\dot{u}|P(\dot{u},a,t)}{m^2}\right)$$
$$-\frac{\partial}{\partial a}\left\{\left(-\frac{\dot{u}(t)}{m} - \frac{a}{m} + \frac{v}{m}\right)P(\dot{u},a,t)\right\}. \tag{39}$$

We are interested in the stationary situation $\partial_t P(\dot{u},a,t) = 0$.

In the limit $m \to 0^+$, the acceleration is divergent since in the ABBM model the disorder generates a white noise with no small-scale cutoff (see Sec. IV C). Analyzing the structure of the Fourier-transformed Fokker-Planck equation

and the moments that follow from it (similarly to Sec. V D), we conclude that one has to introduce a reduced acceleration $\tilde{a} = \sqrt{m}a$ in order to be able to organize the perturbation theory in m. Then, in the region $|\tilde{a}| \gtrsim \sqrt{m}$ and $\dot{u} \gtrsim m > 0$ (we will refer to it as the region 1) we find

$$P^{(1)}(\dot{u},a) = \sqrt{m}e^{-\frac{\tilde{a}^2}{2\dot{u}}-\dot{u}}\sum_{n=0}^{\infty}\frac{F_n(\tilde{a},\dot{u})}{\Gamma(v)\sqrt{2\pi}}\dot{u}^{v-\frac{3+4n}{2}}m^{n/2}. \tag{40}$$

The index (1) denotes that the expression is valid in region 1. Here, F_n satisfies the recursion for $n \geqslant 0$ (and $F_{-1} = 0$):

$$\tilde{a}\partial_{\tilde{a}}F_n - \dot{u}\partial_{\tilde{a}}^2 F_n + \dot{u}^2(v - \dot{u})\partial_{\tilde{a}}F_{n-1} + \tilde{a}\dot{u}^2\partial_{\dot{u}}F_{n-1}$$
$$+ \frac{1}{2}[\tilde{a}^3 - (4n-1)\tilde{a}\dot{u}]F_{n-1} = 0. \tag{41}$$

We start solving Eq. (41) from the smallest $n = 0$. Then, using the solution for F_0, we solve the next equation for $n = 1$ and find F_1. The procedure develops further in the same way. However, if we want to determine F_i, we have to solve all the differential equations (41) with $n \leqslant i + 2$. The reason is that we are interested in a distribution that has all finite moments $\overline{a^k\dot{u}^j}$, and therefore decays faster than algebraically for large $\dot{u}$ and a. This condition has to be satisfied for any mass, hence for any order in the expansion. Taking this into account when analyzing the solution in $(i + 2)$nd order allows us to discard some solutions to the equation appearing in the ith order, i.e., in F_i. The details of the calculation and some intermediate results are given in Appendix A.

For brevity we state here only the first three terms (the further terms are lengthy, and given in Appendix A):

$$F_0 = 1, \tag{42}$$

$$F_1 = \frac{1}{2}\left(\tilde{a}\dot{u} - \frac{\tilde{a}^3}{3}\right) + c_3\dot{u}^2, \tag{43}$$

$$F_2 = \frac{\tilde{a}^6}{72} - \frac{5\tilde{a}^4\dot{u}}{48} - \frac{1}{6}\tilde{a}^3 c_3\dot{u}^2 - \frac{1}{4}\tilde{a}^2\dot{u}^2(\dot{u} - v) + \frac{1}{2}\tilde{a}c_3\dot{u}^3$$
$$+ c_5\dot{u}^4 - \frac{1}{48}\dot{u}^3[24\dot{u}^2 - 48\dot{u}v\ln(\dot{u}) - 24v^2 + 36v - 5]. \tag{44}$$

There still remain undetermined constants c_3 and c_5. They have to be fixed such that $\int da\, d\dot{u}\, P(\dot{u},a) = 1$ for *all* m. This task can not be done now since region 2 may also contribute. It is further complicated by the fact that also negative velocities may contribute, and our expansion does not give a result for those. We discuss this issue in the next section [see Eqs. (91) and (92)] when comparing the analytical results with the numerical solution of Eq. (38).

Integrating out velocities from $P^{(1)}(\dot{u},a)$, one obtains the conditional probability distribution of acceleration when $\dot{u} > m$. Leading two contributions in the region 1 are

$$P^{(1)}(a)da = d\tilde{a}\left[\frac{2^{\frac{3}{4}-\frac{v}{2}}}{\sqrt{\pi}\Gamma(v)}|\tilde{a}|^{v-\frac{1}{2}}K_{\frac{1}{2}-v}(\sqrt{2}|\tilde{a}|)\right.$$
$$+ \sqrt{m}\frac{2^{-\frac{1}{4}-\frac{v}{2}}}{3\sqrt{\pi}\Gamma(v)}|\tilde{a}|^{v-\frac{3}{2}}$$
$$\times[3\sqrt{2}[\tilde{a} + c_3(2v-3)]K_{\frac{3}{2}-v}(\sqrt{2}|\tilde{a}|)$$
$$\left. - 2|\tilde{a}|(\tilde{a} - 3c_3)K_{\frac{5}{2}-v}(\sqrt{2}|\tilde{a}|)]\right]. \tag{45}$$

Here $K_n(z)$ is the modified Bessel function of the second kind. Similarly, by integrating out a from $P^{(1)}(\dot{u},a)$ we obtain the conditional probability distribution of velocities in region 1, for $|\tilde{a}| > \sqrt{m}$, of which we state the first terms (higher-order terms are discussed in Appendix A):

$$P^{(1)}(\dot{u}) = \frac{e^{-\dot{u}} \dot{u}^{v-1}}{\Gamma(v)} + \frac{c_3 \sqrt{m} e^{-\dot{u}} \dot{u}^{v-1}}{\Gamma(v)} + \frac{m e^{-\dot{u}} \dot{u}^{v-2}}{4\Gamma(v)}$$
$$\times [(4c_5 - 1)\dot{u} - 2\dot{u}^2 + 4\dot{u}v\ln(\dot{u}) + 2(v-1)v]. \tag{46}$$

In the limit of $m \to 0$ only the first term survives and we recover the result given by Eq. (8). A note of caution concerning the distributions (45) and (46) is in order: They have been obtained by integrating the joint distribution (40) over all values of a, and over positive $\dot{u}$, while (40) is valid in a more restricted range. These distributions may acquire some correction from other regions, which should be small (and maybe even subdominant to the correction given above, but we can not prove it). In any case, it can not affect the leading-order result, i.e., the first line in Eq. (45), which is the (normalized) distribution of (reduced) acceleration $\tilde{a}$ in the presence of a small inertia, and which is a novel exact result.

Next, we discuss region 2, defined as $|\tilde{a}| \lesssim \sqrt{m}$ and $0 < \dot{u} \lesssim m$. If one naively assumes that the results obtained in region 1 are valid in region 2, one finds nonintegrable divergences in P for small velocities $\dot{u}$. In order to organize the perturbation theory in region 2, we have to introduce $\tilde{\tilde{u}} = \dot{u}/m$ and use $a = \tilde{a}/\sqrt{m}$. Then,

$$P^{(2)}(\dot{u},a) = f(m,v) \sum_{n=0}^{\infty} \tilde{\tilde{P}}_n^{(2)}(a,\tilde{\tilde{u}}) m^n, \tag{47}$$

where f is an undetermined function. Plugging this equation into the Fokker-Planck Eq. (39), we obtain the equations that determine $\tilde{\tilde{P}}_n^{(2)}$.[4] Unfortunately, these equations are as difficult to solve as the full Fokker-Planck equation, and we did not succeed in solving them analytically. However, in Appendix B we demonstrate that Eq. (47) has the correct form and that the perturbation theory is properly organized. We show that $P^{(2)}(\dot{u},a)$ matches at the boundary between regions 1 and 2 the distribution function found in region 1.

C. Large driving velocity $v \gg v_\mu$

A naive argument is that in that limit the noise $\sqrt{|\dot{u}|}\xi(t)$ can be replaced by $\sqrt{v}\xi(t)$, hence becomes Gaussian. One can then directly solve the Langevin equation (in dimensionless units) in frequency space,

$$\dot{u}_\omega = \frac{\sqrt{v}\xi_\omega + 2\pi v\delta(\omega)}{-m\omega^2 + 1 + i\omega}. \tag{48}$$

This leads to a Gaussian distribution for $\dot{u}$ and $\tilde{a}$ with equal-time correlations in the steady state:

$$\overline{[\dot{u}(t) - v]^2} = \int_\omega \frac{2v}{(1 - m\omega^2)^2 + \omega^2} = v, \tag{49}$$

$$\overline{\tilde{a}(t)^2} = -\int_\omega \frac{2vm\omega^2}{(1 - m\omega^2)^2 + \omega^2} = v, \tag{50}$$

with $\overline{\dot{u}(t)\tilde{a}(t)} = 0$ and $\int_\omega = \int \frac{d\omega}{2\pi}$. We used $\overline{\xi_\omega} = 0$. Thus, we find

$$P_{v \gg 1}(\tilde{a},\dot{u}) \approx \frac{1}{2\pi v} \exp\left(-\frac{1}{2v}[\tilde{a}^2 + (\dot{u} - v)^2]\right). \tag{51}$$

Note that since the dynamics being the same for positive $\dot{u}$ this large v result should hold for all three models.

Integrating over the acceleration, this can be identified with a Boltzmann distribution

$$P_{v \gg 1}(\dot{u}) \sim \sqrt{\frac{m}{2\pi T_{\text{eff}}}} e^{-\frac{m(\dot{u}-v)^2}{2T_{\text{eff}}}} \tag{52}$$

in the moving frame for the Hamiltonian of a free particle of mass m. The effective temperature (in dimension-full units) is

$$T_{\text{eff}} = m v_\mu v = m v \frac{\sigma}{\eta \mu^2}. \tag{53}$$

Hence, at large driving velocity, the disorder, the quadratic well, and the damping act together in the moving frame as a thermal noise.[5]

From the above result we could guess that the probability of a negative velocity decays as $e^{-v/(2v_\mu)}$ at large v. We will see below that this is not quite accurate. Indeed, we will go beyond the above argument and show that there is a large-deviation function which describes the deviations from the Gaussian at large driving velocity. These deviations appear in the far tails at $|\dot{u} - v| \sim v$ (see Sec. VI D).

D. Large mass $m \gg 1$

At large mass, the oscillation time $\tau_0 = \sqrt{m}/\mu$ increases but becomes much smaller than the damping time $\tau_m = m/\eta$ (necessary for damping to overcome inertia). Hence, the system is in the under-damped limit and the particle oscillates many times before it comes to rest. It can be seen by rewriting the Langevin equation in dimensionless units:

$$\frac{d\dot{u}}{dt'} = \tilde{a}, \tag{54}$$

$$\frac{d\tilde{a}}{dt'} = -\dot{u} + v + \frac{\sqrt{|\dot{u}|}}{m^{1/4}}\xi(t') - \frac{\tilde{a}}{\sqrt{m}}, \tag{55}$$

where we have used the reduced acceleration and defined the reduced time as $t = \sqrt{m}t'$ in units of the oscillation time. At large m, we see that to leading order we have a Hamiltonian system with $p = \tilde{a}$ and $q = \dot{u} - v$ and $H(p,q) = \frac{1}{2}(p^2 + q^2)$, i.e., a harmonic oscillator, weakly perturbed by (i) a noise and (ii) the damping. Although these terms are small, they will select the steady state as we show now.

---

[4]The function f does not enter them since the Fokker-Planck equation is linear equation in P.

[5]Although this could be interpreted by saying that the effect disorder in the moving frame is the same as an equilibrium white noise of variance $2\eta T_{\text{eff}}$ for a particle in a quadratic well with damping η (i.e., satisfying usual fluctuation-dissipation relations), this would lead to an incorrect value for the noise, hence it is is not a valid interpretation. There is an underlying Hamiltonian system, but it is nonstandard and involves the acceleration (see Sec. VI D). This is because the starting equation of motion can only be written in a Langevin form in terms of velocity.

For large m, the Fokker-Planck equation has a well-defined limit if one scales the probability as

$$P(\dot{u},a,t) = \sqrt{m}\,\tilde{P}(\dot{u},\tilde{a} = a\sqrt{m}, t' = t/\sqrt{m}). \quad (56)$$

The scaling function $\tilde{P}$ satisfies

$$\partial_{t'}\tilde{P} = [(\dot{u}-v)\partial_{\tilde{a}} - a\partial_{\dot{u}}]\tilde{P} + \frac{1}{m^{1/2}}\big[1 + \tilde{a}\partial_{\tilde{a}} + D(\dot{u})\partial_{\tilde{a}}^2\big]\tilde{P}, \quad (57)$$

where we have allowed for a general noise function $D(\dot{u})$. It is equal to $D(\dot{u}) = |\dot{u}|$ for the tree model that we study now, and $D(\dot{u}) = \dot{u}$ for the $\sqrt{\dot{u}}$ model studied below.

This equation is well suited to analyze the time regime $t \sim \tau_0$, i.e., $t' = O(1)$, when the system oscillates. However, at even larger times it will be damped and will reach a steady state. For the latter, we are interested in the limit

$$\lim_{m\to\infty}\lim_{t'\to\infty}\tilde{P}(\dot{u},\tilde{a},t'). \quad (58)$$

We start by searching for the steady state as a time-independent solution in the form

$$\tilde{P}(r,\theta) = \sum_{n=0}^{\infty} m^{-n/2} P_n(r,\theta). \quad (59)$$

It is convenient to use the action-angle variables of the harmonic oscillator,

$$\dot{u} = v + r\sin\theta, \quad (60)$$

$$\tilde{a} = r\cos\theta. \quad (61)$$

In these variables, the Fokker-Planck equation becomes

$$\partial_\theta \tilde{P} = \frac{1}{\sqrt{m}}[1 + r\cos\theta\, O + D(v + r\sin\theta)O^2]\tilde{P}, \quad (62)$$

$$O := \cos\theta\,\partial_r - \frac{\sin\theta}{r}\partial_\theta. \quad (63)$$

This yields the recursion

$$\partial_\theta P_0 = 0,$$
$$\partial_\theta P_{n+1} = [1 + r\cos(\theta)\,O + D(v + r\sin\theta)O^2]P_n, \; n \geqslant 0. \quad (64)$$

Note that the operators O and $D(v + r\sin\theta)$ commute. To leading order the general solution is

$$P_0(r,\theta) = P_0(r), \quad (65)$$

where P_0 is to be normalized as

$$\int_0^\infty 2\pi r\, P_0(r)\,dr = 1. \quad (66)$$

The higher-order terms satisfy

$$\int_0^\infty r\,dr \int_0^{2\pi} d\theta\, P_n(r,\theta) = 0, \quad n \geqslant 1. \quad (67)$$

The function P_0 is selected by the next order equation, as we now discuss:

$$\partial_\theta P_1(r,\theta,t) = \phi(r,\theta) \quad (68)$$

with

$$\phi(r,\theta) = P_0(r) + a(r,\theta)P_0'(r) + b(r,\theta)P_0''(r),$$
$$a(r,\theta) = r\cos^2(\theta) + \frac{1}{r}D(v + r\sin\theta)\sin^2(\theta), \quad (69)$$
$$b(r,\theta) = \cos^2(\theta)D(v + r\sin\theta).$$

The general solution of Eq. (68) is

$$P_1(r,\theta) = \int_0^\theta d\theta'\,\phi(r,\theta') + P_1(r,0). \quad (70)$$

Now, we observe that one can integrate (68), $\int_0^{2\pi} d\theta$, and obtain a condition which must be satisfied, in order for P_1 to be meaningful, i.e., a single-valued function in $e^{i\theta}$:

$$P_1(r,2\pi) - P_1(r,0) = 0 = \int_0^{2\pi} d\theta\,\phi(r,\theta). \quad (71)$$

This leads to a condition which determines the steady state $P_0(r)$ to leading order as

$$P_0(r) + a(r)P_0'(r) + b(r)P_0''(r) = 0. \quad (72)$$

We have defined

$$a(r) = \frac{r}{2} + \frac{1}{r}\int_0^{2\pi}\frac{d\theta}{2\pi}D(v + r\sin\theta)\sin^2(\theta), \quad (73)$$

$$b(r) = \int_0^{2\pi}\frac{d\theta}{2\pi}D(v + r\sin\theta)\cos^2(\theta). \quad (74)$$

The first-order correction reads as

$$P_1(r,\theta) = \int_0^\theta d\theta'\,[a(r,\theta') - a(r)]P_0'(r)$$
$$+ \int_0^\theta d\theta'\,[b(r,\theta') - b(r)]P_0''(r) + P_1(r,0), \quad (75)$$

where $P_1(r,0)$ is determined from the next-order equation using again that P_2 should be single valued and the normalization condition. Let us now analyze this equation for the various models.

1. $D(\dot{u}) = \dot{u}$ model

Consider now the simpler choice $D(\dot{u}) = \dot{u}$, which, anticipating a bit, is the $\sqrt{\dot{u}}$ model defined below. In that case,

$$a(r) = \frac{r}{2} + \frac{v}{2r}, \quad (76)$$

$$b(r) = \frac{v}{2}. \quad (77)$$

Solving the differential equation (72), we find two solutions. One is the Gaussian

$$P_0(r) = \frac{1}{2\pi v}e^{-r^2/(2v)}. \quad (78)$$

The other one decays as $1/r^2$ at large r and thus can not satisfy the normalization condition (66). Going back to variables $\dot{u}$, $\tilde{a}$, this identifies with the Gaussian distribution (51) also found in the large-velocity limit.

The analysis can be continued to higher orders. Writing

$$P_n = \frac{e^{-r^2/(2v)}}{2\pi v}Q_n(r,\theta), \quad (79)$$

where the Q_n are polynomials in r, $\cos\theta$, and $\sin\theta$, which satisfy the recursion

$$Q_0 = 1,$$
$$\partial_\theta Q_{n+1} = [1 + r\cos\theta\,\hat{O} + (v + r\sin\theta)\hat{O}^2]Q_n\,, \quad n \geqslant 0. \tag{80}$$

We have defined

$$\hat{O} = e^{r^2/(2v)} O e^{-r^2/(2v)} = \cos\theta\left(-\frac{r}{v} + \partial_r\right) - \frac{\sin\theta}{r}\partial_\theta.$$

One finds

$$Q_1 = -\frac{r\cos(\theta)[r^2\cos(2\theta) + r^2 - 6v]}{6v^2} = -\frac{a^3 - 3av}{3v^2}. \tag{81}$$

The second order Q_2 is given in Appendix G. The moments $\overline{u^n a^m}$ of the $\sqrt{u}$ model are computed in Sec. V D by another method and we have checked that they agree with the ones obtained here from P to the considered order $(1/m)$.

2. Tree model $D(\dot{u}) = |\dot{u}|$

For the tree model one finds

$$a(r) = \frac{r}{2} + \int_0^{2\pi} \frac{d\theta}{2\pi}\left|\frac{v}{r} + \sin\theta\right|\sin^2(\theta), \tag{82}$$

$$b(r) = r\int_0^{2\pi} \frac{d\theta}{2\pi}\left|\frac{v}{r} + \sin\theta\right|\cos^2(\theta). \tag{83}$$

Explicit calculations give

$$a(r) = \frac{r}{2} + \frac{1}{\pi}\frac{v}{r}\arcsin\left(\frac{v}{r}\right) - \frac{1}{3\pi}\left(\frac{v^2}{r^2} - 4\right)\sqrt{1 - \frac{v^2}{r^2}}, \quad r > v$$

$$a(r) = \frac{r}{2} + \frac{v}{2r}, \quad r < v \tag{84}$$

$$b(r) = \frac{v}{\pi}\arcsin\left(\frac{v}{r}\right) + \frac{r}{3\pi}\left(2 + \frac{v^2}{r^2}\right)\sqrt{1 - \frac{v^2}{r^2}}, \quad r > v$$

$$b(r) = \frac{v}{2}, \quad r < v. \tag{85}$$

We see that for large v one recovers the result of the $\sqrt{u}$ model, namely, the Gaussian. For v of order one, the solution P_0 of (72) can be computed numerically (see Fig. 10). For $v = 0$, one can obtain an analytical expression using $a(r) = r/2 + 4/(3\pi)$ and $b(r) = 2r/(3\pi)$:

$$P_0(r) = \frac{9\pi}{32}e^{-\frac{3\pi}{4}r}. \tag{86}$$

The other solution is excluded since it decays as $1/r^2$ at large r. For the leading correction in m at $v = 0$ we find

$$P_1(r,\theta) = P_0(r)Q_1^+(r,|\theta|)\text{sgn}(\theta), \quad -\pi < \theta < \pi \tag{87}$$

$$Q_1^+(r,\theta) = \tfrac{1}{64}[4(\pi - 2\theta)(3\pi r - 8) - 2\pi\cos(\theta)(12r\sin(\theta) + (3\pi r + 4)\cos(2\theta) + 3\pi r - 20)]. \tag{88}$$

We can check that it has zero angular integral and vanishes at all $\theta = n\pi/2$. The moments are

$$\overline{a^2} = \overline{u^2} = \frac{16}{3\pi^2} + O(1/m), \tag{89}$$
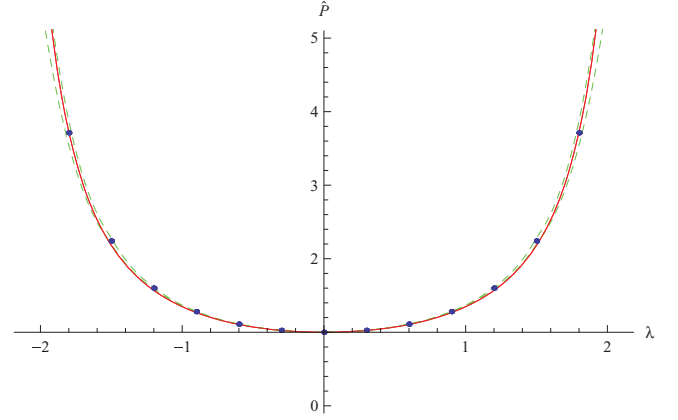

FIG. 4. (Color online) Numerical simulation of the tree model for $v = 0.1$, $m = 100$, $\mu = \eta = 1$, and 5×10^7 data points. In order to eliminate the small asymmetry coming from nonzero velocity, we show symmetrized $\hat{P}$ in λ, i.e., $[\hat{P}(\lambda) + \hat{P}(-\lambda)]/2$. These are the data shown (blue dots), together with a 1σ estimate of their statistical errors (green, dashed line) and the analytical curve (90) (red, solid line). Note that there is no adjustable parameter. For larger values of $|\lambda|$ (not shown), the statistical errors grow and one observes small deviations whose origin could be corrections from $1/m$ or small but finite v.

whereas they would vanish in the limit of $v = 0$ for the $\sqrt{u}$ model, where the Gaussian (78) is valid at zeroth order in $1/m$.

The Laplace transform of Eq. (86) gives, to leading order in $1/m$,

$$\hat{P}(\lambda) = \overline{e^{\lambda\dot{u}}} \approx \int_0^{2\pi} d\theta \int_0^\infty dr\, r\, P_0(r)\, e^{\lambda r\sin\theta}$$
$$= \frac{27\pi^3}{(9\pi^2 - 16\lambda^2)^{3/2}}. \tag{90}$$

This function has a branch-cut singularity starting at $\lambda_c^\pm = \pm\frac{3\pi}{4} = \pm 2.35619$. It is interesting to note that from Eq. (72) and (84) one can conclude directly that for any v, $P_0(r) \sim e^{-\frac{3\pi}{4}r}$ at large $r \gg v$. Hence, the tree model has $\lambda_c^\pm = \pm\frac{3\pi}{4}$ at $m = \infty$ independent of v. Similar branch-cut singularities for the $\sqrt{u}$ model will be discussed in Sec. V B. In Fig. 4, we show a numerical simulation of the equation of motion given by Eqs. (34)–(36) for $v = 0.1$, $m = 100$, $\mu = \eta = 1$, and 5×10^7 data points. The agreement of the simulations with the analytical result (90) is excellent.

E. Numerical solution of the Fokker-Planck equation

In this section, we solve Eq. (39) numerically using the discretization scheme proposed by Scharfetter and Gummel [50] and analyze the probability distribution for different values of the driving velocity v and mass m. The probability distribution of velocities for different masses and fixed driving velocity $v = 5/2$ is shown in Fig. 5. For $m = 0$ there are no negative velocities $\dot{u}$ and the probability reaches its maximum at a higher value than all other curves shown in Fig. 5. The general tendency is an increase of the probability for negative $\dot{u}$ when increasing the mass as well as a decrease of the maximum of the probability. At the same time, the maximum gets shifted
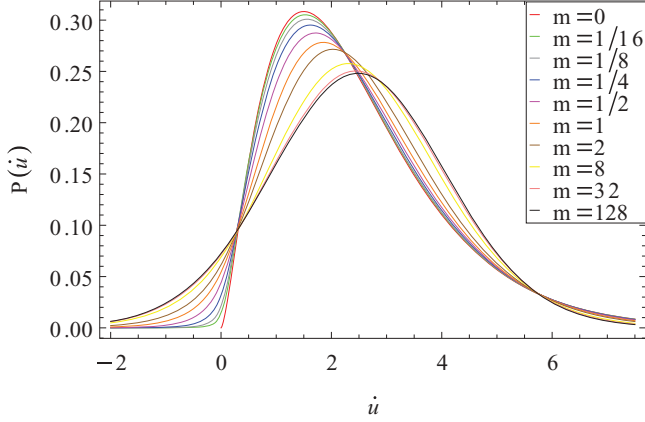
FIG. 5. (Color online) Velocity probability distribution for a fixed driving velocity $v = 5/2$. Different curves correspond to different masses (see the explanation in the main text).

FIG. 7. (Color online) Probability distribution of accelerations for a fixed driving velocity $v = 1/2$. Different curves correspond to different masses (see the explanation in the main text).

towards higher velocities. We see that for $m = 32$ and 128 there is only a small difference in the probability distribution, and for large mass the probability converges to a master curve at $m = \infty$, the behavior of which we discuss in more detail in the next section. Also note that there are two remarkable points where all curves intersect, a feature which remains to be understood.

Figure 6 shows $P(\dot{u})$ for $v = 1/2$ and different masses. We see that the divergence for $m = 0$ seems to disappear in the presence of a small mass, and that at the same time the probability for negative $\dot{u} < 0$ becomes finite. A small mass changes the positive tail of the distribution only slightly. Inertia has the tendency to decrease the maximum of $P(\dot{u})$ as was noticed in Fig. 5 where $v > 1$. This is also manifest for $v < 1$.

Next we analyze the probability distribution of accelerations. Figure 7 shows $P(a)$ for $v = 1/2$ and different masses. The larger the mass is, the more symmetric the distribution becomes, in agreement with results from Sec. IV D. Decreasing the mass, the maximum of $P(a)$ gets lowered, while the distribution broadens and the average of a^2 increases. A similar behavior is observed for $v > 1$.
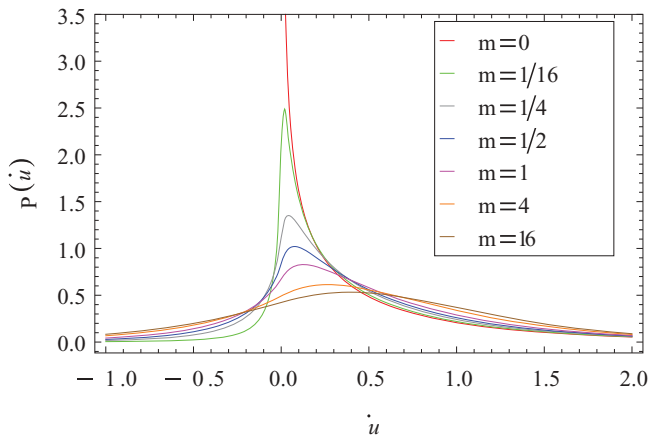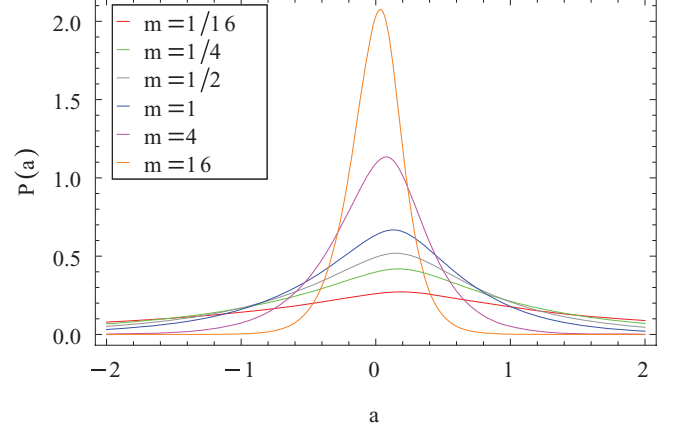
Apart from similarities between the ABBM model and the tree model (discussed in Sec. III), there are also differences. By looking at Figs. 2 and 3, we see that when the probability for negative velocities becomes considerable, a difference between the tree model and the ABBM model with inertia becomes visible. The probability distribution for the tree model is characterized by a smaller peak and larger tails than the ABBM model with inertia.

F. Comparison of the numerical solution of the Fokker-Planck equation with perturbation expansion in m and $1/m$

Here we compare numerical and analytical results from the two previous sections focusing on the behavior at small and large m. We start with small m. We now have to determine the currently undetermined constants entering the distribution function Eqs. (42)–(44). For sufficiently small m and sufficiently large v, negative velocities appear with small probability. Then, we can neglect their contribution to $\int da\, d\dot{u}\, P = 1$ as well as the contribution from the narrow region 2 since the main contribution comes form region 1. We find

$$c_3 = 0, \tag{91}$$

$$c_5 = \tfrac{1}{4} - v\psi(v), \tag{92}$$

where $\psi(x)$ is the digamma function. In this region of parameters, in Appendix A we state higher-order terms in $P(\dot{u})$ and additionally we calculate exactly moments characterizing the distribution function and some other correlations in Secs. V D, V G, and Appendix D.

The numerical solution for the joint probability distribution of acceleration and velocity, integrated over positive velocities for $m = 1/8$ and $v = 5/2$, is shown in Fig. 8 by the full line. The dotted line is the first-order and the dashed line the second-order perturbation theory result of Eq. (45). We see good agreement between analytical and numerical solutions. Also, the agreement increases with increasing order of perturbation theory. The small remaining difference may come from the approximation made when fixing c_3 and c_5, i.e., due to

FIG. 6. (Color online) Velocity probability distribution for a fixed driving velocity $v = 1/2$. Different curves correspond to different masses (see the explanation in the main text).
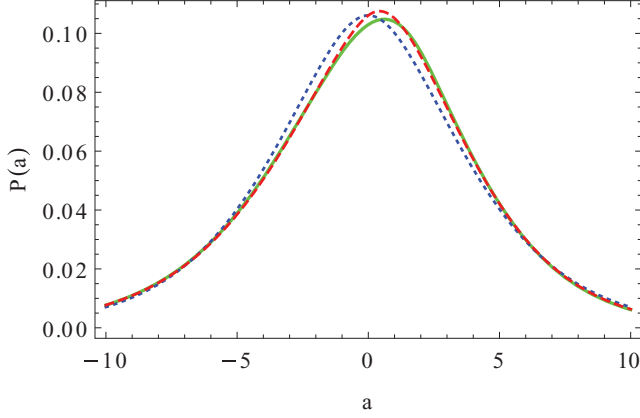
FIG. 8. (Color online) The full green line represents the numerical solution for the joint probability distribution of acceleration and velocity, integrated over positive velocities for $m = 1/8$ and $v = 5/2$. The dashed red line is the result of the second-order perturbation theory (45), while the dotted blue line is the first-order perturbation theory.

neglecting the contributions from negative velocities and from the region 2.

Let us now compare the distribution of velocities. Figure 9 presents $P(\dot{u})$ for $m = 1/4$ and $v = 5/2$. The full line is the numerical solution, the dotted line is $m = 0$, and the dashed line is the perturbation theory result of Eq. (A6). For $P(\dot{u})$ in the region 1 there is very good agreement between perturbation theory and numerical solution.

Next, we compare the perturbation expansion in $1/m$ studied in Sec. IV D with the numerical solution. The distribution function becomes rotationally invariant in the $\dot{u}$-$\tilde{a}$ plane around the point $(v,0)$ in the limit $m \to \infty$ [see Eq. (65)]. Therefore, in Fig. 10 is shown $\tilde{P}(\dot{u} + v, \tilde{a} = 0)$ for fixed mass $m = 100$ and different driving velocities. The definition of $\tilde{P}$ is given by Eq. (56). Numerical solutions are shown by full lines, while dotted lines denote the zeroth order in the expansion given by solutions of the differential Eq. (72) for the tree model. We see good agreement, especially for larger v.
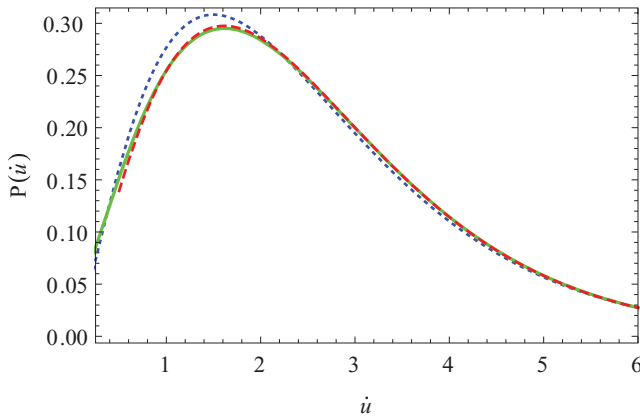

FIG. 9. (Color online) The full green line represents numerical solution for velocity distribution for $m = 1/4$ and $v = 5/2$. Dashed red line is the result of perturbation theory, Eq. (A6). Dotted blue line is $m = 0$ curve.
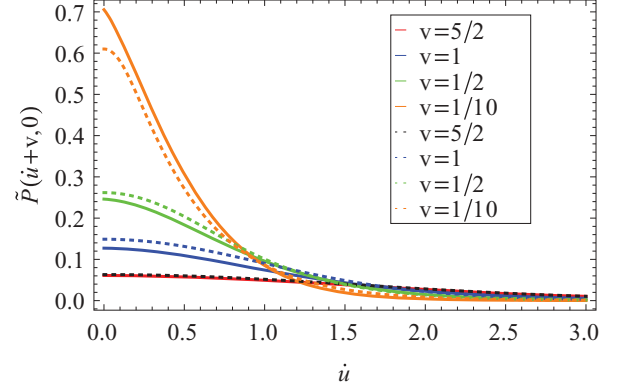

FIG. 10. (Color online) The full lines represent the numerical solution for $\tilde{P}(\dot{u} + v, \tilde{a} = 0)$ for $m = 100$ and different values of v. The dotted lines are the zeroth order of perturbation theory, Eq. (72).

V. $\sqrt{\dot{u}}$ MODEL

A. Strategy

In this section, we define a model which

(i) is equivalent to the ABBM model for all trajectories such that the particle only moves forward;

(ii) is an exact saddle point of the MSR dynamical action, hence allows for some analytical results; in particular the generating function of the one-time velocity distribution is given by

$$\hat{P}(\lambda) := \overline{e^{\lambda \dot{u}(t_0)}} = e^{v Z(\lambda)}, \tag{93}$$

where $Z(\lambda)$ does not depend on v;

(iii) on the downside, $\dot{u}$ may become complex.

Although the MSR saddle-point method for the ABBM model is exact only for $m = 0$, its extension to $m > 0$ provides a natural approximation of the ABBM model in presence of inertia. For instance, let us define $P_{\text{approx}}(\dot{u})$ as the inverse-Laplace transform of $\hat{P}(\lambda)$ on the *real* $\dot{u}$ axis as

$$\hat{P}(\lambda) = \int_{-\infty}^{\infty} d\dot{u} \, P_{\text{approx}}(\dot{u}) \, e^{\lambda \dot{u}} \tag{94}$$

since $Z(\lambda)^* = Z(\lambda^*)$, the function $P_{\text{approx}}^v(\dot{u})$ is real, and since $Z(0) = 0$ (see below) it integrates to unity. As velocities can become complex, using this function as an approximation of a probability distribution (for the ABBM model) makes senses if, and only if

(iv) the function $P_{\text{approx}}(\dot{u})$ is positive.

Although not an obvious fact, we have strong numerical evidence that this is indeed the case. Finally, we will show in Sec. VI that the approximation becomes exact for large v.

B. Definition and basic properties

We define the model in the laboratory frame

$$\frac{d\dot{u}(t)}{dt} = a(t), \tag{95}$$

$$m \frac{da(t)}{dt} = \mu^2 [v - \dot{u}(t)] - \eta a(t) + \sqrt{\dot{u}(t)} \, \xi(t), \tag{96}$$

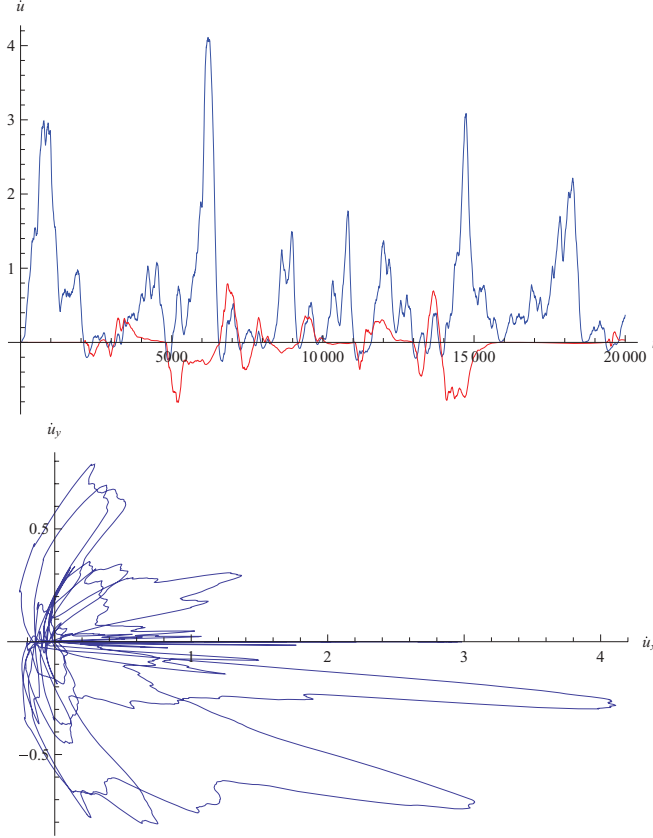$$\langle \xi(t) \xi(t') \rangle = 2\sigma \, \delta(t - t'). \tag{97}$$

FIG. 11. (Color online) Top: real (upper blue line) and imaginary (lower red line) parts of the velocity for one realization of the disorder, and $v = 0.5$. Bottom: phase portrait, i.e., trajectories in the complex plane $\dot{u} = \dot{u}_x + i\dot{u}_y$. Note the different scale in real and imaginary directions.

As long as the velocity is positive, the noise $\sqrt{\dot{u}(t)}\xi(t)$ is real, and the velocity remains real. However, when $\dot{u}$ becomes negative, complex velocities arise. This can be seen on Fig. 11 for one given disorder realization, and driving velocity $v = 0.5$ and $m = 1/4$. Increasing the driving velocity, the trajectories at the bottom of Fig. 11 get closer to the real axis, and less negative events arise. In addition, one sees from Eq. (95) that near the positive real velocity axis a small imaginary part $im\dot{u} = \epsilon$ experiences a linear force $-(\mu^2 - \frac{\xi(t)}{2\sqrt{u}})\epsilon$ which on average brings it back towards the real axis except for small velocities.

Therefore, this model is expected to be a reasonable approximation to the ABBM model with inertia for large v and small m (see Sec. VI). Moreover, in the same limit of parameters, this model works also well for the particle on the tree studied in the previous section. It will be discussed in Sec. V F 6 how good an approximation it can provide beyond this range of parameters. While the velocities in this model can become complex, as we will show now, the generating function for the velocities is given by a single, v-independent function $Z(\lambda)$:

$$\overline{e^{\lambda\dot{u}(t_0)}} = e^{vZ(\lambda)}. \tag{98}$$

The proof is based on the MSR formalism. Replacing $a(t)$ in the second line of the above Langevin equation by $\ddot{u}(t)$, the
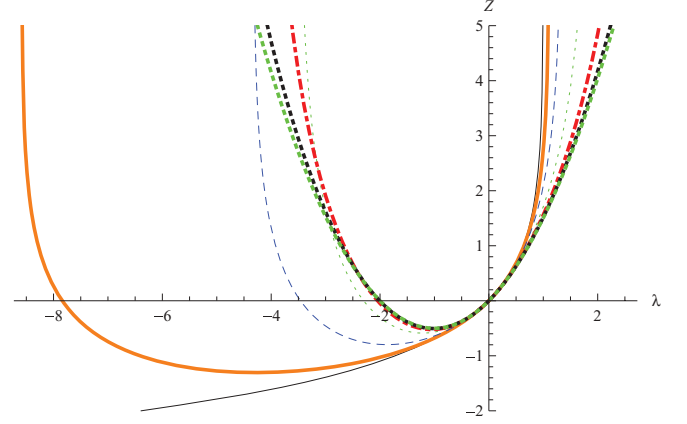

FIG. 12. (Color online) The generating function $Z(\lambda)$ for masses $m = 0$ (thin, solid, black line), $m = 1/4$ (thick orange line), $m = 1$ (blue, dashed line), $m = 4$ (green, dotted line), $m = 16$ (red, dotted-dashed, thick line), $m = 64$ (black, dotted, thick line), $m = 256$ (green, dotted, thick line). All functions diverge at $\lambda = \lambda_c^+$ and $\lambda = \lambda_c^-$.

expectation (98) can be written as Refs. [24–26]

$$\overline{e^{\lambda\dot{u}(t_0)}} = \int \mathcal{D}[\dot{u}]\mathcal{D}[\tilde{u}]e^{\lambda\dot{u}(t_0)-\mathcal{S}[\dot{u},\tilde{u}]} \tag{99}$$

with the dynamical action

$$\mathcal{S}[\dot{u},\tilde{u}] = \int_t \tilde{u}(t)\big[m\partial_t^2\dot{u}(t) + \eta\partial_t\dot{u}(t) + \mu^2(\dot{u}(t) - v)\big] \\ - \sigma\dot{u}(t)\tilde{u}(t)^2. \tag{100}$$

In the square brackets, we recognize the equation of motion without disorder, enforced by the response field $\tilde{u}(t)$. The last term results from the average over the disorder, using (97).

Since the action is *linear* in $\dot{u}$, the saddle point w.r.t. this variable is *exact*, leading to the instanton equation

$$m\partial_t^2\tilde{u}(t) - \eta\partial_t\tilde{u}(t) + \mu^2\tilde{u}(t) - \sigma\tilde{u}(t)^2 = \lambda\delta(t - t_0). \tag{101}$$

This has to be supplemented with the boundary conditions $\tilde{u}(\pm\infty) = 0$. For the case $m > 0$ studied here it turns out to be equivalent to requesting

$$\tilde{u}(t) = 0, \quad \forall\, t \geqslant t_0 \tag{102}$$

which implies $\partial_t\tilde{u}(t) = 0$ for all $t > t_0$.[6] Supposing that (101) holds, the only term which survives in Eq. (99) is the term of order v in Eq. (100), which yields (98) with

$$Z(\lambda) = \mu^2 \int_t \tilde{u}(t). \tag{103}$$

While analytical results for Eqs. (101) and (103) are difficult to obtain, it is quite easy to solve the instanton equation (101) numerically. We do this now in our dimensionless units, i.e., setting $\eta = \mu^2 = \sigma = 1$. On Fig. 12, we show $Z(\lambda)$ for different masses. For real λ, $Z(\lambda)$ diverges at two singularities, one at $\lambda = \lambda_c^+ > 0$, the other at $\lambda = \lambda_c^- < 0$. Their values, as a function of m, are plotted on Fig. 13. Examination of $P_v(\lambda)$

---

[6]Note, however, that for $m < 0$ there are solutions which vanish at infinity and do not satisfy (102).
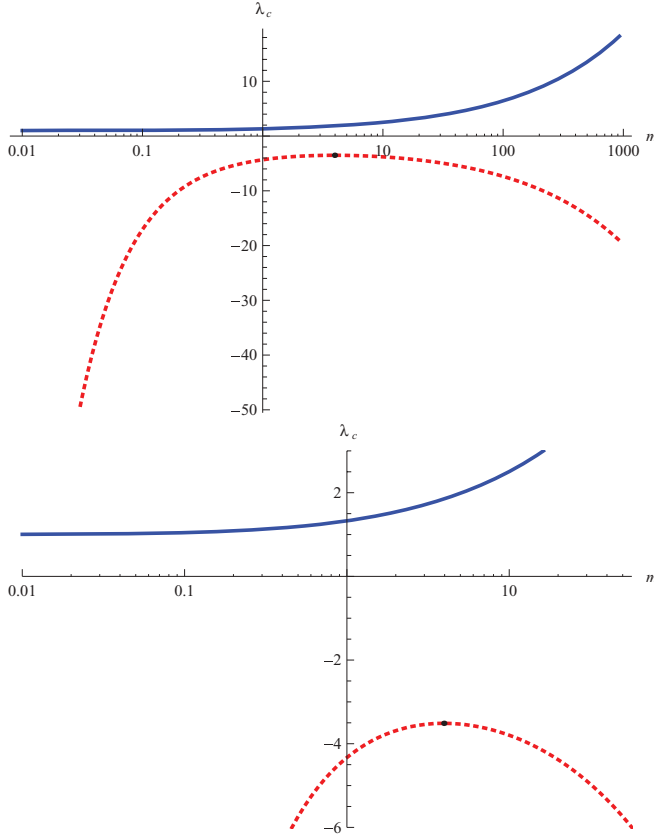
FIG. 13. (Color online) Top: Location of the branch-cut singularity in $Z(\lambda)$, as a function of m. Lower curve (red, dotted) is λ_c^-, upper curve (blue) is λ_c^+. The maximum of λ_c^- is at $m = 3.9540$, $\lambda_c^- = -3.5124$, marked by a dot. Bottom: Blow-up of the same curve.

for complex λ show that they are branch-cut singularities. The branch-cut singularities determine the behavior of the function $P_{approx}^v(\dot{u})$ defined in Eq. (94) at large $\dot{u}$, up to possible power-law pre-exponential factors as

$$P_{approx}(\dot{u}) \sim \begin{cases} e^{-\dot{u}\lambda_c^+} & \text{for } \dot{u} \to +\infty, \\ e^{\dot{u}\lambda_c^-} & \text{for } \dot{u} \to -\infty. \end{cases} \quad (104)$$

It is important to note that this asymptotic behavior holds at *any* driving velocity: Were $P_{approx}^v(\dot{u})$ to decay faster (e.g., with a larger constant in front of, or a higher power of $\dot{u}$ in the exponential), then $\hat{P}(\lambda_c) = e^{vZ(\lambda_c)}$ would be finite, which it is not. Similarly, if it would decay slower, then $\hat{P}(\lambda_c) = e^{vZ(\lambda_c)}$ would not exist up to $\lambda = \lambda_c$. Note that (101) also implies that $Z(\lambda)$ is real for real λ, at least as long as the solution $\tilde{u}(t)$ decays to zero at large times, which is the case for $\lambda_c^- < \lambda < \lambda_c^+$ (see below).

As shown in Fig. 13, by increasing the mass beyond the special value $m^* = 3.95402$, the value of λ_c^- decreases again, i.e., the tail for negative $\dot{u}$ becomes again shorter. For $m \to \infty$, both λ_c^+ and λ_c^- become infinitely large, meaning that $Z(\lambda)$ becomes an analytic function for all λ. This is in agreement with the result found in Sec. IV D where we demonstrate that in the limit $m \to \infty$ the distribution function becomes Gaussian (78).

Beyond allowing us to define the function $P_{approx}(\dot{u})$, $Z(\lambda)$ contains information on the probability distribution $P(\dot{u}_x, \dot{u}_u)$

of the process $\dot{u}(t) = \dot{u}_x + i\dot{u}_y$ in the complex plane (see, e.g., Fig. 11) through

$$\hat{P}(\lambda) = \int_{-\infty}^{\infty} d\dot{u}_x \int_{-\infty}^{\infty} d\dot{u}_y \, e^{\lambda[\dot{u}_x + i\dot{u}_y]} P(\dot{u}_x, \dot{u}_y). \quad (105)$$

It does not allow us, however, to determine $P(\dot{u}_x, \dot{u}_y)$ since we would need a more general generating function for the moments of $\dot{u}^* = \dot{u}_x - i\dot{u}_y$. A question is what information can be extracted, and how does it relate to $P_{approx}(\dot{u})$. For illustration, we can consider a simple toy example such that the probability factorizes $P(\dot{u}_x, \dot{u}_y) = P_x(\dot{u}_x)P_y(\dot{u}_y)$ so that $\hat{P}(\lambda)$ can be written as $\hat{P}(\lambda) = \hat{P}_x(\lambda)\hat{P}_y(i\lambda)$ where $\hat{P}_x(\lambda)$ and $\hat{P}_y(\lambda)$ are the Laplace transforms of $P_x(\dot{u})$ and $P_y(\dot{u})$, respectively. From our numerical studies we find that $P(\dot{u}_x, \dot{u}_y)$ is narrowly distributed in the y direction, with a width which decreases with increasing v. For large v, $P(\dot{u}_x, \dot{u}_y)$ will converge against $P_{approx}(\dot{u}_x)\delta(\dot{u}_y)$, at least for $\dot{u}_x > 0$. For finite v, consider the simplest example, i.e., a Gaussian for $P_y(\dot{u}_y)$ which leads to

$$\hat{P}_v(\lambda) = \hat{P}_x(\lambda)e^{\frac{-\alpha\lambda^2}{2}}. \quad (106)$$

As discussed above, we found that $\hat{P}(\lambda)$ has two branch-cut singularities starting at a finite real λ_c^+ and λ_c^-. Since the latter control the behavior at large $\dot{u}$ and $\dot{u}_x$, both $P_{approx}(\dot{u})$ and $P_x(\dot{u}_x)$ have the same behavior at large (positive or negative) arguments for this toy example. We will not pursue further here the study of $P(\dot{u}_x, \dot{u}_y)$.

C. Connection between instanton approach and Fokker-Planck approach

We saw in Sec. II that the ABBM model *without* inertia can be solved either using the Fokker-Planck equation or the MSR method based on the nonlinear saddle-point equation (the instanton). We recalled their equivalence based on the method of characteristics. The same property holds for the $\sqrt{\dot{u}}$ model, with a small caveat. The caveat is that the correspondence is simple only between the instanton equation and the *Fokker-Planck equation in its Laplace-transformed version* [Eq. (108)]. In real space, it corresponds formally to the Fokker-Planck (FP) equation (39) where the replacement $|\dot{u}| \to \dot{u}$ is made in the diffusion term. This would indeed be the FP equation associated to the Langevin process (95) and (96) if one forgets that $\dot{u}$ can become negative, and consequently complex. Writing an adequate FP equation for such a process requires an extension of $P(\dot{u}, a, t)$ with arguments in the complex plane, a route which we do not follow here.

Instead, consider the evolution equation for the following average over trajectories:

$$\hat{P}(\lambda, \kappa, t) = \overline{e^{\lambda\dot{u}(t) + \kappa a(t)}}. \quad (107)$$

It is in principle an integral $\int d\dot{u} \, da \, e^{\lambda\dot{u} + \kappa a} P(\dot{u}, a, t)$ over the complex $\dot{u}$ and a plane. The average (107) satisfies the Laplace version of the FP equation,

$$\frac{\partial \hat{P}}{\partial t} - \frac{\partial \hat{P}}{\partial \kappa}\left(\lambda - \frac{\kappa}{m}\right) - \frac{\partial \hat{P}}{\partial \lambda}\left(-\frac{\kappa}{m} + \frac{\kappa^2}{m^2}\right) = \frac{\kappa}{m}v\hat{P}, \quad (108)$$

in dimensionless variables. As mentioned above, it is *formally* the Laplace transform (over the real axis) of the FP equation

with a $\dot{u}$ diffusion term. Equation (108) is easily derived from the Langevin equations (95) and (96) by considering the variation of the observable in an infinitesimal time interval dt. The only subtlety arises when expanding the variation $\overline{e^{\frac{\kappa}{m}\sqrt{\dot{u}(t)}d\xi(t)}} = 1 + \frac{1}{2}(\frac{\kappa}{m})^2\dot{u}(t)\overline{d\xi(t)^2} + O(dt^2)$ to second order, with $\overline{d\xi(t)^2} = 2\sigma dt$, using stochastic Itô calculus. This leads to the term $(\kappa^2/m^2)\partial_\lambda\hat{P}$ in Eq. (108).

We now show the connection to the MSR method and the instanton equation. The solution of Eq. (108) can be written in the form

$$\hat{P}(\lambda,\kappa,t) = e^{vZ(\lambda,\kappa,t)}, \qquad (109)$$

where Z is independent of v and satisfies

$$\frac{\partial Z}{\partial t} - \frac{\partial Z}{\partial \kappa}\left(\lambda - \frac{\kappa}{m}\right) - \frac{\partial Z}{\partial \lambda}\left(-\frac{\kappa}{m} + \frac{\kappa^2}{m^2}\right) = \frac{\kappa}{m}. \qquad (110)$$

To solve this equation, we again apply the method of characteristics, and reduce the partial differential equation to a family of ordinary differential equations

$$\dot{\kappa}(t) = -\lambda(t) + \frac{\kappa(t)}{m}, \qquad (111)$$

$$\dot{\lambda}(t) = \frac{\kappa(t)}{m} - \frac{\kappa(t)^2}{m^2}, \qquad (112)$$

$$dZ(t) = \frac{\kappa(t)}{m}dt. \qquad (113)$$

We have defined $Z(t) = Z(\lambda(t),\kappa(t),t)$, as well as $\dot{\kappa}(t) = d\kappa(t)/dt$ and $\dot{\lambda}(t) = d\lambda(t)/dt$.

Let us now introduce

$$\tilde{u}(t) = \kappa(t)/m. \qquad (114)$$

Eliminating $\lambda(t)$ in Eqs. (111) and (112), we find that it satisfies

$$m\ddot{\tilde{u}}(t) - \dot{\tilde{u}}(t) + \tilde{u}(t) - \tilde{u}^2(t) = 0. \qquad (115)$$

If we impose $\tilde{u}(t) = 0$ and $\dot{\tilde{u}}(t) = 0$ for $t > t_0$ and assume $\lambda(t_0) = \lambda$ and $\kappa(t_0) = 0$, this equation becomes the instanton equation (101) in dimensionless units. To obtain the stationary solution $Z(\lambda,\kappa)$ of Eq. (110) we can solve (115) on the interval $t \in]-\infty,t^*]$, with boundary conditions at $t = t^*$:

$$\tilde{u}(t^*) = \frac{\kappa}{m}, \qquad (116)$$

$$\dot{\tilde{u}}(t^*) = -\frac{\lambda}{m} + \frac{\kappa}{m^2}, \qquad (117)$$

and $\tilde{u}(-\infty) = 0$, $\dot{\tilde{u}}(-\infty) = 0$. Then, we compute

$$Z(t^*) = \int_{-\infty}^{t^*}\tilde{u}(t)\,dt := Z(\lambda,\kappa), \qquad (118)$$

which is precisely $Z(\lambda,\kappa)$ if expressed as a function of the boundary condition. Since it does not depend on t^*, we have found the stationary solution.

Hence, we have shown, via Eq. (108), that the observable (107) can be obtained from the solution of the instanton equation, although with a slightly more general boundary condition than in Eq. (101). This is because we now want the joint distribution of velocity and acceleration (at a given time t^*). We can rewrite the observable (107) as

$$\hat{P}(\lambda,\kappa,t) = \overline{e^{\int dt[\lambda\delta(t-t^*)-\kappa\delta'(t-t^*)]\dot{u}(t)}}. \qquad (119)$$

Performing the same manipulations using the dynamical MSR action as in Refs. [24–26] as sketched above in Sec. V B, we arrive at the instanton equation with a source on the right-hand side $\lambda\delta(t - t^*) - \kappa\delta'(t - t^*)$, which is equivalent to the boundary conditions (116) and (117).

To summarize, for the $\sqrt{\dot{u}}$ model, Eq. (108) describes the time evolution of the observable (107) under the Langevin equations (95)–(97), even though $\dot{u}$ and a take values in the complex plane. Solving it is equivalent to solving the instanton equation as a function of λ and κ that determine its boundary conditions (116) and (117). Neither equation admits solutions in closed analytical form for generic values of m, but each has its advantages for numerical or perturbative studies. For instance, from Eq. (108) we can easily obtain the moments for this model, as we now show. Also, note that the Laplace transform of the Fokker-Planck equation for the tree model can also be studied although it is more involved (see Appendix C).

D. Moments of the distribution function

In the stationary case, taking the derivatives $\partial_\lambda^n\partial_\kappa^m$ of Eq. (108) where m and n are positive integers and afterwards setting κ and λ to zero, one obtains a set of linear equations for $\partial_\lambda^n\partial_\kappa^m\hat{P}(\lambda,\kappa)|_{(0,0)}$. By solving them and using $\partial_\lambda^n\partial_\kappa^m\hat{P}(\lambda,\kappa)|_{(0,0)} = \overline{\dot{u}^n a^m}$ and $\hat{P}(0,0) = 1$, one finds[7] the moments characterizing the distribution function for the $\sqrt{\dot{u}}$ model:

$$\overline{\dot{u}^0 a^1} = 0, \qquad (120)$$

$$\overline{\dot{u}^0 a^2} = \frac{v}{m}, \qquad (121)$$

$$\overline{\dot{u}^0 a^3} = -\frac{2v}{m(m+2)}, \qquad (122)$$

$$\overline{\dot{u}^0 a^4} = \frac{3v^2}{m^2} + \frac{6(5m+3)v}{m^2(m+2)(4m+3)}, \qquad (123)$$

$$\overline{\dot{u}^1 a^0} = v, \qquad (124)$$

$$\overline{\dot{u}^1 a^1} = 0, \qquad (125)$$

$$\overline{\dot{u}^1 a^2} = \frac{v^2}{m} + \frac{2v}{m(m+2)}, \qquad (126)$$

$$\overline{\dot{u}^1 a^3} = -\frac{2v^2}{m(m+2)} - \frac{6v}{m(m+2)(4m+3)}, \qquad (127)$$

$$\overline{\dot{u}^2 a^0} = v(v+1), \qquad (128)$$

$$\overline{\dot{u}^2 a^1} = 0, \qquad (129)$$

$$\overline{\dot{u}^2 a^2} = \frac{1}{m(m+2)(4m+3)}(4m^2 v^3 + 4m^2 v^2 + 11mv^3$$
$$+ 27mv^2 + 10mv + 6v^3 + 18v^2 + 12v), \qquad (130)$$

$$\overline{\dot{u}^3 a^0} = \frac{4v}{m+2} + v^3 + 3v^2, \qquad (131)$$

$$\overline{\dot{u}^3 a^1} = 0. \qquad (132)$$

_____

[7]The result is exact in the region of parameters discussed at the very beginning of this section.
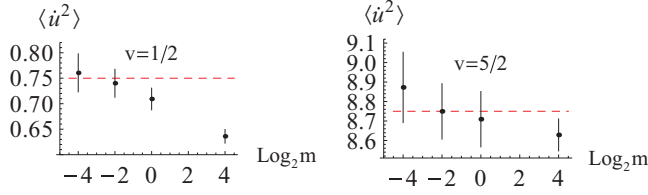
FIG. 14. (Color online) Average value of $\dot{u}^2$ for the ABBM model with inertia as a function of mass m is shown for two driving velocities $v = 1/2$ and $5/2$. Dashed line represents the value $v(v+1)$, while the points are the numerical results.

For brevity, we stated only the first few moments, but the procedure can be easily extended to higher moments. Some of them are given in Appendix D.

While these results are exact for the $\sqrt{\dot{u}}$ model, we can compare them with the ABBM model with inertia and for the particle on the tree model. In Fig. 14 we show $\langle \dot{u}^2 \rangle$ as a function of mass for two different driving velocities for the ABBM model with inertia. For $v = 1/2$ we see disagreement between the above obtained $v(v+1)$ value and the numerical result for $m = 1$, while for the larger velocity the deviation appears at larger values of the mass. Similar behavior is observed for the tree model. In Appendix D, the moments of the velocity are computed using an iterative solution of the instanton equation instead of Fokker-Planck equation.

E. Perturbation at small m for $P(\dot{u})$

In this section, we obtain the perturbative expansion in small m of the generating function $Z(\lambda) = Z(\lambda, \kappa = 0)$ for the steady state velocity distribution function of the $\sqrt{\dot{u}}$ model. To this aim, we will solve perturbatively in m the nonlinear instanton equation (115) and use (118) to obtain $Z(\lambda)$ from the solution. The solution $\tilde{u}(t)$ of Eq. (115) at $m = 0$ is given in Eq. (16). It is nonzero for $t < 0$, zero for $t > 0$, with a jump at $t = 0$. In presence of inertia $m > 0$, we are now looking for a solution nonzero for $t < 0$, zero for $t > 0$, but which vanishes at $t = 0$, i.e., $\tilde{u}(0) = 0$ since we have set $\kappa = 0$, and with $\dot{\tilde{u}}(0) = -\lambda/m$. For small m it is then clear that there is a boundary layer for $t = O(m) < 0$ where the function varies rapidly from values of order 0 to values of order λ. In addition, there is a bulk region $t = O(1) < 0$. We now study both regions and how they match.

As will become clear below, in the boundary layer region $0 < -t \lesssim m$ we can write

$$\tilde{u}(t) = \sum_{n=0}^{\infty} m^n f_n \left(\frac{t}{m} \right) \tag{133}$$

with $\tilde{u}(0) = 0$ and $\dot{\tilde{u}}(0) = -\lambda/m$. By inserting into the instanton equation (115), we then find the following recursion:

$$f_0(t) = \lambda(1 - e^t), \tag{134}$$

$$\ddot{f}_{k+1}(t) - \dot{f}_{k+1}(t) + f_k(t) - \sum_{\ell=0}^{k} f_\ell(t) f_{k-\ell}(t) = 0 \tag{135}$$

for $k \geqslant 0$. Note that the term $f_0(t)$ already exists in absence of disorder and describes the rounding of the disorder-free response function by the mass. We assume $f_n(0) = 0$ and

$\dot{f}_n(0) = 0$ for $n > 0$. Then, we find

$$f_1(t) = \frac{\lambda}{2}[4 - 2t(\lambda - 1) - 5\lambda] + \frac{\lambda^2}{2} e^{2t} + e^t \lambda[2\lambda - 2 - t(2\lambda - 1)]. \tag{136}$$

Higher-order terms can be found, but for brevity are not stated here. In Appendix E, we give f_2. In general, f_n is a sum of exponentials and a polynomial of the form $f_n(t) = \sum_{k=1}^{n+1} e^{kt} C_k^{(n)}(t, \lambda) + \sum_{k=0}^{n} A_k^{(n)}(\lambda)(-t)^k$ further discussed in Appendix E.

In the region $-t = O(1) \gg m$, the solution can be written as

$$\tilde{u}(t) = \sum_{n=0}^{\infty} m^n y_n(t), \tag{137}$$

where y_n satisfy the following differential equations:

$$-\dot{y}_0 + y_0 - y_0^2 = 0, \tag{138}$$

$$\ddot{y}_{k-1}(t) - \dot{y}_k(t) + y_k(t) - \sum_{\ell=0}^{k} y_\ell(t) y_{k-\ell}(t) = 0. \tag{139}$$

The last line is for $k > 0$. The boundary condition is $y_n(-\infty) = 0$. Equations (138) and (139) can be solved recursively. This gives for each $y_n(t)$ a first-order differential equation, for which we need to fix $y_n(0)$ by the condition that solutions in different regions [Eqs. (133) and (137)] match at $-t$ small but $-t/m$ large. We discuss this in detail in Appendix E. Here, we state the solution

$$y_0(t) = \frac{\lambda}{\lambda + (1 - \lambda)e^{-t}}, \tag{140}$$

$$y_1(t) = -\frac{e^{-t}\lambda}{2[-e^{-t}(-1 + \lambda) + \lambda]^2}[4 - 2t(-1 + \lambda) + 5\lambda - 4(-1 + \lambda)\ln(e^{-t} + \lambda - e^{-t}\lambda)]. \tag{141}$$

Additionally, in Appendix E we give $y_2(t)$. Now we can determine

$$Z(\lambda, 0) = \sum_n m^n Z_n(\lambda) \tag{142}$$

given by Eq. (118) with $t^* = 0$. We find $Z_0 = \int_{-\infty}^{0} dt \, y_0(t)$ and $Z_n = \int_{-\infty}^{0} dt \sum_{k=1}^{n} e^{kt} C_k^{(n-1)}(t, \lambda) + \int_{-\infty}^{0} dt \, y_n(t)$. Hence, there is a contribution from both regions. The contribution of the $A_k^{(n)}$ terms is already taken into account through the contribution of the $y_n(t)$ at small t. Calculating the integrals, we obtain

$$Z_0 = -\ln(1 - \lambda), \tag{143}$$

$$Z_1 = -\lambda - \frac{1}{2}\lambda \left(\frac{\lambda}{1 - \lambda} + \frac{2\ln(1 - \lambda)}{\lambda} \right), \tag{144}$$

$$Z_2 = \frac{\lambda\{\lambda[5\lambda(\lambda + 2) - 36] + 24\}}{24(\lambda - 1)^2} + \ln(1 - \lambda). \tag{145}$$

Now, $\hat{P}(\lambda, 0) = \overline{e^{\lambda \dot{u}}} = e^{vZ(\lambda,0)}$ and from that follows the perturbative expansion of the moments $\overline{\dot{u}^k}$ in agreement with the results in Sec. V D. Assuming that for small mass we can ignore contribution in $\hat{P}$ coming from complex velocities,

we perform the inverse Fourier transform of $\hat{P}$ and find the distribution function

$$P_{\text{approx}}(\dot{u}) = \frac{e^{-\dot{u}}\dot{u}^{v-1}}{\Gamma(v)}\theta(\dot{u}) - \frac{me^{-\dot{u}}\dot{u}^{v-2}}{2\Gamma(v)}(-2\dot{u}v\ln(\dot{u})$$
$$+ 2\dot{u}v\psi(v) + \dot{u}^2 - v^2 + v)\theta(\dot{u}) + O(m^2),$$
(146)

where $\theta(x)$ is the Heaviside theta function, and $\psi(v)$ is the digamma function. The result to this order is thus a probability normalized to unity (to this order) for $v > 1$. The correction $O(m^2)$ is given in Appendix A by Eq. (A6) and is a bona fide distribution for $v > 2$. It also gives nonzero contribution for $\dot{u} > 0$ only and it is normalized to zero. Note that there is no *a priori* reason why at a fixed $m > 0$ the inverse-Laplace transform of $Z(\lambda)$ should exist, and furthermore with support on $\dot{u} > 0$ since the present model leads to complex velocities. However, it appears that (i) for large enough driving velocity $v > n$, the perturbative result can be trusted up to order $O(m^n)$, i.e., the negative velocity events are sufficiently rare not to spoil the result to that order; (ii) the perturbative result seems to be correct for any v provided $\dot{u} \gtrsim m$. These findings are consistent with the analysis for the tree model, for which we found the same result (46) in the region $\dot{u} \gtrsim m$, although with unknown constants c_3 and c_5, while for the $\sqrt{\dot{u}}$ model they are fixed by Eqs. (91) and (92).

F. Critical case $m = 1/4$

Here, we analyze the specific case of $m = 1/4$, and work in our dimensionless units. For the system *without disorder*, this is the critical case which separates the over-damped to under-damped regime where the particle starts to oscillate. It is also the mass which brings the particle back to the origin of the parabola in the shortest time. In presence of disorder, there is *a priori* nothing special to this case. Since, however, perturbative formulas simplify for $m = 1/4$, our aim in this section is to obtain to high numerical accuracy the behavior of $Z(\lambda)$ and of $P_{\text{approx}}(\dot{u})$. While the results are specific to $m = 1/4$, they are representative of other masses.

Since neither $Z(\lambda)$ nor $P_{\text{approx}}(\dot{u})$ can be obtained exactly, we consider several schemes to compute them to excellent precision: (i) a perturbative expansion in λ; (ii) an analysis of Z close to the branch cuts, and (iii) the behavior of Z for $\lambda \to \infty$. Each of these schemes gives an estimate of $P_{\text{approx}}(\dot{u})$ [the latter two are are denoted $P_{\text{BC}}(\dot{u})$ and $P_{\text{asymp}}(\dot{u})$ below] depending on which region of the complex plane dominates in the Laplace inversion. They are valid for different values of v and $\dot{u}$, as discussed below. In addition, we use numerical solution of the instanton equation. At the end, we compare our results to the numerical simulations on the ABBM model.

1. Perturbative expansion for $Z(\lambda)$

The response function is

$$R(t) = 4te^{-2t}\Theta(t), \qquad \left(\frac{\partial_t}{2} + 1\right)^2 R(t) = \delta(t). \quad (147)$$

The instanton equation (101) becomes

$$\left(1 - \frac{\partial_t}{2}\right)^2 \tilde{u}_t - \tilde{u}_t^2 = \lambda\delta(t). \quad (148)$$

The boundary conditions are given by Eq. (102). Equation (148) can be solved iteratively in λ, as shown in Appendix D. Integrating over time yields a perturbative expansion of $Z(\lambda)$:

$$Z(\lambda) = \lambda + \frac{\lambda^2}{2} + \frac{8\lambda^3}{27} + \frac{29\lambda^4}{144} + \frac{4094\lambda^5}{28125} + \frac{599431\lambda^6}{5467500}$$
$$+ \frac{650366396\lambda^7}{7657689375} + \frac{4815122286049\lambda^8}{71693475840000}$$
$$+ \frac{2890888542208895511\lambda^9}{5357932381952640000}$$
$$+ \frac{16329405133190713144717\lambda^{10}}{37207863763560000000000}$$
$$+ \frac{478482679990012444082975011879513\lambda^{11}}{1326979721280974188091895000000000}$$
$$+ \frac{8967062566599931521463627770728771141\lambda^{12}}{30017728909617033561025674240000000000}$$
$$+ O(\lambda^{13}). \quad (149)$$

The branch cuts described in Sec. V B are at, see Fig. 15

$$\lambda_c^+ = 1.10647, \quad \lambda_c^- = -8.58563. \quad (150)$$

2. Perturbative expansion for the critical instanton and λ_c^+

The value of the branch cuts can either be obtained from the numerical solution of the instanton equation, or via the following observation: The critical instanton $\tilde{u}_c^+(t) := \tilde{u}_{\lambda_c^+}(t)$ converges for $t \to -\infty$ rapidly against 1 (see Fig. 16). Thus, while $Z(\lambda_c^+) = \infty$, the solution of the instanton equation is still defined at this point. This allows for a series expansion, making the ansatz

$$\tilde{u}_c^+(t + t^*) = 1 - e^{\alpha t} + \sum_{n=2}^{\infty} b_n e^{n\alpha t}. \quad (151)$$

The parameters $\alpha > 0$ and b_n have to be determined, such that (151) satisfies the instanton equation (101), and finally t^* is chosen such that $u_c^+(t^*) = 0$. To find the parameters, expand (151) inserted into the instanton equation (101) in a series in $y := e^{\alpha t}$. At first order in y, the condition is
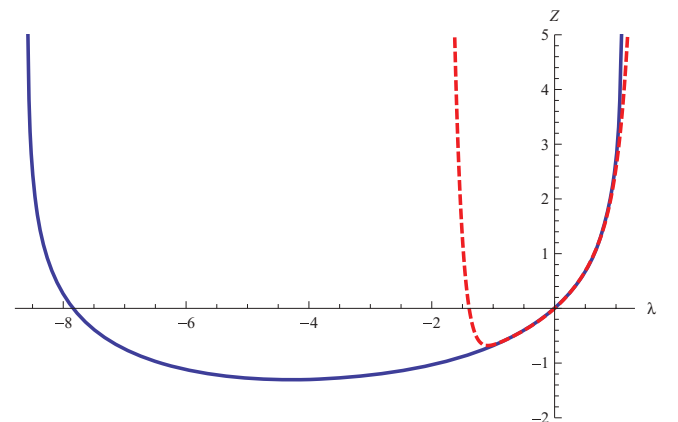

FIG. 15. (Color online) $Z(\lambda)$ in the critical case $m = 1/4$, together with its Taylor expansion (149).
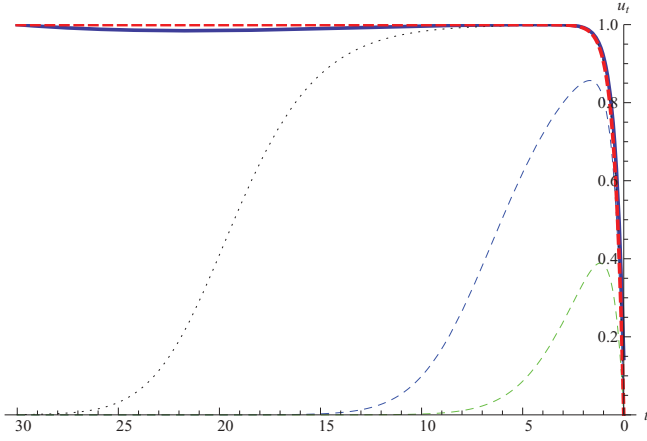
FIG. 16. (Color online) The function $\tilde{u}_t$ is increasing with increasing λ, as seen by numerically integrating the instanton solution: $\lambda = 1/2$ (green, dashed, smallest curve), $\lambda = 1$ (blue, dashed curve), $\lambda = 1.106$ (black, dotted curve), $\lambda = \lambda_c^+$ (red/blue, thick curve). The last curve shows superimposed the numerical solution of the instanton equation, and of the expansion (152).

$4 + 4\alpha - \alpha^2 = 0$, leading to $\alpha = 2(1 + \sqrt{2})$. Then, solve order by order in y, determining the b_n. Finally, find t^* such that $\tilde{u}_c^+(t = 0) = 0$. (This is necessary since the higher orders shift the origin.) The result for the critical instanton is

$$
\begin{aligned}
\tilde{u}_c^+(t) = {} & 1 - 1.08835 y + 0.0935856 y^2 - 0.00550998 y^3 \\
& + 0.000284501 y^4 - 0.00001369 y^5 \\
& + 6.30567 \times 10^{-7} y^6 - 2.81909 \times 10^{-8} y^7 \\
& + 1.23335 \times 10^{-9} y^8 - 5.30802 \times 10^{-11} y^9 \\
& + 2.25516 \times 10^{-12} y^{10} - 9.48217 \times 10^{-14} y^{11} \\
& + 3.95296 \times 10^{-15} y^{12} + O(y^{13}).
\end{aligned}
\tag{152}
$$

This determines $\lambda_c^+ = 1.10647$. Of course, all coefficients could be given explicitly. Also note that already for $n = 2$, one gets λ_c^+ within an error of 0.01. Each further order in n improves the accuracy of λ_c^+ by about one order of magnitude. Thus, one could use this algorithm as an efficient estimator for λ_c^+, as a function of m. A similar solution could be constructed for λ_c^-.

3. A good approximation for $Z(\lambda)$ from the branch cuts

There is an astonishingly good approximation for $Z(\lambda)$, which is dominated by the branch cuts:

$$
Z_{\mathrm{BC}}(\lambda) = -1.20711 \ln\left(\frac{(\lambda - \lambda_c^-)(\lambda - \lambda_c^+)}{\lambda_c^- \lambda_c^+} \right).
\tag{153}
$$

It is obtained by starting from the massless case $Z_{m=0}(\lambda) = -\ln(1 - \lambda/\lambda_c^+)$ with $\lambda_c^+|_{m=0} = 1$, and adding a similar term $-\ln(1 - \lambda/\lambda_c^-)$ for the negative tail. The prefactor was then determined by asking that the highest known moment, in Eq. (149), of order λ^{12} be given exactly. Then,

$$
\begin{aligned}
& Z(\lambda) - Z_{\mathrm{BC}}(\lambda) \\
& = 0.0496465 \lambda - 0.00117287 \lambda^2 \\
& \quad - 0.0000986924 \lambda^3 - 2.769730882007382 \times 10^{-6} \lambda^4
\end{aligned}
$$

$$
\begin{aligned}
& + 2.48119 \times 10^{-8} \lambda^5 - 5.57763 \times 10^{-11} \lambda^6 \\
& - 2.96177 \times 10^{-9} \lambda^7 - 1.82040 \times 10^{-9} \lambda^8 \\
& - 1.04881 \times 10^{-9} \lambda^9 - 5.56368 \times 10^{-10} \lambda^{10} \\
& - 2.25950 \times 10^{-10} \lambda^{11} + O(\lambda^{13}).
\end{aligned}
\tag{154}
$$

What is remarkable about this approximation, besides its accuracy in reproducing higher moments, is that both expected terms $\ln(1 - \lambda/\lambda_c^+)$ and $\ln(1 - \lambda/\lambda_c^-)$ appear with the *same* amplitude. By performing the inverse-Laplace transform for $v > 0$, one finds, defining $\tilde{v} = 1.20711 v$,

$$
\begin{aligned}
P_{\mathrm{BC}}(\dot{u}) = {} & \frac{e^{-\frac{1}{2}\dot{u}(\lambda_c^- + \lambda_c^+)}(-\lambda_c^- \lambda_c^+)^{\tilde{v}} \left(\frac{\dot{u}}{\lambda_c^+ - \lambda_c^-} \right)^{\tilde{v} - \frac{1}{2}}}{\sqrt{\pi}\, \Gamma(\tilde{v})} \\
& \times K_{\tilde{v} - \frac{1}{2}}\left(\frac{1}{2}\dot{u}[\lambda_c^+ - \lambda_c^-] \right) \theta(\dot{u} > 0) \\
& + \frac{e^{-\frac{1}{2}\dot{u}(\lambda_c^- + \lambda_c^+)}(-\lambda_c^- \lambda_c^+)^{\tilde{v}} \left(\frac{\dot{u}}{\lambda_c^- - \lambda_c^+} \right)^{\tilde{v} - \frac{1}{2}}}{\sqrt{\pi}\, \Gamma(\tilde{v})} \\
& \times K_{\tilde{v} - \frac{1}{2}}\left(\frac{1}{2}\dot{u}[\lambda_c^- - \lambda_c^+] \right) \theta(\dot{u} < 0).
\end{aligned}
\tag{155}
$$

K is the Bessel K function. The function $P_{\mathrm{BC}}(\dot{u})$ decays as $e^{-\lambda_c^+ \dot{u}}$ for $\dot{u}$ to ∞, and as $e^{-\lambda_c^- \dot{u}}$ for $\dot{u}$ to $-\infty$. When compared to the numerical inverse-Laplace transform, we find that this is a good approximation for all but small $\dot{u}$.

In the limit of $v = 0^+$, we know (see [24] for more details) that one can expand $\hat{P}(\lambda) = e^{vZ(\lambda)} = 1 + vZ(\lambda) + O(v^2)$, and that upon Laplace inversion one obtains

$$
P(\dot{u}) = (1 - vp')\delta(\dot{u}) + vp'\tilde{P}(\dot{u}) + O(v^2).
\tag{156}
$$

The first term represents events when the particle is pinned, and the second one yields the velocity distribution in an avalanche $\tilde{P}(\dot{u})$ via $Z(\lambda) = vp' \int d\dot{u}(e^{\lambda \dot{u}} - 1)\tilde{P}(\dot{u})$ where vp' is the probability that $t = t_0$ belongs to an avalanche. From the form Eq. (153) for $Z_{\mathrm{BC}}(\lambda)$ we get

$$
p'\tilde{P}_{\mathrm{BC}}(\dot{u}) = 1.20711 \left[\frac{e^{-\dot{u}\lambda_c^+}}{\dot{u}}\theta(\dot{u} > 0) + \frac{e^{-\dot{u}\lambda_c^-}}{|\dot{u}|}\theta(\dot{u} < 0) \right].
\tag{157}
$$

Note that for $\dot{u} > 0$, it is very similar to the result for the ABBM model with $m = 0$ [24] up to the different value for λ_c^+. More interestingly, it also gives a nontrivial prediction for the tail on the negative-velocity side in the avalanche regime.

4. Large-λ behavior

In order to obtain the small-$\dot{u}$ behavior of $P_{\mathrm{approx}}(\dot{u})$, one has to analyze $Z(\lambda)$ for $|\lambda| \to \infty$. For real λ, this is impossible since branch cuts appear at $\lambda = \lambda_c^\pm$. As we show in Appendix F, the behavior for $\lambda \to \pm i\infty$ *on the imaginary axis* can be calculated analytically, and is given by

$$
\begin{aligned}
Z_{\mathrm{asymp}}(\lambda) & = -\frac{15\sqrt[3]{6}\sqrt{\pi}\,\Gamma\left(\frac{5}{6}\right)}{\Gamma\left(\frac{1}{6}\right)^2}(|\lambda|m)^{2/3} \\
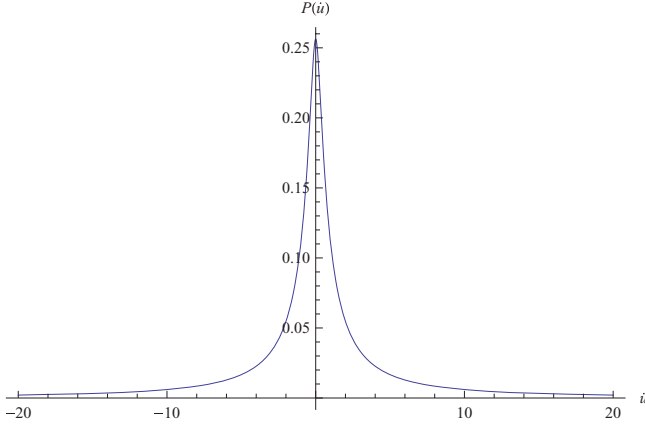& = -1.76006\,(|\lambda|m)^{2/3}.
\end{aligned}
\tag{158}
$$

FIG. 17. (Color online) The contribution of the large-λ behavior (158) to $P_{\text{asymp}}(\dot{u})$ at $v = 2$, $m = 1/4$, as given in Eq. (159).

The contribution of expression (158) to $P_{\text{asymp}}(\dot{u})$ at finite driving velocity v is

$$
\begin{aligned}
P_{\text{asymp}}(\dot{u}) &= \int_0^\infty \frac{d\lambda}{\pi} \cos(\lambda |\dot{u}|) e^{vZ(\lambda i)} \\
&\approx \int_0^\infty \frac{d\lambda}{\pi} \cos(\lambda |\dot{u}|) e^{-1.76006 \lambda^{2/3} v m^{2/3}} \\
&= -\frac{m^{2/3} v \exp\left(\frac{0.403877 m^2 v^3}{\dot{u}^2}\right)}{|\dot{u}|^{7/3}} \\
&\quad \times \left[1.43193 m^{2/3} v \text{Ai}\left(\frac{0.715967 m^{4/3} v^2}{|\dot{u}|^{4/3}}\right) \right. \\
&\quad \left. + 1.6923 |\dot{u}|^{2/3} \text{Ai}'\left(\frac{0.715967 m^{4/3} v^2}{|\dot{u}|^{4/3}}\right) \right].
\end{aligned}
$$

(159)

Ai is the Airy function, and the result Eq. (159) a positive function, peaked around zero, even for relatively large driving velocities (see Fig. 17). Its value at $\dot{u} = 0$ is

$$
P_{\text{asymp}}(0) = \frac{0.181215}{m v^{3/2}}.
$$

(160)

Note that while (159) is relevant at finite v, it does not contribute to the large-deviation function discussed below. We will discuss below its domain of applicability.

5. From $Z(\lambda)$ to $P_{\text{approx}}(\dot{u})$

The instanton equation can be solved numerically for any complex λ away from the branch cuts on the real axis at $\lambda > \lambda_c^+$ or $\lambda < \lambda_c^-$. This yields $Z(\lambda)$ for complex λ. We have performed the numerical inverse-Laplace transform for $Z(\lambda)$. A convenient choice of the contour is $\lambda = \alpha(1 \pm i)$, $\alpha > 0$ for $\dot{u} > 0$ and $\lambda = -\alpha(1 \pm i)$, $\alpha > 0$ for $\dot{u} < 0$. This gives an excellent numerical accuracy, except when $\dot{u}$ and v are both very small (< 0.1).

We can now compare with the asymptotic estimates of $P_{\text{approx}}(\dot{u})$ discussed above (see Fig. 18). Why the different approximations work or fail can be traced to an analysis of the inverse-Laplace transform. Depending on $\dot{u}$ and v, it is dominated by one of the three special points: $\lambda = 0$ for the perturbative approximation, valid for $v \to \infty$, $\lambda = \lambda_c^\pm$ for the
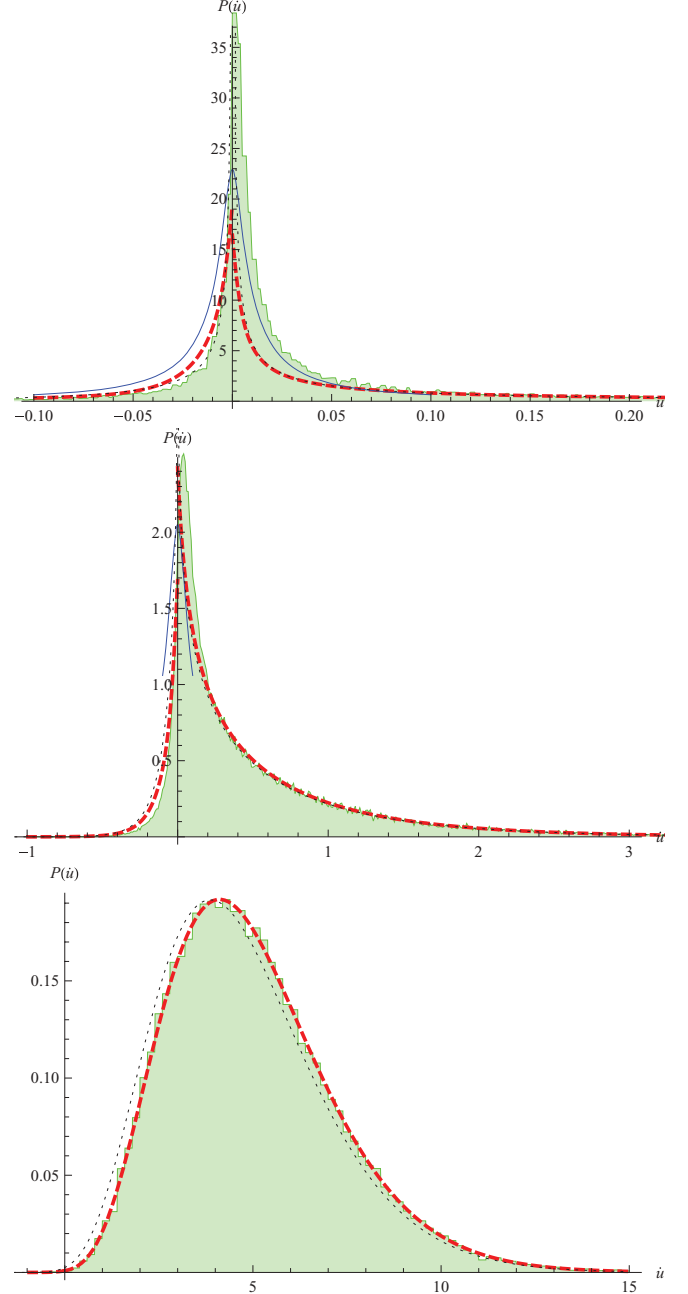

FIG. 18. (Color online) Comparison of $P_{\text{approx}}(\dot{u})$ obtained by numerically inverse-Laplace transforming $e^{vZ(\lambda)}$ (thick red dashed lines) with a simulation of the ABBM model (green shaded histogram plot) and the approximation (155) (black dotted lines). The mass is $m = 1/4$, and the driving velocities are from top to bottom: $v = 1/10$, $v = 1/2$, and $v = 5$. For the two smaller velocities we also plot $P_{\text{asymp}}(\dot{u})$, Eq. (159) (blue solid line).

tails, and $\lambda \to \pm i\infty$, for small $\dot{u}$, as long as v is not large enough so that $\lambda = 0$ dominates.

First the perturbative expansion in λ works well for large v. This will be quantified in Sec. VI, where we discuss the large-deviation function. Second, the branch-cut approximation (155) is a reasonable approximation to $P_{\text{approx}}(\dot{u})$ for all v and all $\dot{u}$, and becomes a good approximation in the tails. The latter can be expected since it uses the knowledge

about the branch-cut singularities at λ_c^+ and λ_c^-. Third, the approximation $P_{\text{asymp}}(\dot{u})$, given in Eq. (159), is a reasonable approximation at small $\dot{u}$, as long as v is small enough. For $v = 1/2$, e.g., it predicts, with relative precision of 10^{-3}, the value of $[P_{\text{approx}}(0^+) + P_{\text{approx}}(0^-)]/2$, where we note that $P_{\text{approx}}(\dot{u})$ jumps at 0, from 1.68172 for $\dot{u} = 0^-$ to 2.42249 at $\dot{u} = 0^+$. The worse disagreement at $v = 0.1$ is probably due to problems in the numerical inverse-Laplace transform [$\hat{P}(\lambda)$ oscillates strongly on the chosen contour]. For $v = 5$, it does not work.

6. The $\sqrt{\dot{u}}$ model as an approximation for ABBM

On Fig. 18, we show the data obtained for the probability distribution $P(\dot{u})$ from a numerical simulation of the ABBM model at $m = 1/4$ (green shaded area), compared to results obtained in this section. The driving velocities are $v = 1/10$, $1/2$, and 5 (from top to bottom). First compare with the result for $P_{\text{approx}}(\dot{u})$, obtained by numerically inverse-Laplace transforming $\hat{P}(\lambda)$ (thick red dashed line). The agreement is excellent for $v = 5$, and reasonable for $v = 1/2$ (it does not give well the peak for $\dot{u}$ close to 0, but quite well the tails), even on the negative side. For $v = 0.1$ only the tails are reasonably well approximated. (We can not, however, exclude numerical problems in the inverse-Laplace transform for $\dot{u} < 0.01$.)

G. Exact results for $m = 6/25$

While Eq. (115) can not be solved in closed form for generic m, and one had to resort to expansions or numerical solutions, there exists a magic value of the mass $m = 6/25$ for which there exist analytic solutions in closed form. These are known in the context of the Fisher-Kolmogorov equation and Abel equations, which are intimately linked to our problem as we now explain.

1. Fisher-Kolmogorov equation

Equation (115) is a second-order differential equation and it has many solutions that are characterized by a different set of values (κ_0, λ_0) defined by Eqs. (116) and (117) where t^* is an arbitrary time. One solution for $m = 6/25$ reads as [51]

$$\tilde{u}(t) = \frac{1}{(1 + De^{-5t/6})^2}, \qquad (161)$$

where D is an arbitrary parameter. Here, we used that traveling wave solutions of the Fisher-Kolmogorov equation satisfy Eq. (115), and that for a special value of the speed of the propagating wave it has the analytic solution Eq. (161) that corresponds to the special value $m = 6/25$ in our case.

For $D > 0$, it follows that $0 < \tilde{u} < 1$, and using Eq. (118) we get

$$Z(\lambda(\kappa),\kappa) = -\tfrac{6}{5}(\ln(1 - \sqrt{25\kappa/6}) + \sqrt{25\kappa/6}), \quad (162)$$

and we determine below which values λ takes as a function of κ. For $D < 0$, solution $\tilde{u}(t)$ [given by Eq. (161)] takes some value that is greater than 1 at two different times. If one chooses $t^* = -6\ln[(1 + \sqrt{6/(25\kappa)})/(-D)]/5$, then

$$Z(\lambda(\kappa),\kappa) = -\tfrac{6}{5}(\ln(1 + \sqrt{25\kappa/6}) - \sqrt{25\kappa/6}). \quad (163)$$

Here, $\tilde{u}$ takes all values greater than zero. If one takes $t^* = -6\ln[(1 - \sqrt{6/(25\kappa)})/(-D)]/5$, then $Z(\lambda(\kappa),\kappa) = \infty$ because the integration in Eq. (118) is over the divergence that happens at $t = 6\ln(|D|)/5$. Taking into account these results, one finds the following correlation functions:

$$\overline{e^{\lambda(\kappa)\dot{u}+\kappa a}} = e^{vZ(\lambda(\kappa),\kappa)}, \qquad (164)$$

$$\lambda(\kappa) = \begin{cases} 5\kappa/2 + 50\kappa^{3/2}/6^{3/2}, & D > 0 \text{ and } 0 \leqslant \kappa < 6/25 \\ 5\kappa/2 - 50\kappa^{3/2}/6^{3/2}, & D < 0 \text{ and } \kappa \geqslant 0. \end{cases}$$
$$(165)$$

In Eq. (164), the first and the second lines of Eq. (165) correspond to $Z(\lambda(\kappa),\kappa)$ given by Eqs. (162) and (163), respectively. Hence, the Laplace transform of the joint distribution of velocities and acceleration is known exactly on the curve $\lambda = \lambda(\kappa)$, which, upon expanding in κ can be translated into nontrivial relations between moments of this distribution.

2. Abel differential equation of the second kind

Next, we find a more general solution of Eq. (115) than in the previous section. Then, using it we obtain an exact result for $Z(\lambda,0)$ for some range of λ values. Additionally, we obtain an analytic expression for λ_c^+ that tells us about behavior of the tails of $P(\dot{u})$ for positive velocities [see Eq. (107)]. Introducing $A = \lambda/m - \kappa/m^2$ and $B = \kappa/m$, the set of Eqs. (111)–(113) can be rewritten as

$$\frac{dA}{dB} = \frac{B^2 - B - A}{mA}, \qquad (166)$$

$$\frac{dZ}{dB} = -\frac{B}{A}. \qquad (167)$$

Equation (166) is the so-called Abel differential equation of the second kind. Its parametric solution reads as Ref. [52]

$$B_C(s) = \frac{1}{4}E^2(s,C)s, \qquad (168)$$

$$A_C(s) = -\frac{5}{24}E^2(s,C)(\sqrt{1+s^3}E(s,C) + 2s), \quad (169)$$

$$E(s,C) = \int_0^s d\tau(1+\tau^3)^{-1/2} + C, \qquad (170)$$

where C is an arbitrary constant. We see that $B_C(0) = 0$ while $A_C(0) = -C^3 5/24$ can be arbitrary, meaning that we have found the family of solutions determined by parameter C. Then,

$$Z(\lambda_C(s),\kappa_C(s)) = -\int ds \frac{B_C(s)}{A_C(s)} \frac{dB_C(s)}{ds} + \text{const}, \quad (171)$$

where the constant is to be determined by knowing that $Z(0,0) = 0$.

For example, if we want to calculate

$$\overline{\exp(-C^3\dot{u}/20)} = \exp[vZ(-C^3/20,0)], \qquad (172)$$

we need to find first

$$Z\left(-\frac{1}{20}C^3,0\right) = -\int_{t_{C0}}^0 ds \frac{B_C(s)}{A_C(s)} \frac{dB_C(s)}{ds}$$

$$= \frac{3}{10}\int_{t_{C0}}^0 ds \frac{s}{\sqrt{1+s^3}}E(s,C), \quad (173)$$

where t_{C0} is defined as $E(t_{C0},C) = 0$. We find the analytic expression for

$$Z\left(-\frac{1}{20}C^3,0\right) = \frac{1}{15}\left(t_{C0}^3 + 1\right) {}_3F_2\left(\frac{5}{6},1,1;\frac{3}{2},2;t_{C0}^3 + 1\right)$$
$$- \frac{3}{5\sqrt{\pi}}\Gamma\left(\frac{7}{6}\right)\Gamma\left(\frac{4}{3}\right)$$
$$\times \sqrt{t_{C0}^3 + 1}\, {}_2F_1\left(\frac{1}{3},\frac{1}{2};\frac{3}{2};t_{C0}^3 + 1\right)$$
$$- \frac{3}{20}Ct_{C0}^2\, {}_2F_1\left(\frac{1}{2},\frac{2}{3};\frac{5}{3};-t_{C0}^3\right)$$
$$- \frac{1}{30}\left[-\sqrt{3}\pi - 3\ln\left(\frac{27}{16}\right)\right]. \quad (174)$$

Here, ${}_2F_1$ is the hypergeometric function and ${}_3F_2$ is the generalized hypergeometric function. t_{C0} is implicitly given by $E(t_{C0},C) = 0$, which could be rewritten as

$$E(t_{C0},0) = -C. \quad (175)$$

We find that $E(s,C) = C + s\, {}_2F_1(1/3,1/2;4/3;-s^3)$. The function $E(s,0)$ becomes complex for $s < -1$. For $s > -1$, it is increasing function of s, and satisfies

$$-\frac{\Gamma\left(\frac{1}{6}\right)\Gamma\left(\frac{4}{3}\right)}{2\sqrt{\pi}} \leqslant E(s,0) \leqslant \frac{\Gamma\left(\frac{1}{6}\right)\Gamma\left(\frac{4}{3}\right)}{\sqrt{\pi}}. \quad (176)$$

We see that for $\lambda_{\min} \leqslant \lambda = -C^3/20 < \lambda_{\max}$, where

$$\lambda_{\min} = -\frac{1}{20}\left[\frac{\Gamma\left(\frac{1}{6}\right)\Gamma\left(\frac{4}{3}\right)}{2\sqrt{\pi}}\right]^3 = -0.137843, \quad (177)$$

$$\lambda_{\max} = \frac{1}{20}\left[\frac{\Gamma\left(\frac{1}{6}\right)\Gamma\left(\frac{4}{3}\right)}{\sqrt{\pi}}\right]^3 = 1.10274, \quad (178)$$

there exists a solution of Eq. (175) and one can find t_{C0}. Since at $s = t_{C0}$ both $\lambda(s)$ and $\kappa(s)$ are zero, this constraint on λ might mean that a solution of Eq. (115) with boundary conditions $\kappa(t = 0) = 0$ and $\dot{\kappa}(t = 0) = \lambda$ reaches $[\dot{\kappa}(t),\kappa(t)] = (0,0)$, i.e., it is convergent, meaning that at large times it goes to zero. By considering numerically this instanton solution of Eq. (115) with given boundary conditions, one indeed sees that it starts to diverge for this value of λ and $\lambda_c^+ = \lambda_{\max}$. However, for $\lambda_{\min}$ the instanton solution is still convergent. The numerics gives $\lambda_c^- = -8.8219 < \lambda_{\min} = -0.1378$. In Fig. 19 we show the numerical result for $Z(\lambda,0)$. We conclude that the parametric solution [Eqs. (168)–(170)] does not "catch" whole $\kappa(t)$ dependence on time with given boundary conditions $\kappa(t = 0) = 0$ and $\dot{\kappa}(t = 0) = \lambda$ for $\lambda < \lambda_{\min}$.

Next, we solve $E(t_{C0},C) = 0$ perturbatively in C and find

$$t_{C0} = -C + \frac{C^4}{8} - \frac{C^7}{112} + \frac{C^{10}}{1792} - \frac{3C^{13}}{93184}$$
$$+ \frac{37C^{16}}{20873216} - \frac{75C^{19}}{793182208} + \mathcal{O}(C^{20}), \quad (179)$$

$$Z(\lambda,0) = \lambda + \frac{\lambda^2}{2} + \frac{25\lambda^3}{84} + \frac{125\lambda^4}{616}$$
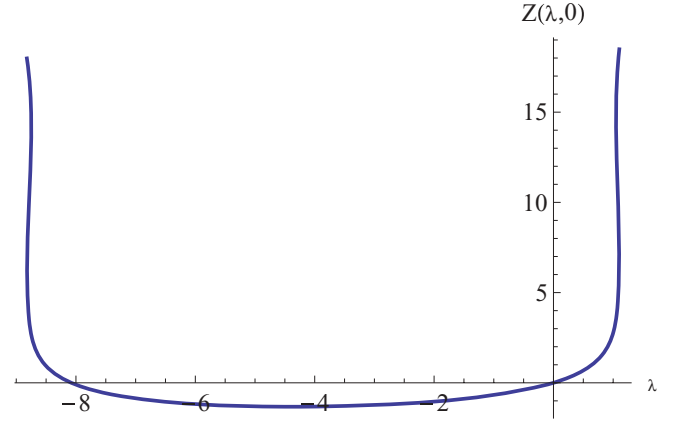$$+ \frac{375\lambda^5}{2548} + \frac{115625\lambda^6}{1039584} + \mathcal{O}(\lambda^7). \quad (180)$$

FIG. 19. (Color online) Numerical result for $Z(\lambda,0)$ is shown for $m = 6/25$.

Now, expanding Eq. (172) in $\lambda = -C^3/20$, one can find the moments $\overline{u^k}$ in agreement with Sec. V D and Appendix D.

VI. LARGE-DEVIATION FUNCTION

A. Definitions and numerical determination

It is suggestive that we "do a good job for large driving velocities" since when the particle does not move backward, all three models considered here are indistinguishable. We actually show below that the so-called *large-deviation* function coincides for all three models for $x > 0$. The large-deviation function is defined as the leading behavior for large driving velocity v of the distribution of instantaneous velocity $P(\dot{u})$ as follows:

$$F_v(x) := -\frac{\ln[P(xv)]}{v}, \quad (181)$$

$$F(x) := \lim_{v \to \infty} F_v(x). \quad (182)$$

Analogously, one defines, if that limit exists,

$$Z_v(\lambda) := \frac{\ln \overline{e^{\lambda\dot{u}}}}{v}, \quad (183)$$

$$Z(\lambda) := \lim_{v \to \infty} Z_v(\lambda). \quad (184)$$

If the limits exist, then for large v the Laplace transform

$$\overline{e^{\lambda\dot{u}}} = e^{vZ_v(\lambda)} = v\int dx\, e^{-vF_v(x)}e^{\lambda xv} \quad (185)$$

can be approximated by its saddle point, and $Z(\lambda)$ and $F(x)$ are related via a Legendre transform:

$$Z(\lambda) + F(x) = \lambda x, \quad (186)$$

$$\frac{d}{dx}F(x) = \lambda, \quad (187)$$

$$\frac{d}{d\lambda}Z(\lambda) = x. \quad (188)$$

It is assumed that $F''(x) > 0$. Note that $Z(\lambda)$ is easier to measure numerically than $F(x)$ since the former does not need binning.

Let us now review our numerical results and how they are consistent with the following scenario: (i) $Z_v(\lambda)$ becomes v

independent at large v for each model in some range of λ. (ii) The asymptotic curves coincide for $\lambda > \lambda^*$,

$$Z(\lambda) = Z_{\sqrt{u}}(\lambda) = Z_{ABBM}(\lambda) = Z_{tree}(\lambda), \qquad (189)$$

where

$$Z'(\lambda^*) = 0, \qquad (190)$$

i.e., the minimum of $Z(\lambda)$ is at λ^*. This corresponds to the point of zero velocity since Eq. (188) implies $x(\lambda^*) = 0$. Another way to state Eq. (189) is to say that, for $x > 0$,

$$F(x) = F_{\sqrt{u}}(x) = F_{ABBM}(x) = F_{tree}(x). \qquad (191)$$

We assumed that $Z'(\lambda) > 0$ for $\lambda > \lambda^*$. A simple argument, which shows that (189) and (191) hold, is given below. For $\lambda < \lambda^*$, the $Z(\lambda)$ for each model is dominated by negative velocities. Since the models differ for these velocities, there is no reason why their $Z(\lambda)$ should be the same, and consequently $F(x)$ for $x < 0$ is expected to be different for the different models.

Our numerical data for $Z_v(\lambda)$ are presented on the left of Fig. 20 for $m = 1/4$. First of all, we have checked through large-scale simulations (5×10^7 data points) that for the $\sqrt{u}$ model $Z_v(\lambda) = Z(\lambda)$ are velocity independent and given by the numerical solution of the instanton equation (101), using (103) (thick orange line). Only data for $v = 0.1$ are presented on the plot (dark gray-blue line, with error bars given by the dashed lines of the same color). Relative errors are $\leqslant 10\%$ for $-4.2 < \lambda < 1$.

We have then checked that $Z_v(\lambda)$ for the tree model converges, for $v \to \infty$, towards the numerical solution of the instanton equation (103) from above, while the ABBM model converges from below. (This fact is consistent with Figs. 2 and 3, where one observes that the probability distribution for the tree model has larger tails than for the ABBM model with inertia.) On Fig. 20, data for $v = 0.5$ and 2 are shown for the tree model, and for $v = 5$ for the ABBM model. Simulations for other velocities (not shown) confirm this picture. Note, however, that we have found convergence of the simulations of $Z_v(\lambda)$ for both ABBM and the tree model to $Z(\lambda)$ of the $\sqrt{u}$ model only in some domain $\lambda > \lambda^*$ and certainly not for $\lambda < \lambda^*$, corresponding to negative velocity, consistent with the above scenario. For $m = 1/4$ we find $\lambda^* = -4.26953$.

Once the $Z(\lambda)$ curves have been measured for each model, one can obtain the corresponding large-deviation functions via a numerical Legendre transform. On Fig. 20 we have plotted the large-deviation function, Legendre transform of $Z(\lambda)$ for the $\sqrt{u}$ model. Its minimum is at $x = 1$, and for large positive x it grows like $F(x) \approx \lambda_c^+ x + \text{const}$, with λ_c^+ given by Eq. (150). For large negative x, the growth is $F(x) \approx \lambda_c^- x + \text{const}$ with λ_c^- also given by Eq. (150). These slopes are indicated by the dashed curves in Fig. 20 (right).

B. Convergence of the large-deviation functions

We now show the main result of this section, namely, that the three models have the same large-deviation function in the region $0 < x < x_+$:

$$F(x) = F_{\sqrt{u}}(x) = F_{tree}(x) = F_{ABBM}(x) \quad \text{for all} \quad 0 < x < x_+, \qquad (192)$$

$$F(x_+) = F(0). \qquad (193)$$

The argument is simple and in fact much more general: Two models, which have the exact same dynamics for positive velocities, have the same large-deviation function in that interval. The idea is the following. Consider a simulation with a set of $N_v = e^{dv}$ data points. If $d > F(0)$, there will be negative velocities in a typical such set (with probability one at large v). But if $d < F(0)$, there will be none, again with probability one at large v. Consider any x such that $F(x) < F(0)$. We can then measure the value of $F(x)$ with arbitrary accuracy (as v becomes large) if we use e^{dv} data points with $F(x) < d < F(0)$ [in fact $d = F(x)^+$ is sufficient]. As stated above, this set almost surely does not contain negative velocities. Since the dynamics for the three models exactly coincides for trajectories with positive velocities, this shows the above property (192), provided at least for one of the models the large-deviation function *exists*. However, the latter is true for the $\sqrt{u}$ model since there $Z(\lambda)$ is v independent, which completes the argument.

The argument is based on considerations of under-sampling of rare events, and is reminiscent of similar considerations used for the multifractal spectrum of wave functions, e.g., when comparing the size-dependence exponents of participation ratios for a typical sample or disorder-averaged ones [53,54]. Here, the additional input is the identification of the dynamics for positive velocities. Note the restriction that $x < x_+$, which means that rare events with positive velocities but as rare as the negative velocity can not be controlled either. In the present case, we do not see a reason why the various functions $F(x)$ would not coincide for $x > x_+$. The restriction comes from the generality of the argument: One could for instance imagine a dynamics such that the particle jumps discontinuously from large positive velocities to negative ones. The above estimates are made more precise in Appendix I.

C. Large-deviation function in perturbation theory for small *m*

1. Expression obtained from previous results

In this section, we compute the large-deviation function for the $\sqrt{u}$ model in a perturbative expansion at small m. For $x > 0$, as argued above, it gives the result for all three models. A further discussion of this equivalence is given in Appendix C. We slightly generalize the discussion of the previous section by considering the large-deviation function for both velocity and acceleration defined as

$$F(x, y) = -\lim_{v \to \infty} \frac{\ln[P(xv, yv)]}{v}, \qquad (194)$$

where $x = \dot{u}/v$ and $y = a/v$. The connection to the generating function introduced in Eqs. (107) and (109) is through a Legendre transform in both variables, namely,

$$Z(\lambda, \kappa) = \max_{x, y} \{-F(x, y) + \lambda x + \kappa y\}. \qquad (195)$$

To compute $F(x, y)$ from $Z(\lambda, \kappa)$, one looks for (x_0, y_0) that satisfy $\partial_x F|_{x_0, y_0} = \lambda$ and $\partial_y F|_{x_0, y_0} = \kappa$ to get

$$F(x_0, y_0) = -Z(\lambda, \kappa) + \lambda x_0 + \kappa y_0. \qquad (196)$$

These formulas assume somehow the convexity of $F(x, y)$ and $Z(\lambda, \kappa)$, which we did not attempt to prove but seems to hold.

Now let us use our results from Sec. IV B to obtain $F(x, y)$ perturbatively in m. To this aim, we use Eq. (194) with
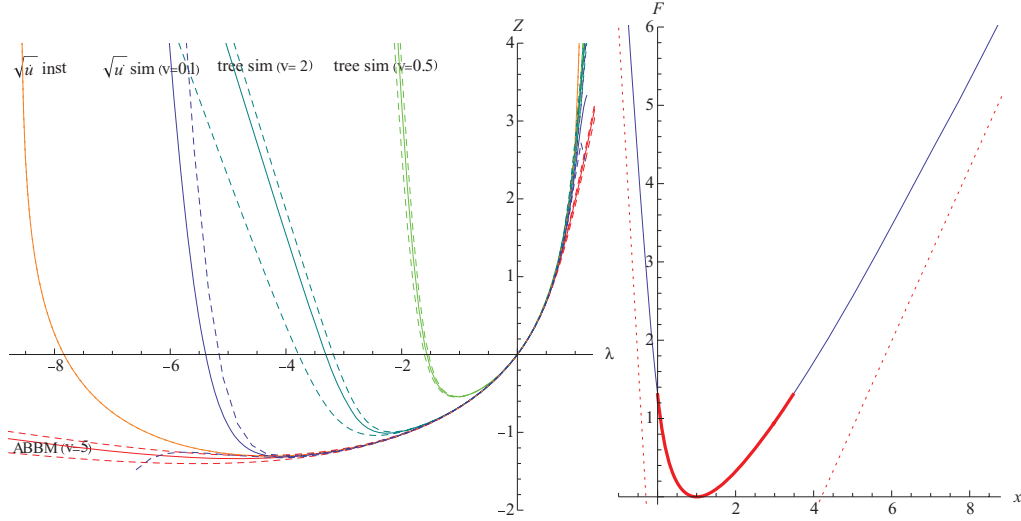
FIG. 20. (Color online) Left panel: Different curves for $Z(\lambda)$, $m = 1/4$: The numerical solution of the instanton equation (101) is used to obtain Z [see Eq. (103)] denoted as $\sqrt{\dot{u}}$ inst and shown by a thick orange line. Numerical simulation of this $\sqrt{\dot{u}}$ model for driving velocity $v = 0.1$ (gray-blue line), with an estimate of the numerical error bars (one-σ error, dashed curves of the same color). Within error bars, the simulation has converged to the orange curve $\sqrt{\dot{u}}$ inst; errors are small for $-4 \leqslant \lambda \leqslant 1$. The simulations for the tree model at $v = 2$ (dark green line) and $v = 0.5$ (bright green line), both with error bars (dashed line), show clear deviations from instanton solution at small v, but get closer to the latter for larger v. The last curve is a simulation of the ABBM model at $v = 5$ (red line). It has also converged to the orange curve within error bars. This is not the case for smaller driving velocities (not shown). All simulations are for 5×10^7 data points, apart from the one for ABBM, which has 93.000 data points. Due to the small number, the error bars in that case are underestimated. Right panel: The large-deviation function $F(x)$, obtained by performing a numerical Legendre transform of $Z(\lambda)$ given by the numerical solution of the instanton equation (101), and Eq. (103). We note $F(0) = F(3.47268) = 1.30459$. The thick red part is the domain for which $F(x) \leqslant F(0)$, which can be obtained with arbitrary precision from a simulation with negligible probability of negative velocity as explained in the text, hence must coincide for the three models. The dashed curves show the asymptotic behavior $\lambda_c^{\pm} x +$ const.

$P(\dot{u}, a)$ given by Eqs. (40) and (42)–(44) where c_3 and c_5 are determined by Eqs. (91) and (92), and $\dot{u}$ is restricted to positive values. We find

$$F(x, y) = \left(\frac{\tilde{y}^2}{2x} + x - \ln(x) - 1 \right) + \frac{\sqrt{m}\tilde{y}^3}{6x^2}$$
$$+ m \left(\frac{\tilde{y}^4}{48x^3} - \frac{\tilde{y}^2}{4x^2} + \frac{\tilde{y}^2}{4x} + \frac{x}{2} - \frac{1}{2x} - \ln(x) \right)$$
$$+ m^{3/2} \left(-\frac{\tilde{y}^5}{240x^4} - \frac{\tilde{y}^3}{36x^3} - \frac{\tilde{y}^3}{18x^2} \right) + \mathcal{O}(m^2), \tag{197}$$

where $\tilde{y} = \sqrt{m}\, y$.

Similarly, we obtain the large-deviation function for the velocity only, defined in Eq. (182). Legendre transforming the results of Sec. V E for $Z(\lambda)$ for small m, using (186), we get

$$F(x) = x - \ln(x) - 1 + m \left(\frac{x}{2} - \frac{1}{2x} - \ln(x) \right)$$
$$+ m^2 \left(-\frac{1}{12x^2} - \frac{5x}{12} + \frac{3}{4x} + \ln(x) - \frac{1}{4} \right) + \mathcal{O}(m^3). \tag{198}$$

We note that $F(x) = F(x, y = 0)$, which presumably holds to all orders.

One can check that convexity $F''(x) > 0$ holds for $x > m/(1 + m)$ for the two first orders in m. This indicates that the expansion is valid at small m only for $x \gg \mathcal{O}(m)$. We will see below, on the example of $m = 1/4$, that indeed the small-m

expansion is accurate for large enough x and breaks down for small x (see Fig. 21).

2. Equation from Fokker-Planck

From the Fokker-Planck equation it is possible to obtain a differential equation for the large-deviation function. Inserting the form $P(\dot{u}, a) = e^{-v F_v(x = \frac{\dot{u}}{v}, y = \frac{a}{v})}$ in the Fokker-Planck
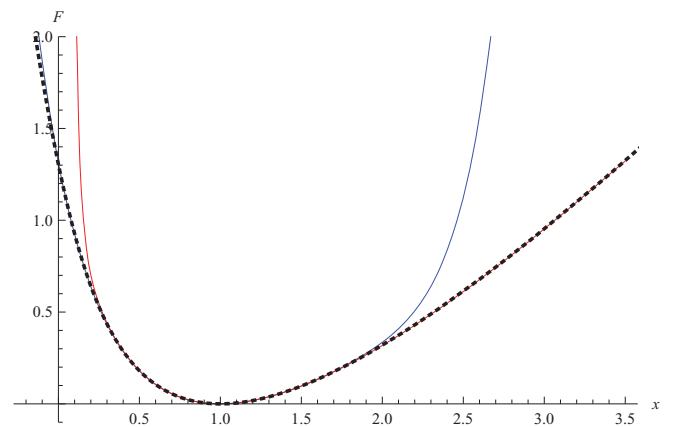

FIG. 21. (Color online) $F(x)$ for $m = 1/4$ as obtained by the numerical solution of the instanton equation (dashed line). Large-m expansion (207) to order $1/m^3$, thus two more orders in $(1 - x)$ as given in Eq. (207) (blue solid line); this approximation substantially deviates for $x > 2$. Small-m expansion (203), which works well at large x, but breaks down at about $x = 1/4$ (red solid line).

equation (39) we find that $F(x, y)$ satisfies, to dominant order at large v,

$$m^2 y \partial_x F - m(x + y - 1)\partial_y F + D(x)(\partial_y F)^2 = 0. \quad (199)$$

Here, $D(x) = x$ for the $\sqrt{u}$ model and $D(x) = |x|$ for the tree model. If we study this equation for $x > 0$, the two equations are the same. While the equation for the tree model can be studied for all x, the meaning of the one for the $\sqrt{u}$ model for $x < 0$ requires further analysis due to possible complex velocities.

We now use Eq. (199) and the emerging structure of the above perturbative results (197) and (198) to construct the expansion in m to higher orders. One way to analyze (199) is to perform a Taylor expansion around $y = 0$:

$$F(x, y) = F_0(x) + \sum_{n \geqslant 2} F_n(x) y^n, \quad (200)$$

where we assume $F(x) = F(x, y = 0)$. Then, the $F_n(x)$ obey the recursion relations $F_1(x) = 0$, $F_2(x) = F_0'(x)/[2(x - 1)]$, and for $k \geqslant 2$,

$$F_{k+1}(x) = \frac{1}{\sqrt{m}(x-1)(k+1)}\left[-kF_k(x) + \sqrt{m}F_{k-1}'(x) \right.$$
$$\left. + x\sum_{p=1}^{k-1}(p+1)(k-p+1)F_{p+1}(x)F_{k-p+1}(x)\right]. \quad (201)$$

If we assume that the structure of (197) holds to higher orders, in particular that there are no poles in $1/(x - 1)$, we find that the conditions for their cancellations order by order in m give enough conditions to determine $F_0(x)$ entirely. The form which we find by inspection is

$$F_k(x) = \sum_{n=0}^{\infty} m^{n + \frac{k-2}{2}} \sum_{p=k-1}^{p=n+k-1} \frac{a_{np}^k}{x^p} \quad (202)$$

for $k > 0$. One checks that the previous result (197) satisfies Eq. (199). One finally obtains

$$F(x) = F_0(x) = [x - \ln(x) - 1] + \frac{1}{2}m\left(x - \frac{1}{x} - 2\ln(x)\right)$$
$$+ m^2\left(\ln(x) - \frac{5x^3 - 9x + 1}{12x^2} - \frac{1}{4}\right)$$
$$+ m^3\left(\frac{x(107x^3 - 240x + 22) + 5}{144x^3} - 2\ln(x) + \frac{53}{72}\right)$$
$$+ m^4\left(\frac{669 - x[x(14809x^3 - 38610x + 2090) + 2905]}{8640x^4}\right.$$
$$\left. + 5\ln(x) - \frac{3895}{1728}\right) + O(m^5). \quad (203)$$

We have fixed the integration constant by requiring that $F(1) = 0$, a consequence of $\bar{u} = v$. Note that the above result satisfies $F'(1) = 0$ and $F''(1) = 1$, which is consistent with our analysis in Sec. IV C, namely, that the bulk of the distribution is the Gaussian (51) in the scaling region $|\dot{u} - v| \sim \sqrt{v}$. The first corrections to the Gaussian arise from $F'''(1) = -4/(2 + m)$

and may already be visible in the tail $|\dot{u} - v| \sim v^{2/3}$. This can be compared to the perturbative expansion of $F(x)$ around $x = 1$, given in Eq. (207) below. The complete large-deviation function describes the far tails $|\dot{u} - v| \sim v$. Another interesting feature is that one obtains an expansion for $\lambda_c^+(m)$ as

$$\lambda_c^+(m) = \lim_{x \to \infty} \frac{F(x)}{x} \quad (204)$$
$$= 1 + \frac{m}{2} - \frac{5m^2}{12} + \frac{107m^3}{144} - \frac{14809m^4}{8640} + O(m^5).$$

Finally, note that for large x, y the large-deviation function takes the form

$$F(x, y) \approx xg(y/x) \quad (205)$$

and that an ordinary differential equation can be written from Eq. (199) for $g(z)$.

D. Large-deviation function for large *m* and matching of small and large *m*

In Appendix C it is explained how to calculate the perturbative solution of $Z(\lambda)$ in powers of λ. Examining the results in powers of λ, keeping the complete m dependence of the coefficients, shows that it actually turns into a large-m expansion. Indeed one finds

$$Z(\lambda) = \lambda + \frac{\lambda^2}{2} + \frac{2\lambda^3}{3m + 6} + \frac{\lambda^4(5m + 6)}{16m^2 + 44m + 24}$$
$$+ \frac{2\lambda^5(103m^2 + 198m + 72)}{5(m + 2)(m + 6)(4m + 3)(9m + 4)}$$
$$+ \frac{\lambda^6(695m^4 + 4396m^3 + 7666m^2 + 4284m + 720)}{3(m + 2)^2(m + 6)(4m + 3)(9m + 4)(16m + 5)}$$
$$+ O(\lambda^7), \quad (206)$$

and each two orders more in λ come with an additional factor of $1/m$ at large m. We have obtained two more orders, which are not displayed here due to their length. Legendre transforming yields

$$F(x) = \frac{1}{2}(x - 1)^2 - \frac{2(x - 1)^3}{3m + 6}$$
$$+ \frac{(12 + 16m - 5m^2)(x - 1)^4}{4(m + 2)^2(4m + 3)}$$
$$+ \frac{4(61m^4 + 420m^3 - 338m^2 - 540m - 144)(x - 1)^5}{5(m + 2)^3(m + 6)(4m + 3)(9m + 4)}$$
$$+ \frac{(x - 1)^6}{6(m + 2)^4(m + 6)(4m + 3)^2(9m + 4)(16m + 5)}$$
$$\times [(17280 + 143136m + 386448m^2 + 239312m^3$$
$$- 488936m^4 - 556346m^5 - 3195m^6 + 5240m^7)]$$
$$+ O(x - 1)^7, \quad (207)$$

which is actually an expansion in $x - 1$ at fixed m, in other words, deviations from the Gaussian solution of Sec. IV C at large velocity. Again, we have obtained two more orders, which are not displayed here due to their length. Since it yields the derivatives $F^{(n)}(1)$ for any m, one can check that at small m they match the result obtained from Eq. (203) above.

From the above expansion one can now obtain a good approximation for $F(0)$, which gives an estimate of the probability

$$p \sim e^{-vF(0)} \tag{208}$$

for negative velocities at large v, and improves on the estimate of Sec. IV C.

As a test, we can compare the small-m expansion (203) and the large-m expansion (207) with the numerical solution of the instanton equation, followed by a Legendre transform (in the form of a parametric representation). The result for $m = 1/4$ is shown on Fig. 21. One sees that the small-m expansion works well for large x, but breaks down for $x \to 0$, while the large-m expansion converges for $x = 0$, but may have a finite radius of convergence in $x - 1$. Taking both expansions together, we have an analytical approximation for the range $0 < x < x_+$ drawn in red in Fig. 20 in its right part of Sec. VI A where the large-deviation functions for the three models have been argued to coincide.

E. Large-deviation function for $m = 6/25$

Here, we determine exactly, in a parametric form, the large-deviation function for the special value of the mass $m = 6/25$ and for a certain range of values for x, using the results obtained in Sec. V G2. One finds $F(x > 0)$, using Eq. (186), where $Z(\lambda = -C^3/20)$ is determined by Eq. (174). In Eq. (187), x takes the values

$$\begin{aligned} x\left(-\frac{C^3}{20}\right) = \frac{1}{3C^2 t_{C0}} &\left[4\sqrt{t_{C0}^3 + 1}\, t_{C0}^3 \,_2F_1\left(\frac{5}{6}, 1; \frac{3}{2}; t_{C0}^3 + 1\right) \right. \\ &- 6C t_{C0}^2 + 3t_{C0}^3 \,_2F_1\left(\frac{1}{2}, \frac{2}{3}; \frac{5}{3}; -t_{C0}^3\right) \\ &\left. + \frac{18\Gamma\left(\frac{7}{6}\right)\Gamma\left(\frac{4}{3}\right)\left(-t_{C0}^3\right)^{2/3}}{\sqrt{\pi}} \right], \end{aligned} \tag{209}$$

where t_{C0} is given by Eq. (175). This expression is real as long as $t_{C0} > -1$.

VII. THERMAL AND QUANTUM FLUCTUATIONS

As long as we neglect backward trajectories, it is possible to include thermal and quantum fluctuations. Here, we obtain some new results within that approximation. We then discuss its expected range of validity.

A. Classical systems: Thermal fluctuations

For a classical system in presence of a thermal noise, we can generalize the equation of motion in the laboratory frame (21) and (22) as

$$m\dddot{u}(t) + \eta\dot{u}(t) = \mu^2[v - \dot{u}(t)] + \partial_t F(u(t)) + \xi_T(t). \tag{210}$$

To remain slightly more general, and cover the case of a colored noise, we define the correlations of the noise as

$$\langle \xi_T(t)\xi_T(t') \rangle = B(t - t'). \tag{211}$$

The standard thermal white noise is

$$B(t) = B_T(t) = 2\eta T\delta(t). \tag{212}$$

Hence, when we can neglect the backward motion, and for $F(u)$ a Brownian landscape, the problem reduces again to a Langevin equation for the velocity,

$$m\dddot{u}(t) + \eta\ddot{u}(t) = \mu^2[v - \dot{u}(t)] + \sqrt{\dot{u}}\xi(t) + \dot{\xi}_T(t), \tag{213}$$

in presence of both a thermal noise and a noise generated by the quenched disorder. It still describes the equation of motion for the center-of-mass velocity of an elastic manifold moving in a Brownian force landscape in presence of a thermal noise, under the same (but more stringent) approximation of neglecting any backward movement of the interface (i.e., even of a piece of it). Indeed, for forward motion, the general argument given in Refs. [24–26] (Sec. IV A) still applies.

Also, note that the Langevin equation (213) defines a noisy version of the $\sqrt{\dot{u}}$ model, as a legitimate model provided one accepts complex velocities which arise from backward trajectories. It turns out that (213) can be solved exactly for an arbitrary noise correlator $B(t)$. This is remarkable since except when $\dot{\xi}(t)$ is a white noise itself (see below), no simple Fokker-Planck version seems to exist. However, within the MSR formalism, the problem is much simpler. The Laplace transform of the velocity distribution can be written as in Eq. (99), where the dynamical action $S[\dot{u}, \tilde{u}]$ contains the additional term

$$-\frac{1}{2} \int_{tt'} \tilde{u}(t)\tilde{u}(t') \partial_t \partial_{t'} B(t - t') \tag{214}$$

$$= -\frac{1}{2} \int_{tt'} \partial_t \tilde{u}(t) \partial_{t'} \tilde{u}(t') B(t - t'). \tag{215}$$

The derivation follows the same steps as in Sec. V B. The action is still linear in $\dot{u}$, hence the instanton equation (101) is unchanged, and inserting this equation in the action gives

$$\overline{\langle e^{\int \lambda \dot{u}(t_0)} \rangle} = e^{vZ(\lambda) + \frac{1}{2}\int_{tt'} \partial_t \tilde{u}(t) \partial_{t'} \tilde{u}(t') B(t - t')} \tag{216}$$

using that $\tilde{u}(t)$ vanishes at $t = \pm\infty$, with the same $Z(\lambda) = \mu^2 \int_t \tilde{u}(t)$ as in Eq. (103). For a thermal noise, it gives

$$\overline{\langle e^{\int \lambda \dot{u}(t_0)} \rangle} = e^{vZ(\lambda) + \eta T \int_t [\partial_t \tilde{u}(t)]^2}. \tag{217}$$

Note that a double average is performed over thermal fluctuations and disorder realizations.[8] Note also that these results can be obtained from the general expression given in Ref. [26] [see Eq. (6) there], valid for an arbitrary forward driving and a forward motion $w(t)$, by substituting $w(t) \to vt + \xi_T(t)/\mu^2$ and performing the Gaussian average over ξ_T.[9]

The calculation of the contribution of the noise requires a small-time cutoff. For standard thermal white noise with no intrinsic cutoff, (217) can be evaluated only for a nonzero inertial mass, which provides the small-time cutoff. Its evaluation turns out to be remarkably simple, as we now show: Multiplying the instanton equation (101) by $\partial_t \tilde{u}$, it can

---

[8]Note that here the natural unit of temperature is $m_\mu v_\mu^2 = \mu^6/\sigma^2$ as can be seen from Eq. (217) and using that the dimension-full instanton solution is $\tilde{u}_{\lambda,m}^{\text{dimfull}}(t) = \frac{\mu^2}{\sigma}\tilde{u}_{\lambda v_\mu, m\mu^2/\eta}^{\text{dimless}}(t/\tau_\mu)$. The model now depends on three dimensionless parameters m, v, and T in the units defined here.

[9]μ here is noted m there.

be rewritten, for $t < t_0$, as

$$-\partial_t \left[\frac{m}{2} [\partial_t \tilde{u}(t)]^2 + W(\tilde{u}(t)) \right] = -\eta [\partial_t \tilde{u}(t)]^2, \quad (218)$$

$$W(\tilde{u}) = \frac{\mu^2}{2} \tilde{u}^2 - \frac{\sigma}{3} \tilde{u}^3. \quad (219)$$

This can be interpreted as a classical particle of position variable $\tilde{u}(t)$, undergoing (backward in time) a damped motion in a potential $W(\tilde{u})$. Integrating over time we find

$$\eta \int_{-\infty}^{t_0} dt (\partial_t \tilde{u})^2 = \left[\frac{m}{2} [\partial_t \tilde{u}(t)]^2 + W(\tilde{u}(t)) \right]_{-\infty}^{0} = \frac{\lambda^2}{2m}, \quad (220)$$

using that $\tilde{u}(t_0) = 0$ and $\tilde{u}'(t_0) = \lambda/m$, as well as that $\tilde{u}(t)$ decays to zero at $t = -\infty$. In other words, the total dissipated energy is the total initial energy since the fictitious particle settles to rest at $t = -\infty$. Hence, we find the exact result for any m and v:

$$\overline{\langle e^{\int \lambda \dot{u}(t_0)} \rangle} = e^{v Z(\lambda) + \frac{T}{2m} \lambda^2}. \quad (221)$$

The new term corresponds to the thermal broadening (i.e., $\dot{u} \to \dot{u} + \delta \dot{u}$) of the $T = 0$ velocity distribution by a Gaussian of variance $\langle \delta \dot{u}^2 \rangle^c = \frac{T}{2m}$. It can be interpreted as the system reaching kinetic-energy equipartition, as in the system without disorder. Keeping only the terms of $O(\lambda)$ and $O(\lambda^2)$ in Eq. (221) leads to the large-v Gaussian distribution (46) with $T_{\text{eff}} \to T_{\text{eff}} + T$, and indicates that at large v negative velocities are negligible when $T + T_{\text{eff}} \ll mv^2$. More precisely, a new large-deviation function at large v can be defined if one scales $T \sim v$, i.e., in the high-temperature, high-driving-velocity limit. The Legendre transform of $Z(\lambda) + \theta \lambda^2/2$ yields to $F_\theta(x)$. Defining $\theta = T/(mv v_\mu^2)$, we have

$$P(\dot{u}) \sim e^{-v F_\theta(x = \frac{\dot{u}}{v})}, \quad (222)$$

$$F'(x) = F_\theta'(x + \theta F'(x)). \quad (223)$$

For the case $m = 0$ (ABBM model without inertia), we find using $F_\theta(1) = 0$

$$F_\theta(x) = (x - 1) \left[\frac{1}{2} + \frac{x - \theta}{x + \theta + \sqrt{4\theta + (x - \theta)^2}} \right]$$
$$- \ln \left(\frac{1}{2} (x - \theta + \sqrt{4\theta + (x - \theta)^2}) \right). \quad (224)$$

The second solution that follows from Eq. (223) is not applicable since it does not give Gaussian distribution expected at large v (Sec. IV C). This formula should, following the general argument given in Sec. VI, also hold in the positive velocity region $x > 0$ for the original ABBM model (without inertia) and with temperature, even though it can not be solved exactly because of possible backward motion due to thermal fluctuations. Extension of Eq. (224) in presence of inertia can be studied using the array of methods introduced in this paper, but we refrain from doing so here.

The result (221) is remarkable since the effect of thermal fluctuations is exactly Gaussian, despite the presence of quenched randomness, which is highly nonlinear. This property can be generalized and traced to the fact that the noise dissipation satisfies the fluctuation dissipation relation (FDR), i.e., for *an equilibrium* thermal bath. To see that, consider a slightly more general bath and response function, in frequency space,

$$R^{-1}(\omega) = -m\omega^2 + \mu^2 + \eta(\omega) i \omega, \quad (225)$$

where $\eta(\omega)$ is an even function in ω. The classical FDR reads as

$$2T \eta(\omega) = B(\omega). \quad (226)$$

Since the response function is changed, the instanton equation becomes different. It involves the transpose of the inverse response and reads as

$$(m \partial_t^2 + \mu) \tilde{u} - \sigma \tilde{u}^2 + \int_\omega e^{i\omega t} \eta(\omega) i \omega \tilde{u}(\omega) = 0. \quad (227)$$

Again, multiplying with $\partial_t \tilde{u}(t)$ and integrating over time yields

$$\frac{\lambda^2}{2m} = \int_\omega \eta(\omega) \omega^2 \tilde{u}(\omega) \tilde{u}(-\omega). \quad (228)$$

Hence,

$$\frac{1}{2} \int_{tt'} \partial_t \tilde{u}(t) \partial_{t'} \tilde{u}(t') B(t - t') = \frac{\lambda^2}{2m} \quad (229)$$

if the FDR holds. Equation (216) again implies Eq. (217).

Formula (216) also allows us to compute $\overline{e^{\lambda \dot{u} + \kappa a}}$ and the joint distribution of velocity and acceleration, replacing $Z(\lambda)$ by $Z(\lambda, \kappa)$ and $\tilde{u}(t)$ by the solution of the instanton equation with boundary conditions (116) and (117). The formula (217), however, can not be used, as it contains a divergent integral since $\tilde{u}(t)$ has a jump of κ/m at t_0. This is because the distribution of acceleration is not well defined, unless we add an intrinsic small-time cutoff to the thermal bath, i.e., the mass is not sufficient to act as a cutoff. It can be seen within the large-v analysis of Sec. IV C since $\langle a^2 \rangle$ is defined by the same integral with an additional ω^2 in the numerator.

A non-Gaussian contribution to the velocity distribution can arise from a Gaussian noise *if it is a nonequilibrium one*, such as, for instance colored noise with a frequency-independent constant-friction dissipation term η. We mention here one simple example, when $\dot{\xi}(t)$ is a white noise, $\langle \dot{\xi}(t) \dot{\xi}(t') \rangle = 2D\delta(t - t')$, i.e., $\xi(t)$ is a Brownian. Then, it is easy to see that for $m = 0$ one recovers the result for the ABBM model without inertia (8) for $P(\dot{u})$ with the replacement

$$P_{v,D}(\dot{u}) = A P_{v+D, D=0}(\dot{u} + D). \quad (230)$$

This is the only case which is amenable to a Fokker-Planck equation (with $\dot{u} \to \dot{u} + D$ in the diffusion term). Not, of course, that negative velocities are simply neglected, hence the normalization factor A.

B. Quantum system

The extension to the quantum system in presence of a bath is straightforward. It can be done by generalizing the MSR methods of Refs. [24,26] to the Keldysh path integral. Let us

write the Keldysh action for a quantum particle in a Brownian-force landscape. The Keldysh path integral over the fields $u(t), \hat{u}(t)$ between an initial and a final time involves e^{-S_K} with Keldysh action $S_K = S_K^0 + S_K^1$ and

$$S_K^0 = \int_{tt'} \int_{t'} i\hat{u}(t) G_0^{-1}(t-t') u(t')$$
$$- \frac{1}{2} \int_{tt'} i\hat{u}(t) B(t-t') i\hat{u}(t'), \quad (231)$$

$$S_K^1 = \frac{i}{\hbar} \int_t \sum_{\epsilon=\pm 1} \epsilon V\left(u(t) + \epsilon \frac{\hbar}{2}\hat{u}(t)\right), \quad (232)$$

$$S_K^2 = \frac{i\mu^2}{2\hbar} \int_t \sum_{\epsilon=\pm 1} \epsilon \left(u(t) + \epsilon \frac{\hbar}{2}\hat{u}(t) - w(t)\right)^2 \quad (233)$$

$$= \int_t i\hat{u}(t) \mu^2 [u(t) - w(t)]. \quad (234)$$

The path integral can be expressed alternatively in terms of the upper and lower Keldysh fields $u^{\pm}(t) = u(t) \pm \frac{\hbar}{2}\hat{u}(t)$. The form of the functions $G_0^{-1}(t)$ and $B(t)$ depends on the details of the bath. One convenient choice is

$$S_K^0 + S_K^2 = \int_t i\hat{u}_t \left(m\partial_t^2 + \eta\partial_t - \mu^2\right) u_t$$
$$- \frac{1}{2} \int_{tt'} i\hat{u}_t B(t-t') i\hat{u}_{t'} + \int_t i\hat{u}_t \mu^2 w_t \quad (235)$$

with

$$B(\omega) = \eta\hbar\omega \coth(\beta\hbar\omega/2), \quad (236)$$

which for $\eta > 0$ represents an Ohmic bath. A realistic bath has a large-frequency cutoff ω_c. After averaging over disorder, the system is described by same Keldysh action with S_K^1 replaced by

$$S_K^1 = \frac{1}{2\hbar^2} \int_{tt'} \sum_{\epsilon,\epsilon'=\pm 1} \epsilon\epsilon' R\left(u_t - u_{t'} + \frac{\hbar}{2}(\epsilon\hat{u}_t - \epsilon'\hat{u}_{t'})\right). \quad (237)$$

This is because the Keldysh path integral is normalized to unity.

In the classical limit $\hbar \to 0$, one recovers the classical MSR functional with the thermal white noise $B(\omega) = 2\eta T$ and the usual disorder part

$$S_1^{\text{classical}} = -\frac{1}{2} \int_{tt'} i\hat{u}_t i\hat{u}_{t'} \Delta(u_{xt} - u_{xt'}). \quad (238)$$

$\Delta(u) = -R''(u)$ is the correlator of the pinning force. Note that $i\hat{u}$ is sometimes denoted by $\hat{u}$ in the MSR formalism.

Now we can treat the case of a Brownian-force landscape, choosing

$$R(u) = R(0) - \Delta(0)\frac{u^2}{2} + \sigma\frac{|u|^3}{6}. \quad (239)$$

This corresponds to $\Delta(u) = \Delta(0) - \sigma u$. Inserting this into Eq. (237), we obtain a complicated expression. However, if

we make the replacement

$$\text{sgn}[u^{\epsilon}(t) - u^{\epsilon'}(t')] \to \text{sgn}(t-t') \quad (240)$$

for all four couples $(\epsilon, \epsilon') = (\pm 1, \pm 1)$, then it simplifies into

$$S_K^1 = \frac{1}{2} \int_{tt'} \hat{u}_t \hat{u}_{t'} [\Delta(0) - \sigma(u_t - u_{t'})\text{sign}(t-t')].$$

The observable we are computing is the following average over the Keldysh action:

$$\hat{P}[\lambda] = \langle e^{\int_t \lambda_t \dot{u}_t} \rangle_{S_K}. \quad (241)$$

The study of more general observable is left for the future. To recover the velocity theory we define

$$i\hat{u}_t = -\partial_t \tilde{u}_t, \quad (242)$$

and consider $\tilde{u}_t$ vanishing at $t = \pm\infty$. It is very similar to what is done in Ref. [26], and to which we refer for details. It yields, after integration by parts,

$$S_K^1 = -\sigma \int_{tt'} \tilde{u}_t \tilde{u}_{t'} \dot{u}_t, \quad (243)$$

$$S_K^0 + S_K^2 = \int_t \tilde{u}_t \left(m\partial_t^2 + \eta\partial_t - \mu^2\right) \dot{u}_t$$
$$- \frac{1}{2} \int_{tt'} \partial_t \tilde{u}_t B(t-t') \partial_{t'} \tilde{u}_{t'} - \int_t i\tilde{u}_t \dot{w}_t. \quad (244)$$

Integration over $\dot{u}_t$ leads to the instanton equation (101), and inserting its solution into the action, we find again for $w(t) = vt$ the same result (216). Note, however, that for any nonzero $\hbar$ the bath cutoff time is needed to get a finite result: the mass only cutoff leads to a logarithmic divergence when inserting into Eq. (216). Since they require the corresponding dissipation related by FDR, we leave explicit calculations to future studies. To summarize, however, one can say that everything works as if the quantum system is described by a semiclassical equation of motion with the noise correlator (236).

Of course, there are two crucial ingredients here: (i) the Brownian-disorder-force landscape; (ii) the approximation (240). For $\epsilon' = \epsilon$, it amounts to neglecting any trajectory with backward motion. We see, however, that for $\epsilon' = -\epsilon$ the approximation can not be correct at short time differences $t - t'$, even for forward-only trajectories. This should be valid if this time scale is much smaller than the other ones considered here. A more detailed discussion of the validity of this approach is left for the future.

VIII. CONCLUSIONS AND DISCUSSION

In this paper, we studied an extension of the ABBM model including inertia, i.e., the motion of a particle of inertial mass m driven at externally imposed average velocity $v > 0$, in a 1D Brownian-random-force landscape in presence of damping. Its main interest, besides modeling a particle, is that in some cases it describes the center-of-mass dynamics of an interface in a Brownian correlated disorder. When all the segments of the interface move forward it is certainly true, and in more general situations it remains to be understood. For any m, this model can also be derived for the center of mass of a manifold with inertia in a short-range disorder potential, in the limit of a fully connected model (infinite-ranged interactions). In that sense,

it is a mean-field approximation. Whether that property also extends to finite-range interactions in high enough internal space dimension d, as is the case for $m = 0$ for $d > d_c$, remains to be understood. Our aim here was to calculate exactly, or using approximate methods, the distribution of the instantaneous velocity and of the acceleration for this particle model.

We started by recalling the $m = 0$ limit, which is exactly solvable (standard ABBM model). It is characterized by a relaxation time scale τ_μ, a spatial scale S_μ, and a velocity scale $v_\mu = S_\mu / \tau_\mu$ (see Sec. II). For $v < v_\mu$, the motion proceeds via avalanches, while for $v > v_\mu$ the motion becomes smoother. In presence of inertia $m > 0$, the ABBM model can not easily be solved because backward motion occurs and induces memory effects. Numerical simulations and qualitative arguments showed new characteristic time scales for oscillations τ_0, and damping τ_m, and new velocity scales $v_0 = S_\mu / \tau_0$ and $v_m = S_\mu / \tau_m$ (Sec. III). An avalanche regime survives for $v < \min(v_m, v_\mu)$ similar to the one for $m = 0$ except that the smallest avalanches have merged into bigger ones. As the mass increases, overshoots and oscillations become more pronounced before the damping allows relaxation into a metastable state. As v increases further, the motion becomes smoother, but oscillations persist. As a general rule, the inertia tends to make the motion less jerky and to smoothen the abrupt jumps of a center-of-mass position in time. At the same time, the distribution of velocities evolves from being strictly positive but with a divergent limit $P(\dot{u} = 0^+) = \infty$ for $m = 0$ and $v < 1$, corresponding to intermittent motion where the particle is part of the time at rest, to developing a finite weight for negative velocities and a finite $P(\dot{u} = 0)$, corresponding to oscillatory motion.

To make quantitative progress we introduced two variants of the model which share the exact same dynamics with the ABBM model for all forward trajectories, and are analytically more tractable. The analysis of the first, the tree model, is based on a Fokker-Planck equation. The study of the second one, the $\sqrt{\dot{u}}$ model, is based on a saddle-point equation of the dynamical action. For both of them, we calculated the joint distribution of acceleration and velocity perturbatively in small and large mass. The $\sqrt{\dot{u}}$ model could also be solved exactly for a magic value of the mass in terms of hypergeometric functions, and was studied with very high precision for other values of the mass. From these variant models we obtained two sets of results for the ABBM model:

(i) *At large driving velocity*: Since by increasing v the probability distribution for negative velocities decreases, all the considered models become more and more similar. The bulk of the velocity distribution, i.e., for velocities $|\dot{u} - v| = O(v)$, then tends to the same Gaussian. To characterize more accurately the tails, we defined for each model the large-deviation function which describes the rare events when the instantaneous velocity $\dot{u}$ deviates from the average v. We proved that these large-deviation functions become identical for positive $\dot{u}$ at large v for the three models, and obtained analytical expressions at small and large m and for the magic value of the mass.

(ii) *At any driving velocity*: We compared the three models and discuss differences and similarities. Although agreement

is not exact anymore, some features of the ABBM model are, in some cases, quite well reproduced.

Finally, we showed how thermal and quantum fluctuations can also be treated within the approximation of neglecting backward trajectories. For thermal fluctuations, it is expected to be a reasonable approximation at fixed v only for small T or for any T at large v. For quantum fluctuations, the discussion is more subtle but basically it should hold within a semiclassical approximation.

In conclusion, this paper proposes a first step to the description of classical and quantum avalanches of pinned elastic systems in presence of inertia, and the effect of driving. A more elaborate theory should incorporate barrier crossing by thermal and quantum fluctuations, and a treatment of memory and oscillation effects. However, we believe that we have introduced a useful framework. For instance, a key observable is $Z(\lambda) = \frac{1}{v} \ln \overline{e^{\lambda \dot{u}}}$, which in the $\sqrt{\dot{u}}$ model is independent of v, and is well characterized by branch-cut singularities describing the tails of the velocity distribution. At the same time, as $v \to 0^+$, it describes the avalanche dynamics. Hence, numerical or experimental determination of this quantity in realistic systems could help developing further understanding.

It would be interesting to extend the current analysis to different time-dependent and space-dependent driving, as well as to analyze the spatial correlations of the probability distribution taking into account the spatial extension of the interface and not just its center-of-mass position. Additionally, due to retardation effects appearing in soft magnets [4], there is a need to generalize the current approaches and to use a more general equation of motion, with a more general response function. Finally, in quantum systems where velocity translates into current, developing a more general connection with the full counting-statistics problem would be very interesting.

APPENDIX A: PERTURBATION THEORY AT SMALL *m* FOR $P(\dot{u})$ FOR THE TREE MODEL

In this Appendix, we give details on the perturbation theory discussed in Sec. IV B. We start with the differential equation (41) with $n = 0$. It has the solution

$$F_0(a, u) = \sqrt{\frac{\pi}{2}} \sqrt{\dot{u}} c_1(\dot{u}) \mathrm{erfi}\left(\frac{a}{\sqrt{2}\sqrt{\dot{u}}}\right) + c_2(\dot{u}), \quad \text{(A1)}$$

where erfi denotes the imaginary error function $\mathrm{erfi}(z) = \mathrm{erf}(iz)/i$. In order to have properly defined moments $\overline{a^i \dot{u}^j}$, the distribution function has to decay exponentially fast at

large a and $\dot{u}$. This implies that $c_1(\dot{u}) = 0$. Next,

$$F_1(a,\dot{u}) = c_4(\dot{u}) + \frac{1}{2}\left[-\frac{1}{3}a^3 c_2(\dot{u}) + a\dot{u}c_2(\dot{u}) - 2a\dot{u}^2 c_2'(\dot{u})\right], \tag{A2}$$

$$F_2(a,\dot{u}) = \frac{1}{2}a^2\dot{u}^3[-vc_2'(\dot{u}) + \dot{u}c_2'(\dot{u}) - \dot{u}c_2''(\dot{u})]_2F_2\left(1,1;\frac{3}{2},2;\frac{a^2}{2\dot{u}}\right) + \frac{1}{72}a^6 c_2(\dot{u}) + \frac{1}{48}a^4\dot{u}[8\dot{u}c_2'(\dot{u}) - 5c_2(\dot{u})] - \frac{1}{6}a^3 c_4(\dot{u})$$

$$+ \frac{1}{4}a^2\dot{u}^2[2\dot{u}^2 c_2''(\dot{u}) + vc_2(\dot{u}) - \dot{u}c_2(\dot{u})] + \sqrt{\frac{\pi}{2}}\sqrt{\dot{u}}c_5(\dot{u})\text{erfi}\left(\frac{a}{\sqrt{2}\sqrt{\dot{u}}}\right) - \frac{1}{2}a\dot{u}[2\dot{u}c_4'(\dot{u}) - 5c_4(\dot{u})] + c_6(\dot{u}), \tag{A3}$$

where $_2F_2(a;b;z)$ is a generalized hypergeometric function. The first line of Eq. (A3) has to vanish due to its large-a behavior, which gives us a differential equation for $c_2(\dot{u})$. Solving it, we obtain

$$c_2(\dot{u}) = c_3(-1)^v\Gamma(1 - v, -\dot{u}) + c_4. \tag{A4}$$

Analyzing it, we conclude that $c_3 = 0$. Then, finally we obtain that $F_0(a,\dot{u}) = c_4$. Since the distribution has to be normalized by $\int da\,d\dot{u}\,P(\dot{u},a) = 1$ for every m, we conclude that $F_0(a,\dot{u}) = 1$.

Also, $c_5(\dot{u})$ appearing in F_2 has to be zero. We proceed further in a similar way. In order to find $c_4(\dot{u})$ entering $F_1(a,\dot{u})$, we have to solve Eq. (41) for $n = 3$, and the procedure continues for higher-order terms in m. To be able to find F_i we have to solve the differential equations (41) for all $n \leqslant i + 2$.

Apart from the already stated Eqs. (43) and (44), we give the final expressions for

$$F_3(a,\dot{u}) = \frac{1}{6}\dot{u}^4 v\ln(\dot{u})(-\tilde{a}^3 + 3\tilde{a}\dot{u} + 6c_3\dot{u}^2) + \frac{-10\tilde{a}^9 + 135\tilde{a}^7\dot{u} + 180\tilde{a}^6 c_3\dot{u}^2}{12960} + \frac{27\tilde{a}^5\dot{u}^2(20\dot{u} - 20v - 3) - 1350\tilde{a}^4 c_3\dot{u}^3}{12960}$$

$$+ \frac{45\tilde{a}^3\dot{u}^3[-4(12c_5 + 5)\dot{u} + 24\dot{u}^2 - 24v^2 + 80v - 17]}{12960} - \frac{3240\tilde{a}^2 c_3\dot{u}^4(\dot{u} - v)}{12960}$$

$$- \frac{135\tilde{a}\dot{u}^4[-8(6c_5 - 5)\dot{u} + 24\dot{u}^2 - 24v^2 + 20v + 9]}{12960} - \frac{270\dot{u}^5[c_3(24\dot{u}^2 - 24v^2 + 36v - 5) - 48c_7\dot{u}]}{12960}. \tag{A5}$$

Higher orders can be calculated in the same manner.

As an approximation for the tree model that seems justified for small enough mass, and large enough driving velocity, one can write $1 = \int_{-\infty}^{\infty}da\int_{-\infty}^{\infty}du\,P \approx \int_{-\infty}^{\infty}da\int_0^{\infty}du\,P^{(1)}$. From this condition follow Eqs. (91) and (92), and we find

$$P_{\text{approx}}(\dot{u}) = \frac{e^{-\dot{u}}\dot{u}^{v-1}}{\Gamma(v)} - \frac{me^{-\dot{u}}\dot{u}^{v-2}}{2\Gamma(v)}(-2\dot{u}v\ln(\dot{u}) + 2\dot{u}v\psi^{(0)}(v) + \dot{u}^2 - v^2 + v) + \frac{m^2 e^{-\dot{u}}\dot{u}^{v-3}}{24\Gamma(v)}$$

$$\times[-12\dot{u}v\ln(\dot{u})[-\dot{u}v\ln(\dot{u}) + \dot{u}(\dot{u} + 2) - v^2 + v] + 12\dot{u}v(\psi(v)[-2\dot{u}v\ln(\dot{u}) + \dot{u}v\psi(v) + \dot{u}(\dot{u} + 2) - v^2 + v]$$

$$- \dot{u}v\psi^{(1)}(v)) - 6\dot{u}^2(v - 4)v + 6\dot{u}(5 - 3v)v + 3\dot{u}^4 + 10\dot{u}^3 + (v - 2)(v - 1)v(3v + 5)]. \tag{A6}$$

A similar analysis can be done for the $\sqrt{\dot{u}}$ model, and there Eq. (A6) is obtained for small mass after neglecting complex velocities, as shown using the instanton solution in Sec. V E.

APPENDIX B: MATCHING OF $\dot{u} \sim m$ AND $\dot{u} \gg m$ AT SMALL MASS

Next we discuss some remaining details of the perturbation theory presented in Sec. IV B. Although we could not solve analytically the equations that determine the solution in region 2, in this Appendix we demonstrate that we properly organized the perturbation theory in region 2. We will prove the matching between the distribution function in regions 1 and 2, without explicitly solving the equations in region 2.

The matching condition at the boundary reads as $P^{(1)}(\dot{u},a) \approx P^{(2)}(\dot{u},a)$. From that follows

$$P^{(2)}(\dot{u},a) = m^{v-1}\sum_{n=0}^{\infty}\tilde{P}_n^{(2)}(a,\check{u})m^n$$

$$+ \ln(m)m^{v-1}\sum_{n=0}^{\infty}\tilde{\mathcal{P}}_n^{(2)}(a,\check{u})m^n + \dots, \tag{B1}$$

where $\dots$ denotes that there are other terms $\sim(\ln m)^i$ where $i > 1$, as well as $\sim m^{v-1/2}$. Note that $\ln(m)$ terms come from the $\ln(u)$ dependence in $P^{(1)}$, while $\sim m^{v-1/2}$ comes from terms like $\sim c_3$ in $P^{(1)}$. Note that $\tilde{\mathcal{P}}_n^{(2)}$ satisfies the same equations as $\tilde{P}_n^{(2)}$, but with different boundary conditions, i.e., it contains only some terms from $\tilde{P}_n^{(2)}$ (see below). The same holds for the omitted terms which can be analyzed in the same manner.

For large enough $a,\check{u}$,

$$\tilde{P}_0^{(2)}(a,\check{u}) \approx e^{-\frac{a^2}{2\check{u}}}\sum_{n=0}^{\infty}\frac{\check{u}^{v-\frac{3}{2}-2n}}{\Gamma(v)\sqrt{2\pi}}\tilde{F}_n(a,\check{u}), \tag{B2}$$

$$\tilde{F}_n(a,\check{u}) = \lim_{m\to 0}\frac{F_n(a\sqrt{m},\check{u}m)}{m^{\frac{3n}{2}}}, \tag{B3}$$

where F_n are determined by Eq. (41). Analyzing expressions for F_n, we find

$$\tilde{F}_n(a,\check{u}) = \sum_{i=0}^{[3n/2]}a^{3n-2i}\,\check{u}^i c_i^n, \tag{B4}$$

where $[x]$ rounds x to an integer such that $[x] \leqslant x$ and c_i^n are numbers. Strictly speaking, Eq. (B4) holds for $n < 7$ and for

$n \geqslant 7$ there might be some additional $(\ln u)^i$ terms, but in that case the discussion would be similar.

By plugging Eq. (B1) into Fokker-Planck Eq. (39), one finds

$$a\frac{\partial \tilde{P}_0^{(2)}}{\partial \tilde{u}} + \frac{\partial}{\partial a}\{(-a+v)\tilde{P}_0^{(2)}\} - \frac{\partial^2}{\partial a^2}(\tilde{u}\tilde{P}_0^{(2)}) = 0. \quad (B5)$$

In order that both Eqs. (B2) and (B5) hold,

$$c_i^n(3n-2i) - c_{i-1}^n(3n-2i+2)(3n-2i+1)$$
$$+ c_{i-1}^{n-1}\left(-\tfrac{1}{2} - 2n + i\right) + \tfrac{1}{2}c_i^{n-1}$$
$$+ c_{i-2}^{n-1}v(3n-2i+1) = 0, \quad (B6)$$

where $c_i^n = 0$ for $i < 0$ as well as for $i > [3n/2]$. Indeed, our results satisfy this structure.

Note that for $i = 0$ we obtain $c_0^n 3n + c_0^{n-1}/2 = 0$. To conclude, using Eq. (B6) and knowing $c_0^0 = 1$, we can find all others coefficients c_i^n. Then, the distribution of velocities has for large enough velocities the form

$$\tilde{P}_0^{(2)}(\tilde{u}) = \sum_{k=0}^{\infty} \frac{\tilde{u}^{v-k-1}}{\Gamma[v]\sqrt{2\pi}} \sum_{i=0}^{3k} 2^{3k-i+1/2}c_i^{2k}\Gamma(3k-i+1/2). \quad (B7)$$

Now we consider the next term in the expansion $\tilde{P}_1^{(2)}$. Knowing $P^{(1)}$, from the matching condition follows that

$$\tilde{P}_1^{(2)}(a,\tilde{u}) \approx e^{-\frac{a^2}{2\tilde{u}}} \sum_{n=0}^{\infty} \frac{\tilde{u}^{v-\frac{3}{2}-2n}}{\Gamma(v)\sqrt{2\pi}}\tilde{Q}_n(a,\tilde{u}), \quad (B8)$$

$$\tilde{Q}_n(a,\tilde{u}) = -\tilde{u}\tilde{F}_n(a,\tilde{u}) + \tilde{u}\sum_{i=2}^{[3n/2]} a^{3n-2i}\tilde{u}^i p_i^n$$
$$+ \tilde{u}\ln\tilde{u}\sum_{i=3}^{[3n/2]} a^{3n-2i}\tilde{u}^i d_i^n, \quad (B9)$$

for large enough velocities. On the other hand, the equation for $\tilde{P}_1^{(2)}(a,\tilde{u})$ reads as

$$a\frac{\partial \tilde{P}_1^{(2)}}{\partial \tilde{u}} + \frac{\partial}{\partial a}[(v-a)\tilde{P}_1^{(2)}] - \frac{\partial^2}{\partial a^2}(\tilde{u}\tilde{P}_1^{(2)}) - \tilde{u}\frac{\partial}{\partial a}\tilde{P}_0^{(2)} = 0. \quad (B10)$$

From Eqs. (B8) and (B10), one obtains

$$p_i^n(3n-2i) - p_{i-1}^n(3n-2i+2)(3n-2i+1)$$
$$+ p_{i-1}^{n-1}\left(\tfrac{1}{2} - 2n + i\right) + \tfrac{1}{2}p_i^{n-1} + p_{i-2}^{n-1}v(3n-2i+1)$$
$$- c_{i-2}^{n-1}(3n-2i+1) + d_i^{n-1} = 0, \quad (B11)$$
$$d_i^n(3n-2i) - d_{i-1}^n(3n-2i+2)(3n-2i+1)$$
$$+ d_{i-1}^{n-1}\left(\tfrac{1}{2} - 2n + i\right) + \tfrac{1}{2}d_i^{n-1} + d_{i-2}^{n-1}v(3n-2i+1) = 0, \quad (B12)$$

where $p_i^n = 0$ for $i < 2$ or $i > [3n/2]$, and $d_i^n = 0$ for $i < 3$ or $i > [3n/2]$. Note that knowing $d_3^2 = v$ we can find all other coefficients. By examining the expressions for $\tilde{Q}_n$ that follow from F_n, we found that both Eqs. (B11) and (B12) hold. One can repeat the procedure for higher-order terms in the same way.

Similarly, we find that in region 1

$$\mathcal{P}_0^{(2)} = 0, \quad (B13)$$

$$\mathcal{P}_1^{(2)} = e^{-\frac{a^2}{2\tilde{u}}} \frac{\tilde{u}^{v-\frac{1}{2}-2n}}{\Gamma(v)\sqrt{2\pi}} \sum_{i=3}^{[3n/2]} a^{3n-2i}\tilde{u}^i d_i^n. \quad (B14)$$

The analysis presented in this Appendix confirms that perturbation theory in region 2 is properly organized, and matching between the distributions in regions 1 and 2 holds.

APPENDIX C: LARGE-DEVIATION FUNCTION

Here, we comment shortly on the Laplace-transformed Fokker-Planck equation for the tree model and then present a calculation of its large-deviation function. It allows us to show that the equivalence of the large-deviation function for the tree and $\sqrt{\tilde{u}}$ model for positive velocities holds self-consistently. It may allow us to obtain a complete proof of the equivalence if one subcase (see below) could be ruled out, but we have not succeeded at this stage in doing so.

The Laplace-transformed Fokker-Planck equation reads as

$$\frac{\partial \hat{P}_+}{\partial t} - \frac{\partial \hat{P}_+}{\partial \kappa}\left(\lambda - \frac{\kappa}{m}\right) - \frac{\partial \hat{P}_+}{\partial \lambda}\left(-\frac{\kappa}{m} + \frac{\kappa^2}{m^2}\right)$$
$$= \frac{\kappa}{m}v\hat{P}_+ + \Phi(\kappa), \quad (C1)$$

$$\frac{\partial \hat{P}_-}{\partial t} - \frac{\partial \hat{P}_-}{\partial \kappa}\left(\lambda - \frac{\kappa}{m}\right) - \frac{\partial \hat{P}_-}{\partial \lambda}\left(-\frac{\kappa}{m} - \frac{\kappa^2}{m^2}\right)$$
$$= \frac{\kappa}{m}v\hat{P}_- - \Phi(\kappa), \quad (C2)$$

where

$$\Phi(\kappa) = \frac{\partial}{\partial \kappa}\int_{-\infty}^{\infty} da\, e^{\kappa a} P(\dot{u} = 0, a). \quad (C3)$$

Here we kept only the one boundary term at $\dot{u} = 0$, assuming that other terms at "infinity" vanish. Here, $\hat{P}_+(\lambda,\kappa) = \int_0^{\infty} d\dot{u}\int_{-\infty}^{\infty} da\, e^{\lambda\dot{u}+\kappa a} P(\dot{u},a)$. We define $\hat{P}_-$ similarly, with the difference that the integration is over negative velocities.

Equation (C1) (which describes the contribution coming from positive velocities) can be compared with the corresponding equation for the $\sqrt{\tilde{u}}$ model (108). One sees that the main difference is the additional boundary term $\Phi(\kappa)$. When this boundary term vanishes, the two models become equivalent.

In the stationary case, introducing the time parametrization as in Eqs. (111) and (112), we obtain

$$\frac{d\hat{P}_+}{dt} - \frac{\kappa(t)}{m}v\hat{P}_+ - \Phi(\kappa(t)) = 0. \quad (C4)$$

The solution of this equation is

$$\hat{P}_+(\lambda_0,\kappa_0) = \hat{P}_+(0,0)e^{vZ(\lambda_0,\kappa_0)}$$
$$+ \int_{-\infty}^{t} e^{v\{Z(\lambda_0,\kappa_0)-Z(\lambda(s),\kappa(s))\}}\Phi(\kappa(s))ds, \quad (C5)$$

where Z is given by Eq. (118) with $\kappa(t) = \kappa_0$ and $\lambda(t) = \lambda_0$.

Introducing $F(x,y)$ as in Eq. (194), we find $\Phi(\kappa) = a_0 e^{v[G(\kappa)-f_0]}$, where $\hat{P}_+(0,0) = e^{-vf_0} = e^{-v\min_{x,y}F(x,y)}$. Here,

$$G(\kappa) - f_0 = -\min_y\{F(0,y) - \kappa y\}, \quad (C6)$$

and a_0 is the corresponding value of the acceleration when the minimum is reached. If we assume that the first term in Eq. (C5) gives the main contribution in the limit $v \to \infty$, we obtain

$$-f_0 + Z(\lambda, \kappa) = -\min_{x,y}\{F(x,y) - \kappa y - \lambda x\}. \quad (C7)$$

Then, indeed the second term is smaller than the first one in Eq. (C5) since it reads as

$$e^{-vf_0}e^{vZ(\lambda,\kappa)} \int_{-\infty}^{t} e^{-v\{Z(\lambda(s),\kappa(s)) - G(\kappa(s))\}}ds$$
$$= e^{-vf_0}e^{vZ(\lambda,\kappa)}e^{-v\min_{s\in(-\infty,t)}\{Z(\lambda(s),\kappa(s)) - G(\kappa(s))\}}, \quad (C8)$$

and using Eqs. (C6) and (C7) it follows that $\phi(\lambda_0, \kappa_0) = \min_{s\in(-\infty,t)}\{Z(\lambda(s),\kappa(s)) - G(\kappa(s))\} \geqslant 0$.

However, if we assume that the second term gives the main contribution, then (C8) implies that

$$-f_0 + Z(\lambda,\kappa) - \phi(\lambda,\kappa) = -\min_{x,y}\{F(x,y) - \kappa y - \lambda x\}. \quad (C9)$$

From this equation and Eq. (C6) follows that $\phi(\lambda_0, \kappa_0) \leqslant Z(\lambda_0, \kappa_0) - G(\kappa_0)$. This statement is not in contradiction with the assumption, but on the other hand it does not follow from Eq. (C9) that $\phi(\lambda_0, \kappa_0) \leqslant 0$, as it should be if the second term is the dominant one. It would be nice to show that this possibility is ruled out, which would provide a proof of the equivalence of large-deviation functions, independent of the one given in the main text.

Note that f_0 is expected to be zero and then (C7) is equivalent to Eq. (195).

APPENDIX D: MOMENTS OF THE DISTRIBUTION FUNCTION FOR $\sqrt{\tilde{u}}$ MODEL

Using the equations derived in Sec. V C, we find the moments characterizing the distribution function of the $\sqrt{\tilde{u}}$

model discussed in Sec. V C. Choosing $t^* = 0$ with a constraint $\tilde{u}(t \geqslant 0) = 0$ and $\dot{\tilde{u}}(0) = -\lambda/m$, we can rewrite Eq. (115) as

$$(m\partial_t^2 - \partial_t + 1)\tilde{u} - \tilde{u}^2 = \lambda\delta(t). \quad (D1)$$

Then, $Z(0,\lambda) = \int_{-\infty}^{0} \tilde{u}(t)dt$.

One can write $\tilde{u} = \sum_{n=0}^{\infty} \tilde{u}_n \lambda^n$, where

$$(m\partial_t^2 - \partial_t + 1)\tilde{u}_n(t) - \sum_{\ell=0}^{n} \tilde{u}_\ell(t)\tilde{u}_{n-\ell}(t) = \delta_{n,1}\delta(t). \quad (D2)$$

A solution of this set of equations is

$$\tilde{u}_0 = 0, \quad (D3)$$

$$\tilde{u}_1(t) = R(t), \quad (D4)$$

$$\tilde{u}_n(t) = \int d\tau\, R(t - \tau) \sum_{\ell=1}^{n} \tilde{u}_\ell(\tau)\tilde{u}_{n-\ell}(\tau) \quad \text{for } n > 1, \quad (D5)$$

with

$$(m\partial_t^2 - \partial_t + 1)R_{t-t'} = \delta(t - t'), \quad (D6)$$

$$R_t = \begin{cases} \frac{2\theta(t)}{\sqrt{4m-1}}e^{t/(2m)} \sin\left(\frac{t}{2m}\sqrt{4m-1}\right), & m > 1/4 \\ \frac{2\theta(t)}{\sqrt{1-4m}}e^{t/(2m)} \sinh\left(\frac{t}{2m}\sqrt{1-4m}\right), & m < 1/4. \end{cases} \quad (D7)$$

The case $m = 1/4$ was treated in Eq. (147). Using that $\hat{P}(\lambda,\kappa) = e^{vZ(\lambda,\kappa)}$ and $\partial_\lambda^n \partial_\kappa^m \hat{P}(\lambda,\kappa)|_{(0,0)} = \overline{\tilde{u}^n a^m}$, we obtain the first few moments exactly:

$$\overline{\tilde{u}} = v, \quad (D8)$$

$$\overline{\tilde{u}^2} = v(\sigma + v), \quad (D9)$$

$$\overline{\tilde{u}^3} = v\left(\frac{4\sigma^2}{m'+2} + 3\sigma v + v^2\right), \quad (D10)$$

$$\overline{\tilde{u}^4} = v\left(\frac{6\sigma^3(5m'+6)}{(m'+2)(4m'+3)} + \frac{\sigma^2(3m'+22)v}{m'+2} + 6\sigma v^2 + v^3\right), \quad (D11)$$

$$\overline{\tilde{u}^5} = v\left(\frac{48\sigma^4[m'(103m'+198)+72]}{(m'+2)(m'+6)(4m'+3)(9m'+4)} + \frac{10\sigma^3(31m'+30)v}{(m'+2)(4m'+3)} + \frac{5\sigma^2(3m'+14)v^2}{m'+2} + 10\sigma v^3 + v^4\right), \quad (D12)$$

$$\overline{\tilde{u}^6} = v\left(\frac{240\sigma^5(m'\{m'[m'(695m'+4396)+7666]+4284\}+720)}{(m'+2)^2(m'+6)(4m'+3)(9m'+4)(16m'+5)}\right.$$
$$+ \frac{2\sigma^4(m'\{m'[9m'(225m'+4138)+130916]+137592\}+39456)v}{(m'+2)^2(m'+6)(4m'+3)(9m'+4)}$$
$$\left.+ \frac{15\sigma^3[m'(4m'+105)+90]v^2}{(m'+2)(4m'+3)} + \frac{5\sigma^2(9m'+34)v^3}{m'+2} + 15\sigma v^4 + v^5\right), \quad (D13)$$

$$\overline{\tilde{u}^7} = v\left(\frac{2880\sigma^6[m'(m'(m'\{m'[m'(22015m'+190244)+521534]+594996\}+277920)+43200]}{(m'+2)^2(m'+6)(m'+12)(4m'+3)(9m'+4)(9m'+10)(16m'+5)}\right.$$
$$+ \frac{168\sigma^5(m'\{m'[m'(20438m'+114479)+179748]+93924\}+15120)v}{(m'+2)^2(m'+6)(4m'+3)(9m'+4)(16m'+5)}$$
$$+ \frac{14\sigma^4\{m'[m'(3105m'^2+39756m'+125468)+122256]+33408\}v^2}{(m'+2)^2(m'+6)(4m'+3)(9m'+4)}$$
$$\left.+ \frac{105\sigma^3[m'(4m'+53)+42]v^3}{(m'+2)(4m'+3)} + \frac{35\sigma^2(3m'+10)v^4}{m'+2} + 21\sigma v^5 + v^6\right), \quad (D14)$$

where $m' = m\mu^2/\eta^2$, $\sigma = \frac{|\Delta'(0^+)|}{(\eta\mu^2)}$. Here we used dimension-full quantities. These results are in agreement with the results from Sec. V D.

APPENDIX E: PERTURBATION THEORY FOR THE INSTANTON SOLUTION

Here, we give more details on the derivation of the perturbative solution of Eq. (115) considered in Sec. V E. We analyze the matching of the expansions in the different regions (133) and (137) at $t \sim -m$ in order to find y_n appearing in (137). After determining f_n (see Sec. V E), we notice that for $n \geqslant 0$ it has the structure

$$f_n(x) = \sum_{k=1}^{n+1} e^{kx} \mathcal{C}_k^{(n)}(x,\lambda) + \sum_{k=0}^{n} \mathcal{A}_k^{(n)}(\lambda)(-x)^k. \quad (E1)$$

From Eq. (135) and by comparing the coefficient in front of x^k, we obtain

$$(k+1)\mathcal{A}_{k+1}^{(k+1)} + \mathcal{A}_k^{(k)} - \sum_{\ell=0}^{k} \mathcal{A}_{k-\ell}^{(k-\ell)} \mathcal{A}_\ell^{(\ell)} = 0. \quad (E2)$$

We find that

$$\mathcal{A}_k^{(k)}(\lambda) = \frac{S_k\left(\frac{\lambda-1}{\lambda}\right)}{k!}, \quad (E3)$$

$$S_k(x) = \sum_{n=0}^{\infty} x^n n^k. \quad (E4)$$

This comes from

$$\sum_{\ell=0}^{k} \frac{k!}{\ell!(k-\ell)!} S_{k-\ell}(x) S_\ell(x) = \sum_{\ell=0}^{k} \binom{k}{\ell} \sum_{a=0}^{\infty} x^a a^{k-\ell} \sum_{b=0}^{\infty} x^b b^\ell$$

$$= \sum_{a,b=0}^{\infty} (a+b)^k x^{a+b} = \sum_{t=0}^{\infty} t^k x^t (t+1) = S_{k+1}(x) + S_k(x).$$
$$(E5)$$

By multiplying Eq. (E5) with $1/k!$, we obtain Eq. (E2), if $\mathcal{A}_k^{(k)}(\lambda) = S_k(x)/k!$. Using the "boundary condition" $S_0(x) = 1/(1-x) = \mathcal{A}_0^{(0)} = \lambda$, we find Eq. (E3).

It follows that the matching condition holds in zeroth order in m if

$$y_0(x) = \sum_{n=0}^{\infty} S_n\left(\frac{\lambda-1}{\lambda}\right) \frac{(-x)^n}{n!}$$

$$= \frac{\lambda}{\lambda + (1-\lambda)e^{-x}}. \quad (E6)$$

In order to have a smooth function $\tilde{u}(t)$ at $t \sim -m$ in each order $n \geqslant 0$ in m, it should hold

$$y_n(x) = \sum_{k=0}^{\infty} \mathcal{A}_k^{(n+k)}(\lambda)(-x)^k. \quad (E7)$$

Then, $y_{n>0}(0) = \mathcal{A}_0^{(n)}$ and we find Eq. (141). Higher-order terms y_n can be found easily. We state here

$$\begin{aligned}
f_2(t) = &-\tfrac{1}{6}e^{3t}\lambda^3 \\
&+ \tfrac{1}{12}e^{2t}\lambda(39\lambda - 12t\lambda - 54\lambda^2 + 24t\lambda^2) \\
&+ \tfrac{1}{12}e^t\lambda(-72 + 36t - 6t^2 + 192\lambda - 144t\lambda + 12t^2\lambda \\
&\quad - 126\lambda^2 + 132t\lambda^2 - 12t^2\lambda^2) \\
&+ \tfrac{1}{12}\lambda(72 + 36t + 6t^2 - 231\lambda - 114t\lambda - 18t^2\lambda \\
&\quad + 182\lambda^2 + 84t\lambda^2 + 12t^2\lambda^2), \quad (E8)
\end{aligned}$$

$$\begin{aligned}
y_2(t) = &-\frac{e^{-t}\lambda}{12[e^{-t}(-1+\lambda)-\lambda]^3} \\
&\times (\lambda[-96 + 6t^2(-1+\lambda) + 141\lambda - 25\lambda^2 \\
&\quad - 6t(-8+9\lambda)] \\
&+ e^{-t}[72 + 6t^2(-1+\lambda)^2 - 135\lambda + 41\lambda^2 + 25\lambda^3 \\
&\quad - 6t(4 - 9\lambda + 5\lambda^2)] \\
&- 12[e^{-t}(-1+\lambda) + \lambda][-6 - 2t(-1+\lambda) + 7\lambda] \\
&\times \ln[e^{-t} + \lambda - e^{-t}\lambda] + 24(-1+\lambda) \\
&\times [e^{-t}(-1+\lambda) + \lambda]\ln[e^{-t} + \lambda - e^{-t}\lambda]^2). \quad (E9)
\end{aligned}$$

APPENDIX F: THE BEHAVIOR OF $Z(\lambda)$ FOR $\lambda \to \pm i\infty$ IN THE $\sqrt{\tilde{u}}$ MODEL

In this Appendix, we derive the large-λ behavior of $Z(\lambda)$ for the $\sqrt{\tilde{u}}$ model. In order to facilitate our thinking, we denote $\tau := -t$, such that the time τ of the instanton goes from zero to ∞. The behavior for $\lambda \to \infty$ is complicated. Analyzing $Z(\lambda)$ for real λ, one finds that there is a branch-cut singularity. On the diagonal in the complex plane, $\lambda \sim 1 + i$, the instanton solution of Eq. (101) looks rather chaotic. For complex λ with vanishing real part, the behavior is slightly simpler: In the complex plane, $\tilde{u}(\tau)$, its derivative $\dot{\tilde{u}}(\tau)$, and the energy

$$E(\tau) := \frac{m}{2}[\partial_\tau \tilde{u}(\tau)]^2 + \frac{\mu^2}{2}\tilde{u}(\tau)^2 - \sigma\frac{\tilde{u}^3(\tau)}{3} \quad (F1)$$

are behaving as indicated on Fig. 22 (blue solid lines).

The energy is dissipated as

$$\frac{d}{d\tau}E(\tau) = -\eta[\partial_\tau\tilde{u}(\tau)]^2. \quad (F2)$$

We are interested in the case when λ is equal to the imaginary unit times a large positive number. We start by neglecting dissipation and the term $\sim\mu^2$. One can check later on the trajectories we find that this approximation is justified.

We will be working in dimensionless units $\sigma = \eta = \mu = 1$. We have to solve

$$m\,\partial_\tau^2\tilde{u}(t) = \tilde{u}(\tau)^2, \quad (F3)$$

$$\partial_\tau\tilde{u}(0) = \lambda/m, \quad (F4)$$

$$\tilde{u}(0) = 0. \quad (F5)$$

The solution for $\partial_\tau\tilde{u} \equiv \dot{\tilde{u}}$ can be parametrized by ϕ,

$$\dot{\tilde{u}}(\phi) = (2e^{i\phi} - 1)\frac{\lambda}{m}. \quad (F6)$$
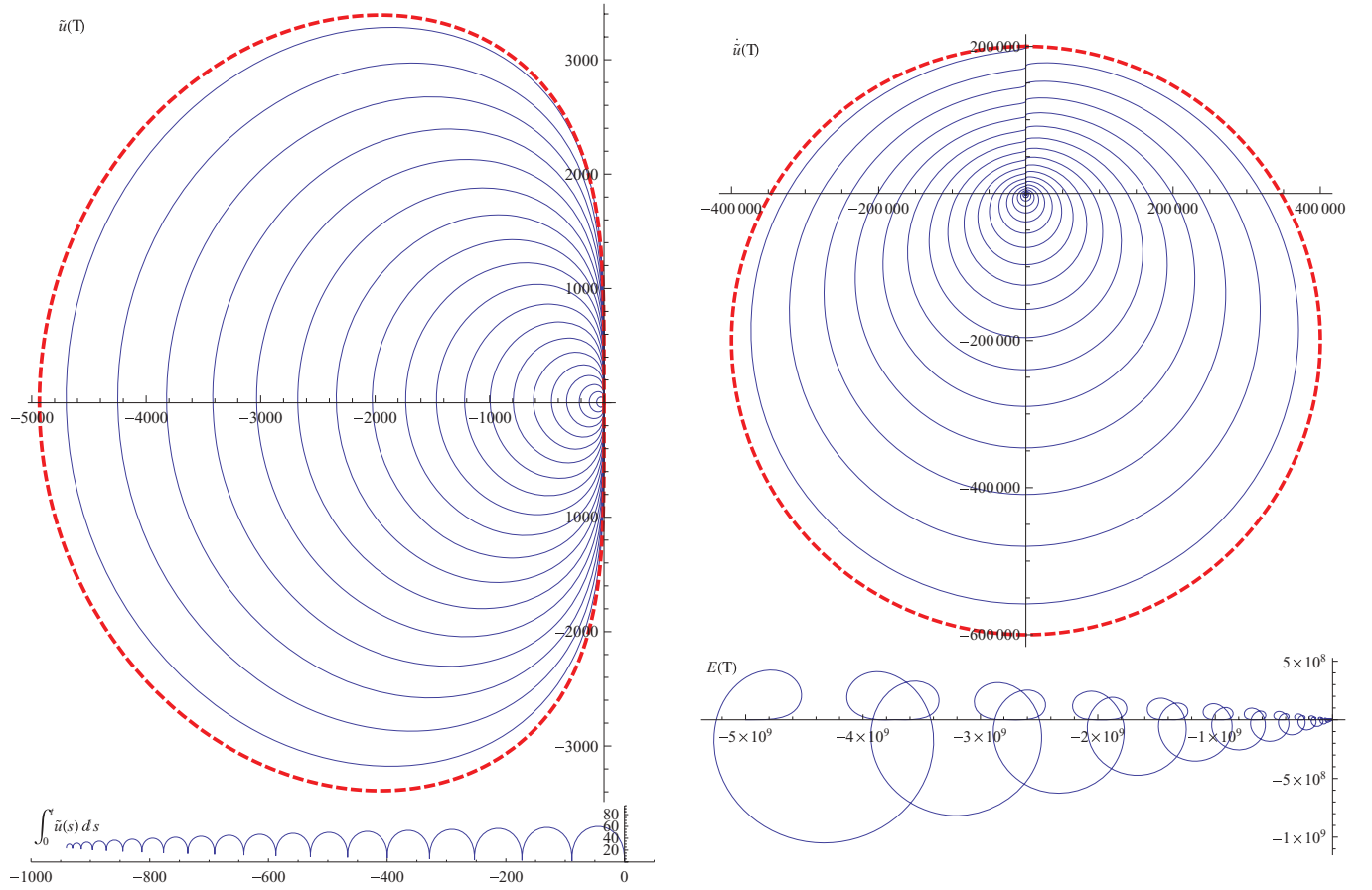
FIG. 22. (Color online) Evolution in the complex plane of $\tilde{u}(\tau)$ (top left), $\dot{\tilde{u}}(\tau)$ (top right), $E_{\text{kin}}(\tau)$ (bottom right), and $\int_0^t ds\, \tilde{u}(s)ds$ (bottom left), for $\lambda = 50\,000i$, $m = 1/4$. The movement of $\tilde{u}(\tau)$ starts at 0, moving in counterclockwise circles inwards. The kinetic energy evolves from left to right, and $\int_0^\tau ds\, \tilde{u}(t)ds$ from zero to the left. The dashed lines are the solution for $\mu = \eta = 0$, given in Eqs. (F6) and (F7).

While this is of course always possible, we claim and check in Eq. (F8) below that ϕ is real, and thus has the natural interpretation of an angle. Using energy conservation, $E(0) = \frac{\lambda^2}{2m}$, and $E(\tau) = \frac{m}{2}[\partial_\tau \tilde{u}(\tau)]^2 - \frac{\tilde{u}^3(\tau)}{3}$, this yields

$$\tilde{u}(\phi) = \sqrt[3]{\frac{-6\lambda^2}{m}} e^{\frac{i\phi}{3} + \frac{2i\pi}{3}} \sqrt[3]{1 - e^{i\phi}}. \tag{F7}$$

This allows us to obtain the "angular velocity" (attention: the prime indicates the derivative w.r.t. the argument ϕ)

$$\dot{\phi}(\phi) = \frac{\dot{\tilde{u}}(\phi)}{\tilde{u}'(\phi)} = \sqrt[3]{\frac{9}{2} \frac{\lambda}{im^2}} e^{\frac{i(5\pi/2 - \phi)}{3}} (1 - e^{i\phi})^{2/3}. \tag{F8}$$

Note that for $\phi \in [0, 2\pi]$, expression (F8) is real, thus the curves are indeed parametrized by a real angle ϕ.

Noting the differential dt,

$$dt = \frac{d\phi}{\dot{\phi}(\phi)}, \tag{F9}$$

this allows us to calculate the period as

$$T = \int_0^{2\pi} \frac{1}{\dot{\phi}(\phi)} d\phi = \frac{2^{2/3} 3^{5/6} \Gamma\left(\frac{1}{3}\right) \Gamma\left(\frac{7}{6}\right)}{\sqrt{\pi}} \sqrt[3]{\frac{im^2}{\lambda}}$$

$$= 5.56022 \sqrt[3]{\frac{im^2}{\lambda}}. \tag{F10}$$

Next we switch on dissipation. It leads to a change in energy, for a time T or the equivalent phase Φ,

$$E(\Phi) - E(0) = E(T) - E(0) = \int_0^T \dot{E}(\tau) d\tau$$

$$= -\int_0^T \dot{\tilde{u}}(\tau)^2 d\tau = -\int_0^\Phi \dot{\tilde{u}}(\phi)^2 \frac{d\phi}{\dot{\phi}(\phi)}. \tag{F11}$$

In principle, the exact trajectory has to be put. Using the dissipationless one, we find for one period

$$E(2\pi) - E(0) \approx -\frac{\Gamma\left(-\frac{5}{6}\right) \Gamma\left(\frac{1}{3}\right)}{2\sqrt[3]{2}\sqrt[6]{3}\sqrt{\pi}\sqrt{m}} \left(\frac{\lambda}{i\sqrt{m}}\right)^{5/3}$$

$$= \frac{3.33613}{\sqrt{m}} \left(\frac{\lambda}{i\sqrt{m}}\right)^{5/3}. \tag{F12}$$

If we call n the number of periods, then

$$-E(0) = -\frac{\lambda^2}{2m} > 0, \tag{F13}$$

$$\frac{d}{dn}[-E(2\pi n)] \approx \frac{\Gamma\left(-\frac{5}{6}\right) \Gamma\left(\frac{1}{3}\right)}{2\sqrt[3]{2}\sqrt[6]{3}\sqrt{\pi}\sqrt{m}}[-2E(2\pi n)]^{5/6}$$

$$= \frac{-3.33613}{\sqrt{m}}[-2E(2\pi n)]^{5/6}, \tag{F14}$$

where we have re-expressed λ by the energy itself in order to allow for an iteration. Defining λ_{eff} by

$$E(2\pi n) =: \frac{\lambda_{\text{eff}}(2\pi n)^2}{2m}, \tag{F15}$$

we get

$$\begin{aligned}
\frac{d}{dn}\frac{\lambda_{\text{eff}}(2\pi n)}{i} &= \frac{d}{dn}\sqrt{-2mE(2\pi n)} \\
&\approx \frac{\Gamma\left(-\frac{5}{6}\right)\Gamma\left(\frac{1}{3}\right)}{2\sqrt[3]{2}\sqrt[6]{3}\sqrt{\pi}}[-2E(2\pi n)]^{1/3} \\
&= \frac{\Gamma\left(-\frac{5}{6}\right)\Gamma\left(\frac{1}{3}\right)}{2\sqrt[3]{2}\sqrt[6]{3}\sqrt{\pi}}\left[\frac{\lambda_{\text{eff}}(2\pi n)}{i\sqrt{m}}\right]^{2/3} \\
&= -3.33613\left[\frac{\lambda_{\text{eff}}(2\pi n)}{i\sqrt{m}}\right]^{2/3}. \tag{F16}
\end{aligned}$$

The integral over one period of $\int_0^T dt\,\tilde{u}(t)$, which contributes to $Z(\lambda)$ is

$$\begin{aligned}
\int_0^T d\tau\,\tilde{u}(t) &= \int_0^{2\pi}\frac{d\phi}{\dot\phi(\phi)}\tilde{u}(\phi) \\
&= \frac{\sqrt[6]{3}\,\Gamma\left(-\frac{1}{6}\right)\Gamma\left(\frac{2}{3}\right)}{2^{2/3}\sqrt{\pi}}\left(\frac{\lambda m}{i}\right)^{1/3} \\
&= -3.91452\left(\frac{\lambda m}{i}\right)^{1/3}. \tag{F17}
\end{aligned}$$

Therefore, using that $Z(\lambda) = \int_0^\infty \tilde{u}(\tau)d\tau$, we have the following relations:

$$\frac{d}{dn}Z(\lambda) = \frac{\sqrt[6]{3}\,\Gamma\left(-\frac{1}{6}\right)\Gamma\left(\frac{2}{3}\right)}{2^{2/3}\sqrt{\pi}}\left(\frac{\lambda m}{i}\right)^{1/3}. \tag{F18}$$

This yields

$$\begin{aligned}
\frac{d}{d(\lambda/i)}Z(\lambda) &= -\frac{\frac{dZ(\lambda)}{dn}}{\frac{d\lambda/i}{dn}} \\
&= -\frac{2\sqrt[3]{6}\sqrt{\pi}\,\Gamma\left(-\frac{1}{6}\right)}{\Gamma\left(-\frac{5}{6}\right)\Gamma\left(\frac{1}{6}\right)}\left(\frac{\lambda}{im^2}\right)^{-1/3} \\
&= -1.17337\left(\frac{\lambda}{im^2}\right)^{-1/3}, \tag{F19}
\end{aligned}$$

where the additional minus sign has been introduced due to the fact that we now integrate in the opposite direction. Integrating over λ, and using that $Z(0) = 0$, we find the asymptotic behavior

$$\begin{aligned}
Z_{\text{asymp}}(\lambda) &= -\frac{15\sqrt[3]{6}\sqrt{\pi}\,\Gamma\left(\frac{5}{6}\right)}{\Gamma\left(\frac{1}{6}\right)^2}\left(\frac{\lambda m}{i}\right)^{2/3} \\
&= -1.76006\left(\frac{\lambda m}{i}\right)^{2/3}. \tag{F20}
\end{aligned}$$

As an example, for $\lambda = 10^7 i$, $m = 1/4$, our formula gives $Z_{\text{asymp}}(10^7 i) = -150483.0$ whereas numerics gives $Z(10^7 i) = -150483.6 + 330.444i$. The subleading imaginary part is consistent with

$$Z_{\text{guess}}(\lambda) = -1.76006\left(\frac{\lambda m}{i}\right)^{2/3} + 1.13i\left(\frac{\lambda m}{i}\right)^{1/3}. \tag{F21}$$

On the negative imaginary axis, the result is the same, i.e., on the whole imaginary axis

$$Z_{\text{asymp}}(\lambda) = -\frac{15\sqrt[3]{6}\sqrt{\pi}\,\Gamma\left(\frac{5}{6}\right)}{\Gamma\left(\frac{1}{6}\right)^2}(|\lambda|m)^{2/3}. \tag{F22}$$

APPENDIX G: LARGE-m EXPANSION TO SECOND ORDER

Here, we state the second order of large-m expansion of the distribution function for $\sqrt{\dot u}$ model (see Sec. IV D):

$$\begin{aligned}
Q_2 = \frac{1}{576v^4}[&r^6\cos(6\theta) + 48r^3v^2\sin(3\theta) \\
&+ 432rv^2\sin(\theta)(r^2 - 4v) \\
&+ 15r^2\cos(2\theta)(r^2 - 12v)(r^2 - 4v) \\
&+ 10(r^6 - 72r^2v^2 + 96v^3) + 6r^4\cos(4\theta)(r^2 - 10v)]. \tag{G1}
\end{aligned}$$

It can be rewritten as

$$\begin{aligned}
Q_2 = \frac{1}{144v^4}(&8\tilde{a}^6 - 75\tilde{a}^4 v + 18\tilde{a}^2 v(\dot u - v)(5\dot u + 3v) \\
&+ 3v\{15\dot u^4 - 28\dot u^3 v - 6\dot u^2 v(v + 20) + 12\dot u v^2(3v + 8) \\
&+ v^2[(24 - 17v)v + 80]\}). \tag{G2}
\end{aligned}$$

Integrating out $\tilde{a}$, we find the distribution for the velocity:

$$\begin{aligned}
P(\dot u) = \frac{1}{\sqrt{2\pi v}}e^{\frac{-(\dot u - v)^2}{2v}}\Big[&1 + \frac{1}{48mv^3}(15\dot u^4 - 28\dot u^3 v \\
&- 6\dot u^2 v(v + 15) + 12\dot u v^2(3v + 7) \\
&+ v^2[(6 - 17v)v + 45]) + O\left(\frac{1}{m^2}\right)\Big] \tag{G3}
\end{aligned}$$

APPENDIX H: EXIT PROBABILITY

In this section, we calculate the probability $E(a,\dot u,t)$ that a particle starting at $t = 0$ with acceleration a and velocity $\dot u > 0$ had a negative velocity at some moment before or at time t. We call it the exit probability. The calculation is valid for all the models studied in the previous sections. The equation for the exit probability reads as

$$\frac{\partial E}{\partial t} = a\frac{\partial E}{\partial \dot u} + \frac{\dot u}{m^2}\frac{\partial^2 E}{\partial a^2} + \frac{1}{m}(-\dot u - a + v)\frac{\partial E}{\partial a} \tag{H1}$$

with the boundary conditions

$$E(a < 0,0,t) = 1, \tag{H2}$$

$$E(a,\dot u > 0,0) = 0. \tag{H3}$$

We assume that the particle starts with a finite acceleration and velocity. Then, introducing $\hat{E}(\kappa,\lambda,t) = \int_{-\infty}^\infty da\int_0^\infty d\dot u\,E(a,\dot u,t)\exp(\kappa a + \lambda\dot u)$, we obtain

$$\begin{aligned}
\frac{\partial\hat{E}}{\partial t} = \frac{\partial\hat{E}}{\partial\lambda}\left(\frac{\kappa^2}{m^2} + \frac{\kappa}{m}\right) + \frac{\partial\hat{E}}{\partial\kappa}\left(-\lambda + \frac{\kappa}{m}\right) \\
+ \frac{\hat{E}}{m}(1 - v\kappa) + \frac{1}{\kappa^2} + f(\kappa), \tag{H4}
\end{aligned}$$

for we used that $\kappa > 0$. The last term $1/\kappa^2 + f(\kappa)$ comes from the boundary term at $\dot u = 0$ obtained by performing

the Laplace transform with respect to $\dot{u}$. Here, $f(\kappa) = -\int_0^\infty da\, a \exp(\kappa a) E(a, \dot{u} = 0, t)$.

Using the method of characteristics, we find

$$\dot{\lambda} = -\frac{\kappa^2}{m^2} - \frac{\kappa}{m}, \tag{H5}$$

$$\dot{\kappa} = \lambda - \frac{\kappa}{m}, \tag{H6}$$

$$\frac{d\hat{E}}{dt} - \frac{\hat{E}(t)}{m}[1 - v\kappa(t)] - \frac{1}{\kappa^2(t)} - f[\kappa(t)] = 0, \tag{H7}$$

where we used $\kappa(t) > 0$. Then, we obtain

$$\hat{E}(\kappa_0 > 0, \lambda_0, t_0 > 0) = \int_0^{t_0} ds \left[\frac{1}{\kappa^2(s)} + f[\kappa(s)] \right] \\ \times \exp\left(\frac{1}{m} \int_s^{t_0} [1 - v\kappa(s')] ds' \right), \tag{H8}$$

where $\kappa(t)$ satisfies the following equation:

$$\ddot{\kappa}(t) + \frac{\dot{\kappa}}{m} + \frac{\kappa^2}{m^2} + \frac{\kappa}{m} = 0 \tag{H9}$$

with conditions $\kappa(t_0) = \kappa_0$ and $\dot{\kappa}(t_0) = \lambda_0 - \kappa_0/m$. If we introduce $\tilde{u}(s) = -\kappa(-s)/m$, then $\tilde{u}(s)$ satisfies Eq. (115) where in Eqs. (116) and (117) it has to be made a change $\kappa_0 -> -\kappa_0$ and $\lambda_0 -> -\lambda_0$. The equation should be solved self-consistently since $f(\kappa)$ is determined by $E(a > 0, 0, t)$. Increasing the driving velocity v and decreasing the mass, the boundary term $f(\kappa)$ decreases. It is expected that the approximation $f(\kappa) = 0$ becomes reasonable good for sufficiently large driving velocity and small mass.

APPENDIX I: SKETCH OF A PROOF FOR CONVERGENCE OF LARGE-DEVIATION FUNCTION

Suppose that we have a numerical simulation of one of the models discussed in this work, at driving velocity v, which gives N data points. This allows us to estimate $F_v(x)$ in a certain domain $x_- < x < x_+$, with $F(x_-) = F(x_+)$. Let us first estimate the probability p that there are data points left of x_-:

$$p \leqslant N \int_{-\infty}^{x_-} dx\, v e^{-v F_v(x)} \approx N \frac{e^{-v F_v(x_-)}}{F'(x_-)} \approx N e^{-v F_v(x_-)}. \tag{I1}$$

This means that the simulation has to be done at velocities large or equal to v_c in order to satisfy (I1), with

$$v_c \approx \frac{\ln(N/p)}{F(x_-)}, \tag{I2}$$

where we have replaced $F_v(x)$ by the limiting function $F(x)$. [For $N = 10^{10}$ and $p = 10^{-4}$, this would give $v_c \approx 21.5$, using for $F_v(0)$ the function for the $\sqrt{u}$ model.]

Let us now estimate which domain of the function $F_v(x)$ we can estimate with relative statistical error smaller than ϵ, at this velocity v_c. The number n of events in the bin around x of size δ is

$$n \approx e^{-v_c F(x)} \delta N \geqslant \frac{1}{\epsilon^2}, \tag{I3}$$

and must as written be larger than $1/\epsilon^2$. Solving for $F(x)$ yields

$$F(x) \leqslant \frac{\ln(\epsilon^2 \delta N)}{v_c} = F(x_0) \frac{\ln(\epsilon^2 \delta N)}{\ln(N/p)}$$

$$\approx F(x_-)\left[1 + \frac{\ln(\epsilon^2 \delta p)}{\ln N} \right], \tag{I4}$$

where in the last line we have supposed that N is large. This is probably a rather crude estimate, but shows that for $N \to \infty$ one can estimate $F(x)$ for all x for which $F(x) < F(x_-)$.

Let us now consider the $\sqrt{u}$ model, for which $Z_v(\lambda)$ does not depend on v, and for which $F_v(x)$ converges against the large-deviation function $F(x)$. The above shows that there exists a simulation, which can estimate, with any given precision, $F(x)$ for all x with $F(x) < F(0)$ (see Fig. 20). For further reference set $x_- = 0$, and $x_+ = 3.47268$ the other root for which $F(x_+) = F(0)$.

We remind that with probability $1 - p \approx 1$, the simulation has never encountered a negative velocity. Now repeat the simulation with the same parameters, with one of the other models. With the same probability $1 - p$, these simulations have no negative velocities, and since then the particle will only move forward, give the same trajectory, and thus the same large-deviation function, within the (small) error bars estimated above. We have thus proven Eq. (192) of the main text.

The only circumstances where the above argument might go wrong are if there are strong correlations in the tails. If, e.g., rare events are correlated such that whenever one gets one rare event (of negative velocity), then one gets with higher probability another one (clustering of rare events). In this case, even the existence of a large-deviation function may be questionable.

[1] D. S. Fisher, Phys. Rep. **301**, 113 (1998).

[2] S. Brazovskii and T. Nattermann, Adv. Phys. **53**, 177 (2004).

[3] P. Le Doussal and T. Giamarchi, Phys. Rev. B **57**, 11356 (1998).

[4] F. Colaiori, Adv. Phys. **57**, 287 (2008).

[5] S. Field, J. Witt, F. Nori, and X. Ling, Phys. Rev. Lett. **74**, 1206 (1995).

[6] G. Gruner, *Density Waves in Solids* (Addison-Wesley, Reading, MA, 1994).

[7] O. Narayan and D. S. Fisher, Phys. Rev. B **46**, 11520 (1992).

[8] F. Perruchot *et al.*, Phys. B (Amsterdam) **284-288**, 1984 (2000).

[9] C. Reichhardt, C. J. Olson, N. Gronbech-Jensen, and F. Nori, Phys. Rev. Lett. **86**, 4354 (2001).

[10] R. Chitra and T. Giamarchi, Eur. Phys. J. B **44**, 455 (2005).

[11] L. F. Cugliandolo, T. Giamarchi, and P. Le Doussal, Phys. Rev. Lett. **96**, 217203 (2006).

[12] D. Wilkinson and J. F. Willemsen, J. Phys. A: Math. Gen. **16**, 3365 (1983).

[13] J. Stokes, D. Weitz, A. D. J. P. Gollub, M. Robbins, P. Chaikin, and H. Lindsay, J. Phys. A: Math. Gen. **57**, 1718 (1986).

[14] S. Ramanathan and D. S. Fisher, Phys. Rev. B **58**, 6026 (1998).

[15] J. S. Urbach, R. C. Madison, and J. T. Markert, Phys. Rev. Lett. **75**, 276 (1995).

[16] D.-H. Kim, S.-B. Choe, and S.-C. Shin, Phys. Rev. Lett. **90**, 087203 (2003).

[17] B. Alessandro, C. Beatrice, G. Bertotti, and A. Montorsi, J. Appl. Phys. **68**, 2901 (1990).

[18] B. Alessandro, C. Beatrice, G. Bertotti, and A. Montorsi, J. Appl. Phys. **68**, 2908 (1990).

[19] P. Cizeau, S. Zapperi, G. Durin, and H. E. Stanley, Phys. Rev. Lett. **79**, 4669 (1997).

[20] S. Zapperi, P. Cizeau, G. Durin, and H. E. Stanley, Phys. Rev. B **58**, 6353 (1998).

[21] G. Durin and S. Zapperi, Phys. Rev. Lett. **84**, 4705 (2000).

[22] P. Cizeau, S. Zapperi, G. Durin, and H. E. Stanley, Phys. Rev. Lett. **79**, 4669 (1997).

[23] P. Le Doussal and K. J. Wiese, Phys. Rev. E **79**, 051106 (2009).

[24] P. Le Doussal and K. J. Wiese, Europhys. Lett. **97**, 46004 (2012).

[25] P. Le Doussal and K. J. Wiese (unpublished).

[26] A. Dobrinevski, P. Le Doussal, and K. J. Wiese, Phys. Rev. E **85**, 031105 (2012).

[27] J. M. Schwarz and D. S. Fisher, Phys. Rev. Lett. **87**, 096107 (2001).

[28] J. M. Schwarz and D. S. Fisher, Phys. Rev. E **67**, 021603 (2003).

[29] A. P. Mehta, A. C. Mills, K. Dahmen, and J. P. Sethna, Phys. Rev. E **65**, 046139 (2002).

[30] D. Spasojević, S. Bukvić, S. Milošević, and H. E. Stanley, Phys. Rev. E **54**, 2531 (1996).

[31] G. Durin and S. Zapperi, J. Magn. Magn. Mater. **242**, 1085 (2002).

[32] G. Durin, F. Colaiori, C. Castellano, and S. Zapperi, J. Magn. Magn. Mater. **316**, 436 (2007).

[33] S. Zapperi, C. Castellano, F. Colaiori, and G. Durin, Nat. Phys. **1**, 46 (2007).

[34] W. Döering, Z. Naturforsch. A **3**, 373 (1948).

[35] V. Lecomte, S. E. Barnes, J.-P. Eckmann, and T. Giamarchi, Phys. Rev. B **80**, 054413 (2009).

[36] D. Bernard and B. Doyon, arXiv:1202.0239.

[37] L. S. Levitov, in *Quantum Noise in Mesoscopic Physics*, NATO Science Series, Vol. 97, edited by Y. V. Nazarov (Springer, Netherlands, 2003), pp. 373–396.

[38] C. W. J. Beenakker and C. Schonenberger, Phys. Today **56**(5), 37 (2003).

[39] P.-E. Roche, B. Derrida, and B. Doucot, Eur. Phys. J. B **43**, 529 (2005).

[40] I. Klich, in *Quantum Noise in Mesoscopic Physics*, NATO Science Series, edited by Y. V. Nazarov (Kluwer, Dordrecht, 2003).

[41] J. Gabelli and B. Reulet, Phys. Rev. B **80**, 161203 (2009).

[42] D. A. Gorokhov, D. S. Fisher, and G. Blatter, Phys. Rev. B **66**, 214203 (2002).

[43] T. Nattermann, T. Giamarchi, and P. Le Doussal, Phys. Rev. Lett. **91**, 056603 (2003).

[44] V. Repain, M. Bauer, J.-P. Jamet, J. Ferré, A. Mougin, C. Chappert, and H. Bernas, Europhys. Lett. **68**, 460 (2004).

[45] A. A. Middleton, Phys. Rev. Lett. **68**, 670 (1992).

[46] J. M. Schwarz and R. Maimon, Phys. Rev. E **64**, 016120 (2001).

[47] Y. G. Sinai, Theor. Math. Phys. **90**, 219 (1992).

[48] T. W. Burkhardt, J. Phys. A: Math. Gen. **26**, L1157 (1993).

[49] P. Le Doussal and K. J. Wiese, Phys. Rev. E **79**, 051105 (2009).

[50] D. L. Scharfetter and H. K. Gummel, IEEE Trans. Electron Devices **ED-16**, 64 (1969).

[51] M. J. Ablowitz and A. Zeppetella, Bull. Math. Biol. **41**, 835 (1979).

[52] A. D. Polyanin and V. F. Zaitsev, *Handbook of Exact Solutions for Ordinary Differential Equations* (CRC Press, Boca Raton, FL, 1995).

[53] F. Evers and A. D. Mirlin, Rev. Mod. Phys. **80**, 1355 (2008).

[54] Y. Fyodorov, J. Stat. Mech. (2009) P07022.